Modeling, Control, and Design Study of Balanced Pneumatic Suspension for Improved Roll Stability in Heavy Trucks

Yang Chen

Dissertation submitted to the Faculty of the Virginia Polytechnic Institute and State University in partial fulfillment of the requirements for the degree of

Doctor of Philosophy
In
Mechanical Engineering

Mehdi Ahmadian, Chair
Clinton L. Dancey
Farrokh Jazizadeh Karimi
Steve C. Southward
Saied Taheri

April 18, 2017
Blacksburg, Virginia

Keywords: Pneumatic suspension, heavy truck, multi-domain modeling, co-simulation

Modeling, Control, and Design Study of Balanced Pneumatic Suspension for Improved Roll Stability in Heavy Trucks

Yang Chen

Abstract

This research investigates a novel arrangement to pneumatic suspensions that are commonly used in heavy trucks, toward providing a dynamically balanced system that resists body roll and provides added roll stability to the vehicle. The new suspension, referred to as "balanced suspension," is implemented by retrofitting a conventional pneumatic suspension with two leveling valves and a symmetric plumbing arrangement to provide a balanced airflow and air pressure in the airsprings. This new design contributes to a balanced force distribution among the axles, which enables the suspension to maintain the body in a leveled position both statically and dynamically. This is in contrast to conventional heavy truck pneumatic suspensions that are mainly adjusted quasi-statically to level the body in response to load variations. The main objectives of the research are to discover and analyze the effects of various pneumatic components on the suspension dynamic response and numerically study the benefits of the pneumatically balanced suspension system. A pneumatic suspension model is established to capture the details of airsprings, leveling valves, check valves, pipes, and air tank based on the laws of fluid mechanics and thermodynamics. Experiments are designed and conducted to help determine and verify the modeling parameters and components. Co-simulation technique is applied to establish a multi-domain model that couples highly non-linear fluid dynamics of the pneumatic suspension with complex multi-body dynamics of an articulated vehicle. The model is used to extensively study effects of pneumatic balanced control of the suspensions on the tractor and trailer combination dynamics. The simulations indicate that the dual leveling valve arrangement of the balanced suspension provides better adjustments to the body roll by charging the airsprings on the jounce side, while purging air from the rebound side. Such an adjustment allows maintaining a larger difference in suspension force from side to side, which resists the vehicle sway and levels the truck body during cornering. Additionally, the balanced suspension better equalizes the front and rear drive axle air pressures, for a better dynamic load sharing and pitch control. It is evident from the simulation results that the balanced suspension increases roll stiffness without affecting vertical stiffness, and thereby it can serve as an anti-roll bar that results in a more stable body roll during steering maneuvers. Moreover, the Failure Mode and Effects Analysis (FMEA) study suggests that when one side of the balanced suspension fails, the other side acts to compensate for the failure. On the other hand, if the trailer is also equipped with dual leveling valves, such an arrangement will bring an additional stabilizing effect to the vehicle in case of the tractor suspension failure. The overall research results presented show that significant improvements on vehicle roll dynamics and suspension dynamic responsiveness can be achieved from the balanced suspension system.

Modeling, Control, and Design Study of Balanced Pneumatic Suspension for Improved Roll Stability in Heavy Trucks

Yang Chen

General Audience Abstract

Over the last decade or so, air suspension has been widely equipped on heavy truck for a better ride and height control. The conventional air suspension employs one leveling valve to adjust airspring pressure in order to maintain ride height for various loads, which, however, hardly provides roll stability control when a truck undergoes a turn, accelerating, or breaking. A new air suspension system, referred to as balanced suspension, is proposed by implementing two leveling valves and a symmetric plumbing arrangement. The suspension pneumatics are designed to provide balanced air flow and pressure in the airsprings such that they are able to better respond to truck body motion in real time. The main objective of this research is to provide a simulation evaluation of the effect of maintaining the balanced airflow in heavy truck air suspensions on vehicle roll stability. The analysis is performed based on a complex model including fluid dynamics of the pneumatic suspension and multi-body dynamics of the heavy truck. Experiments are conducted to determine some parameters necessary for the modeling and to provide verification for the pneumatic suspension model. The simulation results show that, as a truck performs a cornering, the proposed balanced suspension can supply air to the compressed suspension while purging air from the extended suspension. These adjustments result in balanced suspension force to improve the dynamic responsiveness of the suspension to steering, causing less body roll, in comparison with the conventional air suspension. Additionally, the Failure Mode and Effects Analysis (FMEA) study indicates that one-side component failure of the balanced suspension does not completely disable the system, the unaffected side works to keep the system functioning until the failure is corrected. Overall research results suggest that the truck roll dynamics and suspension dynamic responsiveness are improved for the balanced suspension. Moreover, this study contributes to a simulation platform that can serve as an effective virtual design and simulation tool for analyzing, improving, and engineering the pneumatic suspension system.

Dedication

I would like to dedicate this dissertation to my parents, Baian Chen and Min Liu, without whose love, support, and encouragement I would not complete what I have done today. I also dedicate this work to my wife, Yuanyuan Lu, who has always been there to support and encourage me during those difficult and trying times. I also want to dedicate my work to my sister, Xuanyu Chen, to encourage her to work hard for achieving her goal in life.

Acknowledgements

I would like to express my deepest gratitude to my advisor, Dr. Mehdi Ahmadian, whose guideline on both research and my career has been priceless. Thank you for offering me a home in your lab and support over the years, and for academically mentoring me with patience and immense knowledge. I would not achieve the research and writing of the dissertation without your valuable guidance and help. I also truly appreciate you for being supportive and understanding throughout my doctoral process, especially during the hardest time in my life, making me feel the love more than I ever thought. You have been a tremendous mentor, not only in academic research but also in my life.

I am also grateful to my committee members, Dr. Clinton L. Dancey, Dr. Farrokh Jazizadeh Karimi, Dr. Steve C. Southward, and Dr. Saied Taheri, for providing supports and brilliant suggestions on this research.

I want to thank all the staff and students at the Center for Vehicle Systems & Safety for all their contributions of time, ideas, and technical expertise to help me complete such a big project. The past four years I worked with them has been very enjoyable and memorable.

I would like to especially thank to my family and my friends for their love, support and encouragement throughout the course of this research.

Table of Contents

Abstract ii

General Audience Abstract iii

Dedication iv

Acknowledgements v

Table of Contents vi

List of Figures x

List of Tables xv

CHAPTER 1 INTRODUCTION 1

1.1 MOTIVATION 1
1.2 OBJECTIVES 3
1.3 CHALLENGES 4
1.4 APPROACHES 4
1.5 CONTRIBUTIONS 6
1.6 OUTLINE 7

CHAPTER 2 BACKGROUND AND LITERATURE REVIEW 8

2.1 BACKGROUND OF HEAVY TRUCK PNEUMATIC SUSPENSION SYSTEMS 8
2.1.1 Working Principles of Airsprings 10
2.1.2 Working Principles of Height Control Valves 12
2.2 OVERVIEW OF PNEUMATIC SUSPENSION DESIGN AND MODELING 13
2.2.1 Non-linear Characteristic Study of Airsprings 13
2.2.2 Pneumatic Suspension System Design 15
2.2.3 Modeling of Pneumatic Suspension Systems 17

CHAPTER 3 NON-LINEAR MATHEMATICAL MODEL OF A PNEUMATIC SUSPENSION SYSTEM .20

3.1 INTRODUCTION 20
3.2 MATHEMATICAL MODELING OF A PNEUMATIC SUSPENSION SYSTEM 22
3.2.1 Mathematic Equations of the Airspring Model 23
3.2.2 Mathematic Equations of the Valve Model 26
3.2.3 Mathematic Equations of the Pipe Model 30
3.2.4 Mathematic Equation of the Tee-junction Model 32

CHAPTER 4 MODELING AND VALIDATION OF THE PNEUMATIC SUSPENSION 33

4.1 INTRODUCTION 33
4.2 AIRSPRING MODELING DESCRIPTION 34
4.2.1 Development of the Airspring Model 34
4.2.2 Test-based Determinations of Effective Area Change and Volume Variation 36
4.2.3 Validation of the Airspring Model with Simulink Model 40
4.2.4 Validation of the Airspring Model with Experimental Results 42
4.3 VALVE MODELING DESCRIPTION 44
4.3.1 Model Development and Experimental Characterization for the Leveling Valve 44
4.3.2 Validation of the Leveling Valve Model with Experimental Results 47
4.3.3 Development of the Check Valve Model 48
4.4 PIPE MODELING DESCRIPTION 49
4.4.1 Dissipative Effect of the Pipe Model 49
4.4.2 Combination of Dissipative and Compressive Effects 50
4.5 PNEUMATIC SUSPENSION SUBSYSTEM MODELING DESCRIPTION 53
4.6 PNEUMATIC SUSPENSION SYSTEM TEST AND MODEL VALIDATION 55

CHAPTER 5 SIMULATION STUDY OF A 9-DOF TRUCK DYNAMIC MODEL WITH PNEUMATIC SUSPENSION DYNAMICS 60

5.1 TRUCK MODELING DESCRIPTION 60
5.1.1 Development of a Truck Dynamic Model with 9 DOF 60
5.1.2 Validation of the Truck Dynamic Model with Simulink Model 63
5.1.3 Integration with Pneumatic Suspension System 64
5.2 SIMULATION RESULTS 65
5.3 CONCLUSIONS 71

CHAPTER 6 ACHIEVING PNEUMATIC ANTI-ROLL BAR THROUGH SUSPENSION BALANCING CONTROL FOR A SEMI-TRAILER TRUCK 72

6.1 SIMULATION DYNAMIC MODEL 72
6.1.1 Tractor Model 73
6.1.2 53-ft Trailer Model 73
6.1.3 Fifth-wheel Coupling Model 74
6.1.4 Pneumatic Suspension System Model 74
6.1.5 Development of Co-simulation Environment 76
6.2 SIMULATION MANEUVERS 76
6.3 SIMULATION RESULTS AND ANALYSIS 78
6.4 SUMMARY OF SIMULATION RESULTS 83

6.5 CONCLUSION 85

CHAPTER 7 FAILURE MODE AND EFFECTS ANALYSIS OF DUAL LEVELING VALVE AIRSPRING SUSPENSIONS ON TRUCK DYNAMICS 87

7.1 INTRODUCTION 87
7.2 FAILURE CAUSE AND EFFECT STUDIES FOR A SEMI-TRUCK PNEUMATIC SUSPENSION SYSTEM 90
7.3 PNEUMATIC SUSPENSION AND TRUCK DYNAMIC SIMULATION MODEL 92
7.3.1 Modeling of Fully-blocked and Control Rod Bending of the Leveling Valve 92
7.3.2 Modeling of Suspenison System Air Leak 93
7.3.3 Full-truck Multi-body Dynamics Model Integration 94
7.4 SIMULATION ANALYSIS OF THE SUSPENSION FAILURES 95
7.4.1 Simulation Maneuver 95
7.4.2 Effect of Fully blocked Leveling Valve on the Truck's Roll Dynamics 96
7.4.3 Effect of Control Rod Bending on the Truck's Roll Dynamics 97
7.4.4 Effect of Suspension System Air Loss on the Truck's Roll Dynamics 99
7.5 CONCLUSION 100

CHAPTER 8 PNEUMATIC SUSPENSION BALANCING CONTROL FOR IMPROVED ROLL DYNAMICS OF A SEMI-TRAILER TRUCK CARRYING NON-UNIFORM LOAD 102

8.1 INTRODUCTION 102
8.2 SIMULATION MODEL 104
8.2.1 Uneven-loaded Semi-trailer Truck Model 104
8.2.2 Partially-filled Tank Truck Model 105
8.3 RESULTS AND DISCUSSION 109
8.3.1 Effect of the Balanced Suspension on Roll Dynamics of the Truck with Lateral Uneven Load 109
8.3.2 Effect of the Balanced Suspension on Roll Dynamics of the Partially-filled Tank Truck 111

CHAPTER 9 SUMMARY AND FUTURE WORK 116

9.1 SUMMARY 116
9.2 FUTURE WORK 117

REFERENCES 118

APPENDIX A EFFECTIVE AREA CHANGE AND VOLUME VARIATION FOR AIRSPRING OF 53-FT TRAILER 127

APPENDIX B SCHEMATICS OF 9-DOF TRUCK DYNAMIC MODEL AND PARAMETERS USED IN SIMULATION 128

APPENDIX C SCHEMATICS OF HYBRID MODELS AND PARAMETERS USED IN CO-SIMULATION 132

APPENDIX D SCHEMATICS OF THE LIQUID CARGO TANK TRUCK MODEL AND PARAMETERS USED IN THE SIMULATION.....135

List of Figures

FIGURE 1-1. SCHEMATIC OF THE OE SUSPENSION PLUMBING CONFIGURATION 2
FIGURE 1-2. SCHEMATIC OF THE BALANCED SUSPENSION PLUMBING CONFIGURATION 3
FIGURE 2-1. PICTURES OF THE AIRSPRINGS INSTALLED ON THE (A) TRACTOR AND (B) TRAILER 9
FIGURE 2-2. (A) CONVOLUTED BELLOW AND (B) CONVENTIONAL ROLLING LOBE [19] 10
FIGURE 2-3. CHARACTERISTIC VARIATION DUE TO PISTON SHAPES AND FLEXIBLE MEMBER SIZE [18] 11
FIGURE 2-4. TYPICAL HEIGHT CONTROL VALVE MOUNTING AND CONNECTION TO AXLE [22] 12
FIGURE 2-5. BASIC PNEUMATIC DIAGRAM OF A THREE-PORT, THREE-POSITION LEVELING VALVE 13
FIGURE 2-6. DYNAMIC VERTICAL STIFFNESS OF AIRSPRINGS [31] 15
FIGURE 2-7. SCHEMATICS OF A QUARTER CAR MODEL WITH THE DOUBLE-ACTING CYLINDER SUSPENSION [37] 16
FIGURE 2-8. SCHEMATICS OF PNEUMATIC SUSPENSION 16
FIGURE 2-9. PROPOSED DESIGN WITH MULTIPLE AUXILIARY TANKS CONNECTED TO AIRSPRING BY ON-OFF VALVES [41] 17
FIGURE 3-1. PNEUMATIC SUSPENSION SYSTEM 21
FIGURE 3-2. BLOCK DIAGRAM DRAWING FOR ONE SIDE OF THE BALANCED SUSPENSION 21
FIGURE 3-3. BOND GRAPH OF A HALF-BALANCED SUSPENSION 22
FIGURE 3-4. DIAGRAM OF EXTERNAL VARIABLES OF THE AIRSPRING MODEL 23
FIGURE 3-5. DIAGRAM OF EXTERNAL VARIABLES OF THE ORIFICE MODEL 26
FIGURE 3-6. SCHEMATIC OF AIR EXHAUST THROUGH A SMALL ORIFICE 28
FIGURE 3-7. DIAGRAM OF EXTERNAL VARIABLES OF THE PIPE MODEL 30
FIGURE 3-8. DIAGRAM OF EXTERNAL VARIABLES OF THE TEE-JUNCTION MODEL 32
FIGURE 3-9. DIAGRAM OF EXTERNAL VARIABLES OF PRESSURE SOURCE MODEL 32
FIGURE 4-1. MODEL OF AIRSPRING IN AMESIM 35
FIGURE 4-2. TEST FOR AIRSPRING EFFECTIVE AREA 36
FIGURE 4-3. EXPERIMENTAL RESULTS OF AIRSPRING FORCE VERSUS HEIGHT FOR 10 PSI, 15 PSI, AND 20 PSI (AIRSPRING MODEL: VOLVO 556-24-3-110) 37
FIGURE 4-4. EXPERIMENTAL RESULTS OF AIRSPRING EFFECTIVE AREA VERSUS HEIGHT FOR 10 PSI, 15 PSI, AND 20 PSI (AIRSPRING MODEL: VOLVO 556-24-3-110) 37
FIGURE 4-5. AIRSPRING VOLUME TESTING: (A) FULLY FILLING THE AIRSPRING WITH WATER AND (B) MEASURING THE AIRSPRING HEIGHT SUNJECT TO A CONSTANT LOAD 38
FIGURE 4-6. AIRSPRING VOLUME TESTING: (A) HYDRAULIC JACK AND (B) AIRSPRING 39
FIGURE 4-7. EXPERIMENTAL RESULTS OF AIRSPRING VOLUME VERSUS HEIGHT (AIRSPRING MODEL: VOLVO 556-24-3-110) 40
FIGURE 4-8. MODEL USED FOR VALIDATION OF THE AIRSPRING MODEL 41
FIGURE 4-9. AIRSPRING MODEL IN MATLAB/SIMULINK 41

FIGURE 4-10. COMPARISON RESULTS OF AIRSPRING PRESSURE, TEMPERATURE, FORCE, AND VOLUME SUJECTED TO A 1-INCH SINUSOIDAL EXCITATION AT 0.25 HZ 42
FIGURE 4-11. FORCE RESPONSE FOR SINUSOIDAL MOTION EXCITATION AT 0.1HZ, 0.5HZ, AND 1HZ (THE 0.1 HZ AND 1 HZ ARE SHOWN RESPECTIVELY 200 LBF HIGHER AND LOWER THAN ACTUAL VALUES. INITIAL PRESSURE IS SET TO BE 10 PSI) 44
FIGURE 4-12. LEVELING VALVE MODEL IN AMESIM 45
FIGURE 4-13. MOUNTING POSITION OF THE LEVELING VALVE ON THE TRACTOR 45
FIGURE 4-14. TEST SETUP TO DETERMINE THE FLOW CHARACTERIZATION OF THE LEVELING VALVE 46
FIGURE 4-15. EFFECT OF THE SUSPENSION DEFLECTION ON THE FLOW AREA OF THE LEVELING VALVE FOR (A) BALANCED SUSPENSION AND (B) OE SUSPENSION 47
FIGURE 4-16. MODEL USED FOR VALIDATION OF THE LEVELING VALVE MODEL 47
FIGURE 4-17. EFFECTS OF SUSPENSION DEFLECTION ON MASS FLOW RATE FOR (A) LEVELING VALVE OF BALANCED SUSPENSION AND (B) LEVELING VALVE OF OE SUSPENSION 48
FIGURE 4-18. MASS FLOW RATE AS A FUNCTION OF THE PRESSURE RATIO 49
FIGURE 4-19. MODEL USED FOR EVALUATING THE EFFECT OF THE PIPE FRICTION 49
FIGURE 4-20. EFFECT OF DIFFERENT (A) PIPE DIAMETERS AND (B) PIPE LENGTHS ON THE PRESSURE CHANGE AT OUTLET 50
FIGURE 4-21. PIPE MODELS (A) DEVELOPED BY COUPLING PNEUMATIC CHAMBER AND FRICTION SUBMODEL AND (B) ORIGINALLY IN THE PNEUMATIC LIBRARY OF AMESIM 51
FIGURE 4-22. SIMULATION RESULTS COMPARISON BETWEEN THE ORIGINAL PIPE MODEL (PNL0001) AND THE COMBINED MODEL : (A) PRESSURE AT PORT 1, (B) PRESSURE AT PORT 2, (C) MASS FLOW RATE AT PORT 2, AND (D) TEMPERATURE AT PORT 2 52
FIGURE 4-23. EFFECT OF DIFFERENT PIPE LENGTHS ON ATTENUATING THE MASS FLOW RATE AT THE OUTLET 53
FIGURE 4-24. MODEL USED FOR VERIFYING ONE SIDE OF THE BALANCED AIR SUSPENSIONS 53
FIGURE 4-25. TIME TRACE OF SUSPENSION DEFLECTION ON MIDDLE AXLE (A) AND REAR AXLE (B) WITH A 3-INCH BUMP INPUT 54
FIGURE 4-26. TIME TRACE OF AIRSPRING PRESSURE 54
FIGURE 4-27. TIME TRACE OF MASS FLOW RATE AT LEVELING VALVE 55
FIGURE 4-28. DIAGRAM OF THE TEST FOR (A) INFLATION PROCESS AND (B) DEFLATION PROCESS 56
FIGURE 4-29. TEST SETUP FOR THE PNEUMATIC SUSPENSION SYSTEM ON THE TRUCK TANDEM REAR AXLES 56
FIGURE 4-30. INSTALLATION OF THE STRING POT ON ONE SIDE OF THE BOGIE AIR SUSPENSION 57
FIGURE 4-31. RELATIONSHIP BETWEEN AIRSPRING HEIGHT AND STRING POT DATA 57
FIGURE 4-32. MODEL USED FOR VERIFYING THE PNEUMATIC SUSPENSION SYSTEM WITH EXPERIMENTS 58
FIGURE 4-33. COMPARISON BETWEEN SIMULATION AND EXPERIMENTAL RESULTS FOR CHARGING THE AIRSPRINGS BY UPWARD MOVEMENT OF THE LEVELER ARM 59
FIGURE 4-34. COMPARISON BETWEEN SIMULATION AND EXPERIMENTAL RESULTS FOR DISCHARGING THE AIRSPRINGS BY DOWNWARD MOVEMENT OF THE LEVELER ARM 59

FIGURE 5-1. TRUCK MULTI-BODY DYNAMIC MODEL SCHEMATICS 61
FIGURE 5-2. TRUCK MULTI-BODY DYNAMIC MODEL VALIDATION WITH SIMULINK MODEL FOR A 0.2G SINUSOIDAL LATERAL ACCELERATION AT 0.5 HZ 63
FIGURE 5-3. RELATIONSHIP BETWEEN THE TRUCK DYNAMIC MODEL AND THE PNEUMATIC SYSTEM MODEL 64
FIGURE 5-4. ALIGNED TRUCK DYNAMIC MODEL WITH BALANCED PNEUMATIC SUSPENSIONS IN AMESIM 65
FIGURE 5-5. LATERAL ACCELERATION FOR (A) RIGHT-HAND TURN AND (B) AN S-TURN 66
FIGURE 5-6. TIME TRACE OF AIRSPRING PRESSURE ON TANDEM DRIVING AXLES AND FOR RIGHT-HAND CORNERING AND AN S-TURN 67
FIGURE 5-7. TIME TRACE OF AIRSPRING FORCE ON TANDEM DRIVING AXLES FOR RIGHT-HAND CORNERING AND AN S-TURN 68
FIGURE 5-8. TIME TRACE OF SUSPENSION DEFLECTION ON TANDEM REAR AXLES FOR RIGHT-HAND CORNERING AND AN S-TURN 69
FIGURE 5-9. TIME TRACE OF FLOW RATE AT LEVELING VALVES FOR CORNERING AND S-TURN 69
FIGURE 5-10. TIME TRACE OF ROLL ANGLE AND PITCH ANGLE FOR CORNERING AND S-TURN 70
FIGURE 6-1. A 6X4 TRACTOR MODEL IN TRUCKSIM 73
FIGURE 6-2. A 53-FT SEMI-TRAILER TRUCK MODEL IN TRUCKSIM 73
FIGURE 6-3. CAD MODEL OF FIFTH-WHEEL COUPLING 74
FIGURE 6-4. PLUMBING CONFIGURATIONS OF HEAVY TRUCK PNEUMATIC SUSPENSIONS: (A) OE/OE SUSPENSIONS, (B) BALANCED/OE SUSPENSIONS, (C) OE/BALANCED SUSPENSIONS, AND (D) BALANCED / BALANCED SUSPENSIONS 75
FIGURE 6-5. CO-SIMULATION ENVIRONMENT 76
FIGURE 6-6. TARGET PATH FOR THE SINGLE LANE CHANGE MANEUVER 77
FIGURE 6-7. TARGET PATH FOR THE SINGLE LANE CHANGE MANEUVER 78
FIGURE 6-8. SIMULATION RESULTS OF LATERAL ACCELERATIONS ON THE TRACTOR AND TRAILER FOR (A) SINGLE LANE CHANGE AND (B) STEADY-STATE CORNERING 78
FIGURE 6-9. SIMULATION RESULTS OF ROLL ANGLES ON THE TRACTOR AND TRAILER FOR (A, C) SINGLE LANE CHANGE AND (B, D) STEADY-STATE CORNERING 79
FIGURE 6-10. SIMULATION RESULTS OF MASS FLOW RATE AT THE LEVELING VALVES ON THE TRACTOR AND TRAILER FOR (A, C) SINGLE LANE CHANGE AND (B, D) STEADY-STATE CORNERING 80
FIGURE 6-11. SIMULATION RESULTS OF AIRSPRING PRESSURES ON THE TRACTOR AND TRAILER FOR (A, C) SINGLE LANE CHANGE AND (B, D) STEADY-STATE CORNERING 81
FIGURE 6-12. SIMULATION RESULTS OF ANTI-ROLL MOMENT VERSUS ROLL ANGLE ON THE TRACTOR AND TRAILER FOR (A, C) SINGLE LANE CHANGE AND (B, D) STEADY-STATE CORNERING 82
FIGURE 6-13. SIMULATION RESULTS OF ROLL STIFFNESS VERSUS ROLL ANGLE ON THE TRACTOR AND TRAILER FOR (A, C) SINGLE LANE CHANGE AND (B, D) STEADY-STATE CORNERING 83
FIGURE 6-14. SUMMARY OF PEAK-TO-PEAK VALUE ON THE TRACTOR AND TRAILER FOR (A, B) EMPTY, (C, D) HALF LOAD, AND (E, F) FULL LOAD DURING THE SINGLE LANE CHANGE 84

FIGURE 6-15. SUMMARY OF PEAK-TO-PEAK VALUE ON THE TRACTOR AND TRAILER FOR (A, B) EMPTY, (C, D) HALF LOAD, AND (E, F) FULL LOAD DURING STEADY-STATE CORNERING....85
FIGURE 7-1. (A) ORIGINAL EQUIPMENT (OE) AND (B) BALANCED (BA) CONFIGURATIONS ON THE SEMI-TRUCK DRIVE AXLES....89
FIGURE 7-2. PNEUMATIC SUSPENSION SYSTEM: (A) AIR FITTING AND AIR HOSE, AND (B) LEVELING VALVE....90
FIGURE 7-3. THE EFFECT OF THE CONTROL ROD'S BENDING ON FLOW CHARACTERISTICS OF THE LEVELING VALVE....93
FIGURE 7-4. PNEUMATIC SUSPENSION AIR LEAK MODEL IN AMESIM....93
FIGURE 7-5. FAILURE CASES OF (A) ORIGINAL EQUIPMENT (OE) AND (B) BALANCED (BA) SUSPENSION ON THE SEMI-TRUCK DRIVE AXLES....94
FIGURE 7-6. WB-67 SEMI-TRAILER TRUCK MODEL IN TRUCKSIM....95
FIGURE 7-7. PATH TRACK FOR STEADY STATE CORNERING....95
FIGURE 7-8. SIMULATION RESULTS FOR THE FAILURE CASE OF THE FULLY-BLOCKED LEVELING VALVE: (A) MASS FLOW RATE AT THE LEVELING VALVE, (B) ROLL ANGLE, (C) AIRSPRING FORCE, AND (D) SUSPENSION DEFLECTION....97
FIGURE 7-9. SIMULATION RESULTS FOR THE FAILURE OF THE CONTROL ROD BENDING: (A) MASS FLOW RATE AT THE LEVELING VALVE, (B) ROLL ANGLE, (C) AIRSPRING FORCE, AND (D) SUSPENSION DEFLECTION....98
FIGURE 7-10. SIMULATION RESULTS FOR THE FAILURE CASE OF AIR LOSS: (A) MASS FLOW RATE AT THE LEVELING VALVE AND AIR LEAK, (B) ROLL ANGLE, (C) AIRSPRING FORCE, AND (D) SUSPENSION DEFLECTION....100
FIGURE 8-1. BACK VIEW OF THE TRUCK MODEL WITH LATERAL UNEVEN LOAD....104
FIGURE 8-2. ROLL PLANE REPRESENTATION OF THE PARTIALLY-FILLED TANK TRAILER....106
FIGURE 8-3. CO-SIMULATION SCHEME FOR EVALUATING THE EFFECT OF A PNEUMATIC SUSPENSION ON ROLL DYNAMICS ANALYSIS OF A PARTIALLY-FILLED TANK TRUCK....107
FIGURE 8-4. TIME TRACE OF (A) ROLL ANGLE AND (B) ROLL RATE RESPONSES OF THE SEMI-TRAILER TRUCK WITH FIXED UNBALANCED LOAD (CG LATERAL OFFSET OF15 IN) SUBJECTED TO A 0.1 G LATERAL ACCELERATION...110
FIGURE 8-5. COMPARISONS OF (A) PEAK ROLL ANGLE AND (B) PEAK ROLL RATE BETWEEN THE BALANCED AND OE SUSPENSIONS FOR VARIOUS LATERAL OFFSETS OF UNEVEN FIXED LOAD SUBJECTED TO A 0.1 G LATERAL ACCELERATION....111
FIGURE 8-6. TIME TRACE OF (A) ROLL ANGLE AND (B) ROLL RATE RESPONSES OF A 60%-VOLUME FILLED TANK TRUCK SUBJECTED TO A 0.14 G LATERAL ACCELERATION....112
FIGURE 8-7. COMPARISONS OF (A) PEAK ROLL ANGLE AND (B) PEAK ROLL RATE BETWEEN THE BALANCED AND OE SUSPENSIONS FOR VARIOUS TANK FILLS SUBJECTED TO A 0.14 G LATERAL ACCELERATION....112
FIGURE 8-8. TIME TRACE OF (A) LATERAL AND (B) VERTICAL VARIATIONS OF LIQUID CARGO MASS CENTER OF A 60%-VOLUME FILLED TANK SUBJECTED TO A 0.14 G LATERAL ACCELERATION....113
FIGURE 8-9. COMPARISONS OF MAXIMUM (A) LATERAL AND (B) VERTICAL SHIFTS OF LIQUID CARGO MASS CENTER BETWEEN THE BALANCED AND OE SUSPENSIONS FOR VARIOUS TANK FILLS SUBJECTED TO A 0.14 G LATERAL ACCELERATION....114
FIGURE 8-10. TIME TRACE OF (A) EFFECTIVE MOMENT ARM AND (B) ROLL MASS MOMENT OF INERTIA CHANGE OF A 60%-VOLUME FILLED TANK TRUCK SUBJECTED TO A 0.14 G LATERAL ACCELERATION....115

FIGURE 8-11. COMPARISONS OF (A) MAXIMUM EFFECTIVE MOMENT ARM AND (B) MAXIMUM ROLL MASS MOMENT OF INERTIA VARIATION BETWEEN THE BALANCED AND OE SUSPENSIONS FOR VARIOUS TANK FILLS SUBJECTED TO A 0.14 G LATERAL ACCELERATION 115
FIGURE A-1. TRAILER'S AIRSPRING EFFECTIVE AREA VERSUS HEIGHTS 127
FIGURE A-2. TRAILER'S AIRSPRING VOLUME VERSUS HEIGHTS 127
FIGURE B-1. 9-DOF TRUCK MODEL IN AMESIM 128
FIGURE B-2. 9-DOF TRUCK DYNAMIC MODEL IN SIMULINK 129
FIGURE B-3. ALIGNED TRUCK DYNAMIC MODEL WITH OE SUSPENSIONS IN AMESIM 130
FIGURE C-1. TRACTOR AND TRAILER SUSPENSION SYSTEM MODEL IN AMESIM: A) OE/OE SUSPENSIONS (B) BALANCED/OE SUSPENSIONS (C) OE/BALANCED SUSPENSIONS (D) BALANCED/BALANCED SUSPENSIONS 132
FIGURE C-2. CO-SIMULATION MODEL IN MATLAB/SIMULINK 132
FIGURE D-1. CO-SIMULATION MODEL DEVELOPED USING AMESIM, SIMULINK, AND TRUCKSIM 136
FIGURE D-2. SIMULINK DIAGRAM FOR CALCULATION OF THE ADDITIONAL MOMENT CAUSED BY THE LIQUID LOAD SHIFT 137
FIGURE D-3. SOLIDWORK MODELS OF LIQUID CARGO: (A) 30% FILL VOLUME, (B) 60% FILL VOLUME, AND (C) 90% FILL VOLUME 137

List of Tables

TABLE 4-1. TEST DATA OF THE AIRSPRING VOLUME WITH DIFFERENT HEIGHTS 39
TABLE 4-2. PARAMETERS USED IN TESTING THE AIRSPRING 41
TABLE 4-3. PARAMETERS USED IN VERIFYING THE ORIGINAL PIPE MODEL 51
TABLE 6-1. THREE DIFFERENT LOAD CONDITIONS 74
TABLE 7-1. FMEA SPREADSHEET FOR THE PNEUMATIC SUSPENSION SYSTEM 92
TABLE 8-1. TANK SEMI-TRAILER SIMULATION PARAMETERS [70] 108
TABLE 8-2. FLUID CARGO SIMULATION PARAMETERS 108
TABLE B-1. MAIN PARAMETERS SELECTED FOR THE 9-DOF TRUCK DYNAMIC SIMULATION 131
TABLE B-2. MAIN PARAMETERS SELECTED FOR PNEUMATIC SUSPENSION SIMULATION 131
TABLE C-1. MAIN PARAMETERS SELECTED FOR TRUCK DYNAMIC SIMULATION 133
TABLE C-2. MAIN PARAMETERS SELECTED FOR PNEUMATIC SUSPENSION SIMULATION 134

Chapter 1 Introduction

1.1 Motivation

As differentiated from passenger vehicles, heavy trucks carry a considerably large load with a high center of gravity (CG) and while maintaining a relatively small track due to the road width limit. These properties make the heavy trucks yield larger lateral load transfers during cornering, thus exhibiting low roll stability and poor handling. As reported by the Large Truck Crash Facts, there were 4,321 fatal crashes involving large trucks during 2006 [1 – 2].

Vehicle suspension design plays a vital role in improving the vehicle dynamic performance. During the last two decades, pneumatic suspensions employing airsprings have become the new industry "standard," replacing traditional leaf springs. This change is due to the airspring's benefits in reduced weight, ride height adjustment, increased ride comfort, lower damage to cargo, and reduced structure-borne noise among actors [3]. The pneumatic suspensions of heavy trucks typically include a set of various pneumatic components, such as airsprings, leveling valves, pipes, an air tank, and hose fittings to maintain the ride height of the truck in response to load variations. These components could be arranged in different configurations to meet different needs as they relate to truck dynamics.

A typical Class-8 vehicle has the tractor's rear tandem axles and the trailer's dual axles equipped with pneumatic suspensions, as shown in Figure 1-1. This original design, also known as the original equipment (OE), utilized a single three-port, three-position leveling valve for low cost, simple installation, and easy maintenance. It is placed at an offset from the centerline of the track and on the vehicle frame beam on the left side with a linkage arrangement attached to the axles in order to detect the suspension deflection. A circular pneumatic circuit connects the leveling valve to all of the airsprings. The OE pneumatic suspensions are designed for adjusting to load variations that occur quasi-statically. Several studies [4 – 5] have mentioned that the OE pneumatic suspensions are not suitable for responding to the dynamic force resulting from steering maneuvers. Lambert [6] also found

that the OE pneumatic suspension provides poor dynamic load sharing among the axles. Regarding roll stability, some extra anti-roll devices, such as anti-roll bars, might be included to increase roll stiffness, which resists the body roll motion [7 – 11]. However, the use of the anti-roll bar tends to add unnecessary weight and negatively affects ride responses [9 – 10]. Alternatively, there are a number of semi-active and active pneumatic suspension designs currently available for improving roll performance of road vehicles. However, applications of these pneumatic suspension systems for heavy trucks has been limited due to the concerns of cost, weight, complex packaging, and system reliability [3]. Thus, a more cost-efficient pneumatic suspension system for heavy truck application is desired to address the shortcomings of the OE suspension.

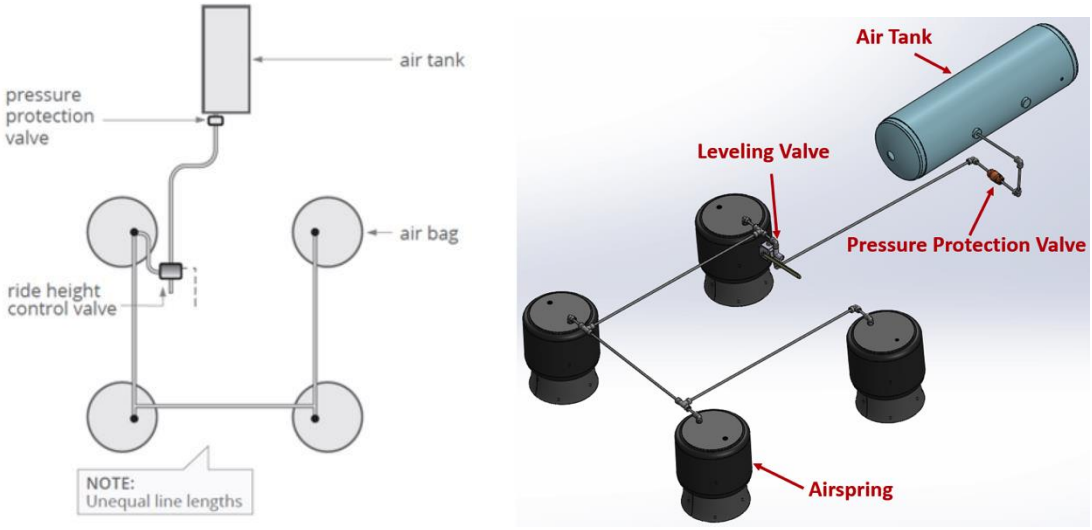

Figure 1-1. Schematic of the OE suspension plumbing configuration

An innovative cost-efficient design for a heavy truck suspension was proposed by simply reconfiguring the OE suspension. The new suspension, referred to as a balanced suspension, includes two leveling valves (one per side) and a symmetric plumbing arrangement, as shown in Figure 1-2, which increases the system's dynamic bandwidth and roll stiffness without changing vertical stiffness. The suspension pneumatics are designed to better respond to body motion in real time. The supplier Hadley manufactures the leveling valve, which is able to provide a larger flow rate with a smaller dynamic dead band. Larger air pipes are utilized for reduced line flow resistances. All air pipes are of equal length from the air tank to the leveling valves, and also from the leveling valves to the airsprings. The

symmetric arrangement is designed to provide equivalent volumetric airflow to the airsprings. The independent control for either side yields a variable roll stiffness, which aids the truck roll dynamics in steering maneuvers. Test data from Richardson et al. [5] have indicated that the truck with the balanced suspension exhibits better handling than the truck with the OE suspension. However, no detailed explanation is presented and regarding how the balanced suspension improves the vehicle dynamics. The present investigation aims to establish the balanced suspension's benefits based on simulation, and to explore the scientific principles behind the control system, which will assist in future design improvement.

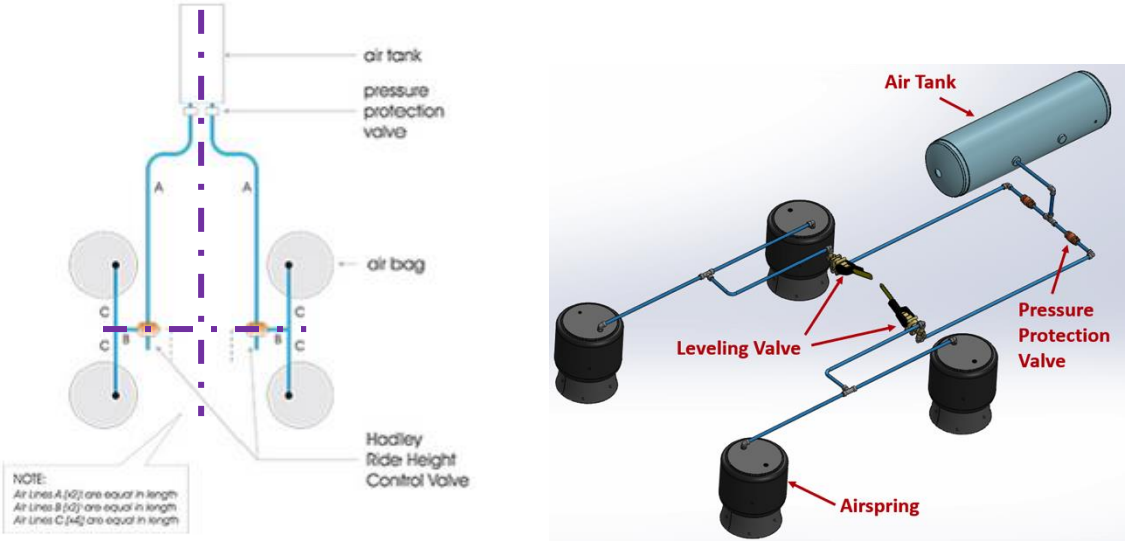

Figure 1-2. Schematic of the balanced suspension plumbing configuration

1.2 Objectives

The primary objectives of this investigation are to:

- Develop a hybrid model including detailed pneumatic suspension dynamics and truck multi-body dynamics.
- Provide a simulation evaluation of the effect of the balanced suspension control system on truck roll dynamics.
- Conduct Failure Mode and Effect Analysis (FMEA) for the pneuamtic suspenison to study the influence of the pneumatic suspension component's shortcomings on the vehicle roll performance.

1.3 Challenges

The following challenges are faced in the investigation:

- Difficulty in modeling highly non-linear fluid dynamics of the pneumatic suspension system.
    - Difficult to develop an analytical model accurately depicting the hysteresis effect and the dynamic behavior of an airspring.
    - Establishing a leveling valve model that can accurately capture the non-linear flow is challenging.
    - Evaluating the pneumatic losses and delays in plumbing arrangement requires parameters and data that is not readily available.
- Combining the detailed pneumatic suspension dynamics and full multi-body dynamics of tractor and trailer combinations in multi-domain modeling is difficult to develop and debug successfully.
- The topic of this study is an innovative and new technique, for which very limited information is available in the open literature.

1.4 Approaches

The following approaches are used to overcome the challenges mentioned in this study:

- The bond graph method is used to help identify flow information and extract equations in a systematic manner for the pneumatic suspension system modeling.
- By applying the principles of fluid dynamics and thermodynamics, mathematic equations of the pneumatic suspension components are derived.
- Based on the mathematic equations, the pneumatic suspension system is modeled using commercial software, AMEsim. The component model and the system model are validated experimentally and analytically.
    - Airspring model (thermo-dynamic effect)
        - The change in the airspring's effective area with respect to height is defined experimentally. The volume of the airspring is determined by a test designed using water. These two properties are necessary for modeling the airspring.

        - The modeling results of pressure, temperature, force, and volume are compared with a Matlab/Simulink model under a sinusoidal excitation.
        - The nonlinear characteristics of the airspring model is also validated with experimental data.
    - Leveling valve model (balanced and OE)
        - The characterization of the valve opening is calculated based on experimental data.
        - The non-linear flow characteristics of the two leveling valve models are respectively verified with experimental data.
    - Check valve model
        - The effect of the difference between downstream and upstream pressures on the mass flow rate is examined by simulation.
    - Pipe model (dissipative effect and compressive effect)
        - The effects of the pipe's diameter and length on pressure drop are tested by simulation.
        - The impact of pipe length on the mass flow rate attenuation at the outlet is tested through simulation.
        - A new lumped model is developed in AMEsim to verify the dissipative and compressive effects of the original model.
    - Subsystem model (one side of the balanced suspension system)
        - Suspension behavior, including deflection, pressure change, and mass flow rate at the leveling valve, is tested by simulation, with no vehicle body dynamics and a road step input.
    - System model
        - Static truck tests are conducted to verify the pneumatic suspension system model. The tests include raising and lowering the truck body via moving the lever arm up and down, Respectively, with a triangle control signal. Experimental results of the airspring pressure and travel are compared with the simulation.
- A 9-DOF truck dynamic model, combined with detailed pneumatic dynamics of a drive-axle suspension, is developed in AMEsim. The model is used to better understand air flow dynamics of the balanced suspension and how they couple with vehicle dynamics.
    - The pure multi-body dynamics of the AMEsim truck model are verified by a Simulink model.

- To extend the investigation to the tractor and trailer combination, a hybrid model is introduced by coupling a WB-67 truck model with a pneumatic suspension. A co-simulation scheme is established by using TruckSim, Matlab/Simulink, and AMEsim. Extensive simulations are performed to evaluate the performance of the pneumatic suspension under different steering maneuvers, driving speeds, and load conditions.
- Failure Mode and Effect Analysis (FMEA) is performed for the pneumatic suspension.
    - The potential failure modes, causes, and effects are analyzed for the pneumatic suspension control system.
    - The failure effects on vehicle roll dynamics are compared between the balanced and OE suspensions via modeling and simulation.
- The influence of the suspension balancing control is evaluated through simulation for the truck carrying non-uniform lateral loads due to uneven loading or cargo shift (liquid sloshing).
    - A semi-trailer truck with a fixed uneven load and a partially-filled tank truck with liquid cargo are modeled separately.
    - Roll angle and roll rate responses are compared between the balanced and OE suspensions for different lateral offsets of the fixed uneven load.
    - Relative movement of liquid CG, effective moment arm, change in moment of inertia, roll angle, and roll rate are compared between the balanced and OE suspensions for different fill volumes in the tank truck.

1.5 Contributions

The primary contributions of this research include:

- More accurate modeling of commercial vehicle pneumatic dynamics
- Improved tools for analyzing, improving, and engineering pneumatic suspensions
    - A verified pneumatic suspension model that can capture highly non-linear fluid dynamic behavior of the truck suspension
    - A multi-domain model that includes pneumatic suspension fluid dynamics and truck multi-body dynamics for heavy truck suspension study and development
    - Introduction of FMEA for pneumatic suspensions with the aide of simulation

    - A coupled tank-vehicle-suspension simulation platform that serves as a virtual design and simulation tool for pneumatic suspension development on tank truck applications
- A complete performance evaluation of an innovative pneumatic suspension system (balanced suspension) on truck roll dynamics

1.6 Outline

- Chapter 1 introduces the study and provides the objectives, challenges, approaches, potential contributions from the research, and an outline of the dissertation.
- Chapter 2 gives some background knowledge on pneumatic suspensions, working principles of airsprings and the height control valves, and an overview of previous modeling work on pneumatic suspension systems.
- Chapter 3 discusses the bond graph approach and mathematic model of a pneumatic suspension system.
- Chapter 4 details computer-aided modeling based on the equations of Chapter 3. Experimental validations of the component model and system model are performed.
- Chapter 5 presents a simulation study of the balanced suspension based on a 9-DOF truck dynamic model with detailed suspension pneumatics on the rear tandem axles.
- Chapter 6 evaluates the effect of the balanced suspensions on tractor and trailer combination dynamics by a co-simulation technique.
- Chapter 7 introduces a simulation-based study of Failure Mode and Effect Analysis (FMEA) for the pneumatic suspension.
- Chapter 8 studies benefits of the balanced suspension on roll dynamics of trucks carrying fixed uneven load or liquid.
- Chapter 9 discusses future work this study leaves open for further investigation.

Chapter 2 Background and Literature Review

This chapter gives some background on fundamental knowledge of heavy truck pneumatic suspension systems and discusses the work done by previous researchers on design and modeling of air suspensions. These studies offer suggestions for my present research of modeling and simulation. Firstly, the chapter briefly introduces the historic development of pneumatic suspensions, along with a discussion of working principles and classifications of airspring and leveling valves. Subsequently, an overview of previous studies regarding airspring dynamics and pneumatic suspension design is presented, followed by a summary of previous modeling works on pneumatic suspension systems.

2.1 Background of Heavy Truck Pneumatic Suspension Systems

The first airspring concept, a 'pneumatic spring for vehicles,' was proposed by Willian W. Humphreys in 1901 [12]. However, the airspring was not produced successfully by the U.S. until the 1950s due to the lack of reinforcement material necessary for the development of flexible rubber-fiber components [12]. All original airsprings at that time belonged to the double convolutes, which had only been applied to buses in the U.S. and Europe. Later, the U.S. started to design air systems for heavy trucks to achieve self-leveling suspensions with adjustable air pressure. This application was later applied to cars in subsequent years [13]. Gradually, the double-convoluted airsprings were substituted by rolling lobe designs because of their greater design height and favorable stroke for their application in road chassis. During the last two decades, an innovation occurred for most heavy trucks to replace traditional leaf springs with airsprings as a result of the increasing recognition of the airspring's benefits [5]. By 1996, air suspensions accounted for 36% of all heavy truck suspension systems. Today, the application of pneumatic suspensions on heavy trucks has increased to 75% [14]. The popularity of this heavy truck application is undoubtedly attributed to the advantages of air suspensions compared to leaf springs as described below [15 – 16]:

- Airsprings are designed with lighter weight and reduced structural-borne noise among actors.
- Compared to traditional leaf springs, the stiffness of the airsprings is lower, providing a better ride for both the cargo and the driver.
- The natural frequency of leaf spring suspensions changes as the load varies, while airspring systems can keep a constant natural frequency over a wide range of load conditions. This can be achieved by adjusting the pressure while setting the same airsprings' static height.
- The desired height of air suspensions can be tuned by charging or discharging the airsprings through connecting valve(s) and air supply, whereas the static height of the leaf spring suspensions has to change with the load variation.
- The stiffness of airsprings can be modulated by changing pressure, while traditional leaf springs have constant stiffness.

A typical design mounts the top of the airspring to the truck frame and the bottom to a trailing beam. The other end of the trailing beam is pivoted on the truck frame, as shown in Figure 2-1 (a). The axle is placed around the middle of the trailing arm such that the airspring height changes by 1.5 to 2.0 times the change in the height of the axle [6]. Contrasting the method of mounting airsprings to the tractor, airsprings on the semi-trailer are typically placed directly between the frame and axle, as shown in Figure 2-1 (b). The design height of the airspring on the trailer is lower than the airspring on the tractor due to vertical space limitations.

(a) (b)

Figure 2-1. Pictures of the airsprings installed on the (a) tractor and (b) trailer

2.1.1 Working Principles of Airsprings

The airspring is composed of a flexible member, upper and lower retainers, and a piston, which establishes a sealed pneumatic chamber. The flexible member of the airspring consists of special reinforcing cords sandwiched between rubber membranes to provide strength [17]. The pressure of compressed air is utilized as the force medium for the airspring. The spring stiffness is a non-linear curve defined by the change in effective area and the change in air pressure. The spring stiffness increases with increased supported mass to retain uniform natural frequency [17].

Two typical types of airsprings exist: convoluted bellow and rolling lobe, as presented in Figure 2-2. Figure 2-2 (a) shows an example of a convoluted bellow, which is a double convolute bellow considering the number of convolutions in the flexible member. A girdle ring constrains sections of the flexible member to form the number of convolutions, which can include up to three. The warping portion of the flexible member allows the convoluted airspring to possess a larger stiffness (high natural frequency) and a larger variation of the effective area compared to the other type of airspring [18]. The effective area is a nominal area, generally smaller than the actual cross-sectional area, calculated by dividing the load supported by the internal pressure at any specified height [19]. However, the stroke is limited to a small range, making this type of airspring suitable only for small-deflection applications, such as railway suspensions.

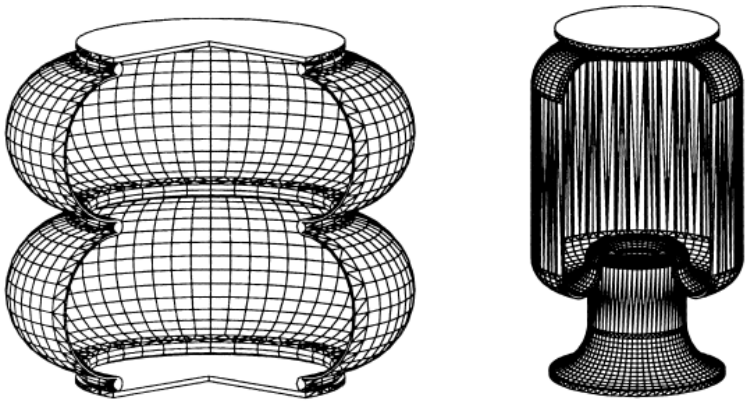

(a) (b)

Figure 2-2. (a) Convoluted bellow and (b) conventional rolling lobe [19]

Currently, heavy truck suspensions typically employ rolling lobe airsprings, as shown in Figure 2-2 (b). This type of airspring includes a piston at the bottom that allows the flexible member to roll along the surface of the piston, providing a relatively large ride height and allowing for a large deflection. Moreover, compared to the convoluted bellow, the rolling lobe possesses modest variation in effective area. For the rolling lobe airspring, research has demonstrated that the variation in the effective area primarily depends on the suspension deflection, rather than internal pressure. As presented in the study by Quaglia and Nieto [19 – 20], the influence of pressure on the effective area is so small that it can be negligible; the effective area can instead be approximated as a function of suspension deflection only. Additionally, the curve of the effective area is different for various types of pistons. Figure 2-3 shows the effect of piston shape on both the effective area and spring force with respect to the spring deflection. Figure 2-3 (a) illustrates the curve on a straight wall piston, most commonly utilized on trucks' airspings. In this case, the effective area changes slightly and increases only in jounce. Therefore, the spring force is mostly determined by the internal pressure. Figure 2-3 (b) shows a back-tapered piston in which the effective area curve varies as a result of the shape of the piston. Figure 2-3 (c) represents a positive-tapered piston where the effective area increases in jounce and decreases in rebound quickly [17].

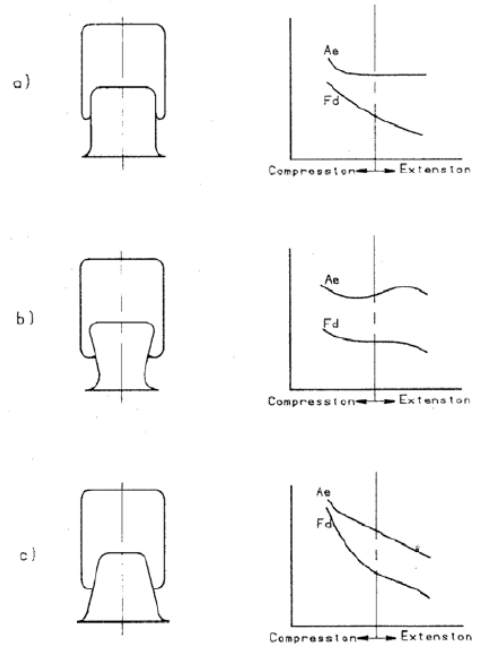

Figure 2-3. Characteristic variation due to piston shapes and flexible member size [18]

2.1.2 Working Principles of Height Control Valves

The air suspension systems on heavy trucks generally utilize height control valve(s) to adjust air volume within the airsprings and the vehicle's set height. The heavy truck's air suspensions most often employ the mechanical height control valve (leveling valve) to achieve self-leveling adjustments, even though the electric control valve is available [21]. Compared to the electric control valve, the leveling valve costs less and has higher reliability. The leveling valve is typically mounted to the vehicle frame with brackets and utilizes a lever arm attached to the axle via a linkage arrangement (control rod), as shown in Figure 2-4. If the truck body moves down due to added loads, the lever arm rotates up, opening the leveling valve for air charging. This allows pressurized air from the air supply to enter the airsprings through the leveling valve to maintain the truck's height as it sinks from the added load. Conversely, if the truck body moves up due to the removal of a load, the lever arm rotates in the opposite direction and activates the leveling valve for air discharging, allowing pressurized air from the airsprings to exhaust out into the atmosphere through the leveling valve [22 – 23].

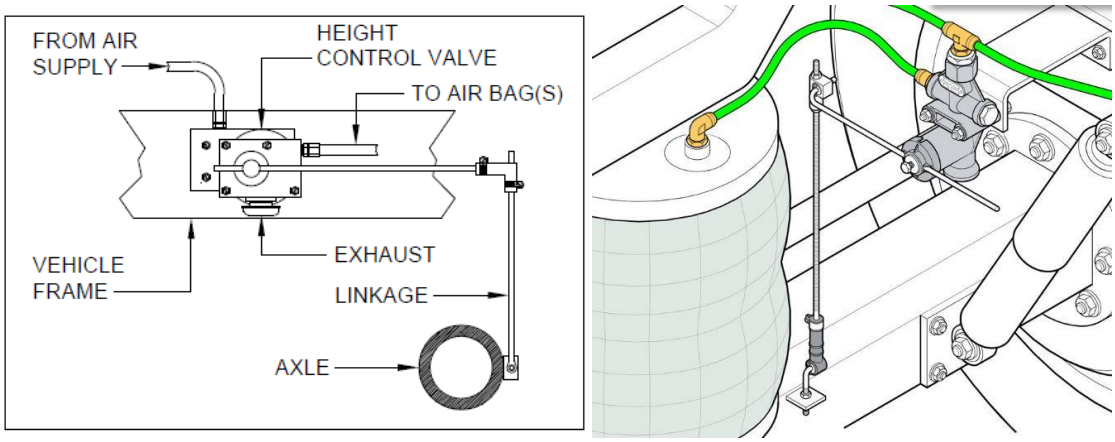

Figure 2-4. Typical height control valve mounting and connection to axle [22]

Three-position, three-port leveling valves are commonly applied to the truck suspension; their pneumatic schematics are shown in Figure 2-5. Port A connects to the airsprings, and ports P and T connect to the air supply and the atmosphere, respectively. The dead band location within the valve prevents airflow for small deflections around the neutral position for the purpose of preventing chattering in high-frequency road excitation. If the

lever arm is rotated down past the dead band, the valve moves to the left position where ports A and T are connected to discharge air out from the airsprings, as shown in Figure 2-5. If the lever arm is pulled up over the dead band, the right position is activated such that ports A and P are connected for charging the airsprings.

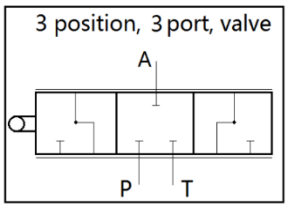

Figure 2-5. Basic pneumatic diagram of a three-port, three-position leveling valve

The leveling valve can be divided into two types: an instant response valve and a delay valve [21]. The instant response valve is able to inflate or deflate the airsprings as soon as the activation lever arm moves. This sort of leveling valve can open for inflation or deflation as the axle chatters vertically, resulting in significiant air consumption and noise. One method of mitigating this problem is to add an extra orifice to the leveling valve to increase the flow resistance. The other method is to enlarge the dead band by increasing the length of the lever arm or changing the installation position [18]. The delay valve, as its name implies, has a slight delay in the reaction of the lever arm rotation due to the elastic characteristics of the control rod and hydraulic damping. This delay action keeps the valve for chattering under high-frequency road excitation, reducing air consumption and saving the valve's lifespan.

2.2 Overview of Pneumatic Suspension Design and Modeling

2.2.1 Non-linear Characteristic Study of Airsprings

Due to the high non-linearities in the stiffness and the hysteresis effects, it is particularly difficult to establish a general model of airsprings. However, for the sake of investigating the dynamics of the air suspension system, it is necessary and significant to develop an analytic model of the airspring that both captures the non-linear characteristics of the airspring and connects to airspring models that control air spring height and stiffness.

The difference between the temperature in the airspring and the ambient temperature gives rise to some heat transfer through the rubber bellow. Some studies have been performed on how the transfer coefficients affect the dynamic performance of airsprings [24] and vehicle dynamics [25]. This research suggests that the assumption of an adiabatic airspring system is valid for short excitations, but it is not reasonable for long-term maneuvers. Currently, a significant amount of research has been carried out to derive an analytic model for an airspring involving its thermodynamic characteristics by applying the energy conservation law. Lee, Hao et al., and Locken et al. [16, 26 – 27] have developed a general analytic model of the airspring on the basis of thermodynamics, and have verified the model through experimentation. Their model revealed that the stiffness depends on volume variation, heat transfer, and variations of air mass and the effective area. The hysteresis primarily is affected by heat transfer and change of effective area. Berg [28] proposed a non-linear model involving the three-dimensional motion of an airspring used for railway vehicles, along with investigation of hysteresis damping caused by friction. He also presented a one-dimensional, non-linear airspring model by integrating elastic, friction, and viscous forces [29]. It is very difficult to accurately define the heat exchange coefficient. In dealing with this problem, Lee [16] suggests that the area of thermal exchange can be calculated from measured geometric data; the heat transfer coefficient is then adjusted through the comparison between simulation and experimental results.

The thermodynamic effects of the airspring have been modeled and studied from the point view of dynamic stiffness by Docquier et al. [30 – 31] and Sayyaadi et al. [32]. Docquier [30] introduced the concept of vertical dynamic stiffness for a better analysis of the bellow-tank system over a wide range of excitation frequencies. The dynamic stiffness is computed as shown in Figure 2-6. The hysteresis effect becomes more obvious while the airspring is interconnected with an auxiliary tank.

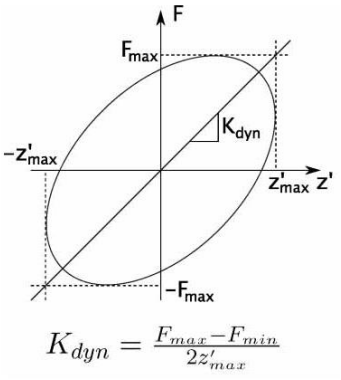

Figure 2-6. Dynamic vertical stiffness of airsprings [31]

When compressing or stretching the airspring, the rubber bellow rolls along the piston and exhibits lateral deformation. The changes of volume and the effective area of the airsprings with respect to height are non-linear, which can be defined experimentally [19 – 20, 33]. Apart from the airspring analytic model, Lee et al., Liu et al., and Bao [34 – 35, 18] applied the method of finite element analysis to study the non-linear stiffness characteristics of the airsprings. These previous studies will be used in studying the non-linear characteristics of the truck airspring analytically and experimentally in this research.

2.2.2 Pneumatic Suspension System Design

The pneumatic suspension system is able to provide an adjustable stiffness, adjustable load-carrying capability, and simplicity of height control. These characteristics allow the vehicle to better adapt to different maneuvers, road roughness, and varied load conditions via active and semi-active pneumatic suspension designs.

For instance, a recent study by Yin et al. has [36] proposed a new pneumatic spring design comprised of a double-acting pneumatic cylinder, as shown in Figure 2-7. It can achieve independent control of stiffness and ride height by adjusting the pressure in each acting chamber individually to better suit road conditions and driver preference. The model of the new pneumatic spring was formulated and corresponding experiments were carried out at different ride heights and chamber pressure settings to verify the new suspension system.

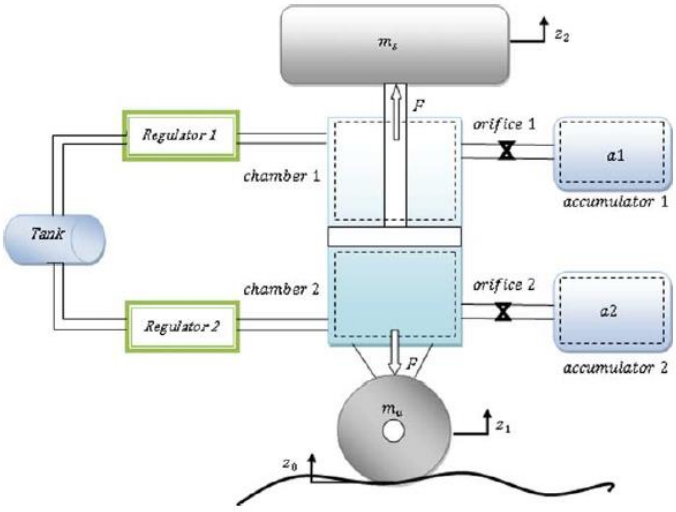

Figure 2-7. Schematics of a quarter car model with the double-acting cylinder suspension [37]

Nieto et al. [37] has proposed and modeled an adaptive vehicle pneumatic suspension system, which can improve ride comfort and handling by changing the diameter of the pipe between the airspring and the auxiliary tank, as shown in Figure 2-8. In his design, a global positioning system (GPS) allowed transmission of road information, which was used to determine which of the plumbing configurations should be activated. There are a number of studies [19 – 20, 38 – 40] done on airspring-tank arrangements, considering the link between the airspring and auxiliary tank via pipe, pipe orifice, or valve. The recent study by Nieto et al. [20] found that, for better vibration isolation, the airspring should use high flow resistance between the airspring and the tank when excitation frequency is lower than the "transition frequency," and low flow resistance when the frequency surpasses that point. The flow resistance can be adjusted by changing pipe diameter, pipe length, or orifice flow area.

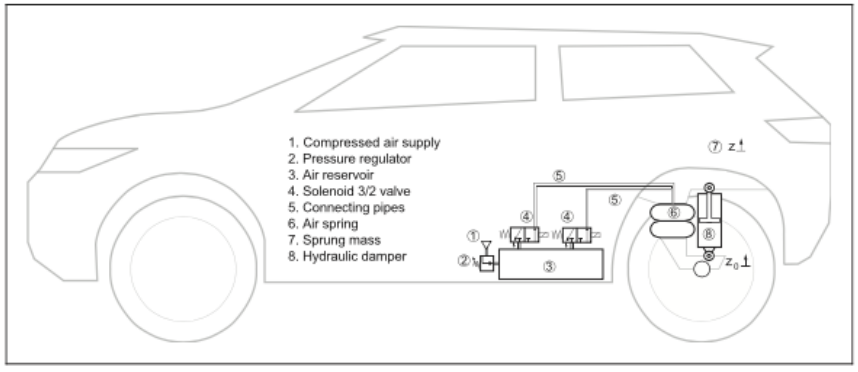

Figure 2-8. Schematics of pneumatic suspension

Additionally, Deo and Suh [41 – 42] have proposed a novel pneumatic automotive suspension system where the airspring stiffness can be changed by varying the volume of the auxiliary tank, as shown in Figure 2-9. Damping can also be adjusted via the on-off valve opening between the airspring and the auxiliary tank. Lambert et al. [6] proposed an increase in the diameter of the air line of longitudinally-connected airsprings on heavy truck dual axles for better dynamic load sharing on the axles.

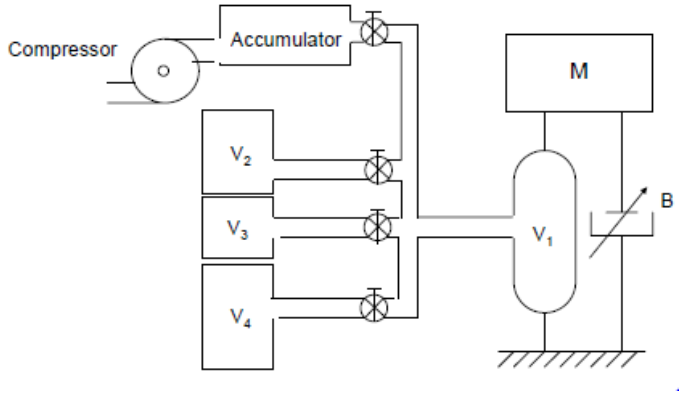

Figure 2-9. Proposed design with multiple auxiliary tanks connected to airspring by on-off valves [41]

2.2.3 Modeling of Pneumatic Suspension Systems

Simulation-based design and analysis reduce the development time and cost of the product and result in prototypes that are much closer to the final product [43]. Computer simulations for vehicle pneumatic suspensions could aid in performance evaluation, further design improvement, test repeatability, and risk prediction. Many studies have been carried out to develop the model of pneumatic suspension systems in order to better understand their dynamic behavior. Different modeling methods can be utilized according to the desired area of study of the suspension. The purpose of this section is to summarize the previous research on pneumatic suspension modeling, which influences the modeling work in this investigation.

Some work has been carried out to substantiate an analytic model of pneumatic suspension systems. Nieto et al. [20] obtained an analytic model of a pneumatic suspension based on an experimental characterization. The non-linear model and its linearized

approximation were defined. Chang and Lu [44] produced a dynamic model of an airspring that accounted for the heat transfer process of the airspring, which was validated by the experimental results. Deo and Suh [41 – 42] derived a thermodynamic model of an airspring connected with multiple auxiliary volumes through the solenoid valve control. However, their study is limited in simulation analysis without the support of experimental results. Xu et al. [45] established a pneumatic suspension model in Simulink to design the electronic ride height control for buses. However, the thermal effects in the pipe and airspring are not taken into account. Robinson et al. [38 – 39] established an analytical model for an airspring-valve-accumulator pneumatic system. The plant model was verified by experimentation and can be used in model-based semi-active control design. Nakajima et al. [46] have developed an air suspension model capturing the high non-linear flow dynamics between the airspring, leveling valves, and differential pressure valves. This behavior is integrated into the multi-body railroad vehicle model to study the effect of different leveling valves on vehicle dynamics. In their pneumatic model, the mass flow rate through the leveling valve is determined by a look-up table of experimental data, allowing for straightforward modeling of the highly non-linear characteristics of the valve. Qi et al. [47] established a pneumatic suspension system model for railway vehicles using AMEsim; the simulation and experimental results were in good agreement. Moshchuk [48] developed a pneumatic suspension model using AMEsim for the comparison study of 4-corners and rear 2-cornering air suspension arrangements. Chen et al. [49] formulated a novel non-linear model for a multi-axle semi-trailer coupled with longitudinally-connected air suspension, but no thermodynamic effect was considered in their airspring model. White [50] has developed a pneumatic suspension model and studied the effect of different leveling valve configurations on the roll stability of a heavy truck. However, there were too many simplifications on modeling the non-linear characteristics of the leveling valve and airspring, including overlooking the effect of pipe plumbing. His study is also limited to the simulation study due to the lack of validation of the pneumatic suspension model.

Co-simulation techniques are favored by many previous modelers to address multi-domain modeling by taking advantage of different software. Qocquier et al. [30 – 31, 51] developed a complete railway pneumatic suspension model containing various pneumatic

components such as tanks, pipes, orifices, and leveling valves in Simulink. The pneumatic model was integrated into a multi-body vehicle model in SimPack to analyze the behavior of the full vehicle. Chang and Lu [44] applied the same co-simulation approach by using Simulink and ADAMS. Kim and Lee [52] proposed a multi-domain simulation that combined an air suspension model, vehicle model, and controller. The air suspension model was developed in AMEsim, where the change in the effective area of the air spring and the effect of the pipe were not considered. Chen [53] entered the co-simulation environment by using AMEsim and CarSim to perform the simulation evaluation of hydro-pneumatic suspensions on different driving conditions. These previous researchers give extensive suggestions on developing a multi-domain model coupling fluid dynamics of pneumatic suspension with the multi-body dynamics of heavy trucks, which are very important for the present investigation.

Chapter 3 Non-linear Mathematical Model of a Pneumatic Suspension System

This chapter describes the development of the fluid dynamic equations of a pneumatic suspension system to be modeled. The ultimate purpose of this chapter is to aid in constructing and verifying the pneumatic suspension model. In this chapter, the pneumatic suspension system is broken down into capacitive and resistive components, followed by the development of the system bond graph. Some assumptions are made for developing the modeling equations. Finally, by applying the principles of fluid dynamics and thermodynamics, mathematic equations of pneumatic suspension components are formulated.

3.1 Introduction

This chapter starts with extracting the flow information of a pneumatic suspension system by the bond graph approach. Firstly, we should clearly distinguish three types of pneumatic elements [54]. The first one is the capacitive element, referring to the volume in which the temperature and the pressure (referred to as effects) are computed from the enthalpy flow and the volume flow rate (referred to as flows) at their ports. Another type of pneumatic element is the resistive element in which the enthalpy flow and volume flow rate are evaluated from the temperature and pressure inputs at their ports. The last one is the ideal source element in which either the flow or the effect is maintained reasonably constant, independent of the supply. The air tank can be assumed as an ideal source element considering that the change in pressure due to charging the airspring is negligible if the tank volume is large enough. Otherwise, the air tank is a capacitive component. Usually three interconnected 10-gallon air tanks are used in the heavy truck to supply air for air suspension and breaking system. In the present investigation, the air tank is modeled as an ideal constant-pressure source. Airsprings and valves are considered as capacitive and resistive components, respectively, as shown in

Figure 3-1. Some pneumatic components such as the pipe may include effects of both the capacitive element and the resistive element.

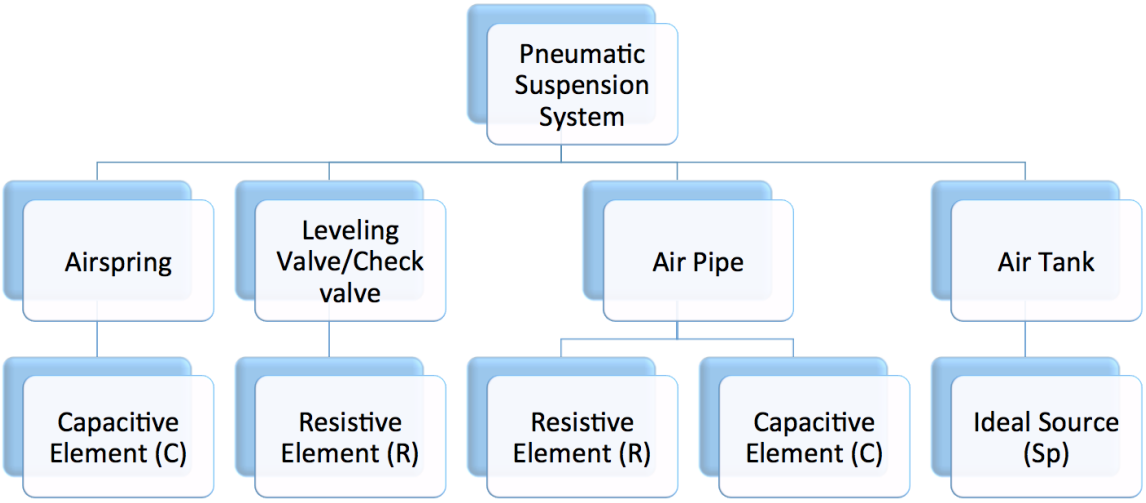

Figure 3-1. Pneumatic suspension system

It is important to note that an aligned pneumatic system model is always built in such a way that an extreme resistive element is always connected to an extreme capacitive element, complying with the causality law of the bond graph approach [54]. As an example in Figure 3-2, a block diagram is drawn from the physical system of one side of the balanced suspension system. The aim of the block diagram is to provide a better understanding of the input and output flows of each component and to assist in developing a bond graph. As can be observed, fluid dynamic systems, thermal dynamic systems, and mechanical systems are coupled in the model. As shown in Figure 3-2, the pipe is modeled in different combinations of resistive and capacitive elements in order to connect different types of components in the pneumatic circuit.

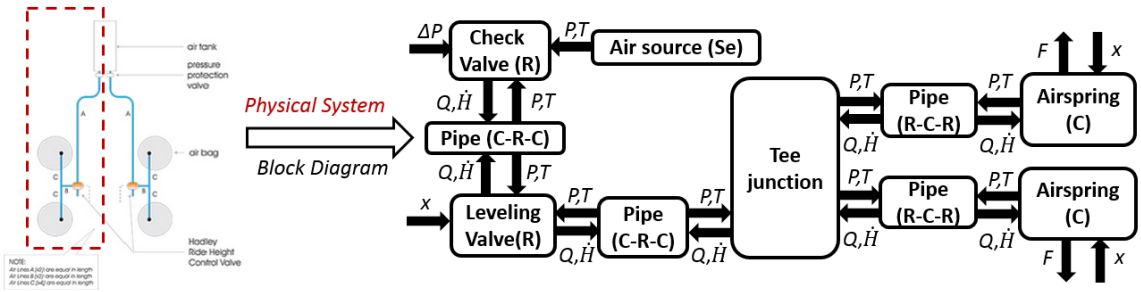

Figure 3-2. Block diagram drawing for one side of the balanced suspension

The bond graph is developed for the suspension subsystem as shown in Figure 3-3, which helps extract equations of motion in a systematic manner and assemble the lumped parameter systems [54]. Due to the non-linear characteristics of the pneumatic component, it is impossible to express the element by linear equations. However, the strokes and junctions help identify the input and output flow, which is desired for mathematic modeling of each component and construction of the system model.

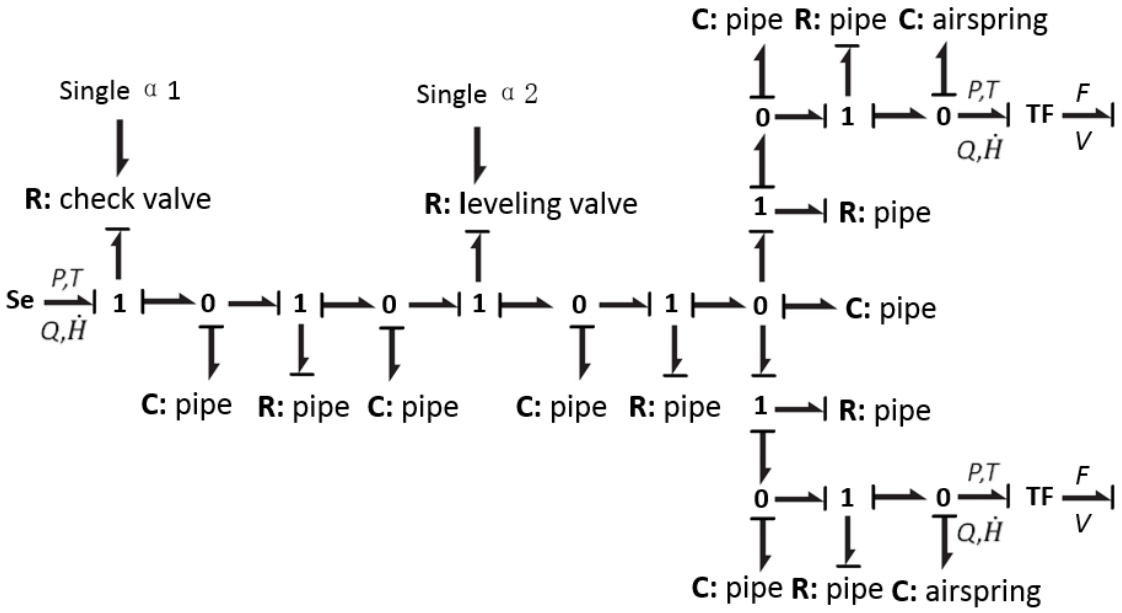

Figure 3-3. Bond graph of a half-balanced suspension

3.2 Mathematical Modeling of a Pneumatic Suspension System

Some assumptions are made for developing the mathematic equations of each component, as listed below:

- The flow is one-dimensional.
- The gas is considered to be a perfect gas with negligible kinetic energy.
- The gravitation and the inertia effect of the gas are assumed to be negligible.
- Pressure and temperature are assumed to be average values and homogeneous throughout the entire volume (airspring and air pipes).
- There is no leakage in the suspension pneumatics.

- The air tank is an ideal air source where pressure and temperature are outputted at constant values regardless of inflow air.
- Friction loss in T- and L-fittings is negligible.
- The thermodynamic parameters of the airspring are constant.

3.2.1 Mathematic Equations of the Airspring Model

The airsprings operate similarly to a pneumatic chamber in which the pressure and the temperature vary due to the airflow and volume variation. The pneumatic chamber works as a non-linear fluid capacitive element with two state variables, pressure and temperature, which are calculated from the inputs of mass variation and volume variation as described in Figure 3-4.

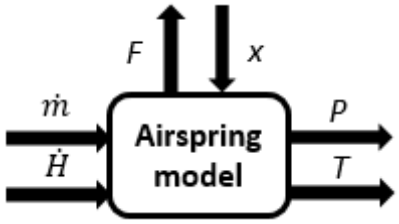

Figure 3-4. Diagram of external variables of the airspring model

In the following paragraph, an approach is introduced to develop the relationship between the input and output variables. By applying the continuity equation, the mass flow rate ($\dot{m}_s$) can be expressed as [16, 26]:

$$\dot{m}_s = \frac{d(\rho_s V_s)}{dt} = \dot{\rho}_s V_s + \rho_s \dot{V}_s \quad (1)$$

where ρ_s represents the air density of the airspring, and V_s is the volume of the airspring. The mass flow rate is positive during inflating of the airspring, and negative while exhausting the air from the airspring. Differentiating the perfect gas equation with respect to time yields an expression of first order differential equation of the air density as:

$$\dot{\rho}_S = \frac{\dot{P}_S}{RT_S} - \frac{P_S \dot{T}_S}{RT_S{}^2} \quad (2)$$

Here, P_s, T_s are, respectively, the pressure and temperature of the airspring, and R is the specific gas constant (universal gas constant divided by the molar mass of the gas). By substituting equation (2) into equation (1), the rate of pressure variation can be explained as:

$$\dot{P}_s = \frac{P_s}{T_s}\dot{T}_s + \frac{RT_s}{V_s}\dot{m}_s - \frac{P_s}{V_s}\dot{V}_s \quad (3)$$

The equation (3) indicates that the pressure variation in the airspring depends on the temperature variation, mass flow rate, and volume variation. Next, using the First Law of Thermodynamics to derive the temperature rate:

$$\dot{U}_s = \dot{m}_s h_{in} + \dot{Q}_s + \dot{W}_s \quad (4)$$

where $\dot{U}_s$ is the internal energy change with respect to time, $\dot{m}_s h_{in}$ is the total enthalpy flow rate into the airspring that is equal to the product of mass flow rate and enthalpy per mass unit at the input port, $\dot{W}_s$ is the time rate of the work supplied by the airspring, and $\dot{Q}_s$ is the heat exchange rate, which can be expressed as:

$$\dot{Q}_s = k_s S_s (T_{ext} - T_s) \quad (5)$$

where k_s is the thermal exchange coefficient, S_s is the thermal exchange area, and T_{ext} is the ambient temperature. The external work done by the airspring ($\dot{W}_s$) due to mechanical displacement can be written by:

$$\dot{W}_s = -P_s \dot{V}_s \quad (6)$$

Since the kinetic and potential energy are ignored, the total energy of the airspring is the same as the internal energy:

$$\dot{U}_s = \frac{d(m_s u_s)}{dt} = u_s \dot{m}_s + m_s \dot{u}_s \quad (7)$$

The internal energy per mass unit can be expressed by $u_s = h_s - P_s v$, where v is the specific volume and h_s is the internal enthalpy per mass unit. Then equation (7) becomes:

$$\dot{U}_s = (h_s - P_s v)\dot{m}_s + m_s \frac{d(h_s - P_s v)}{dt} \quad (8)$$

$$\dot{U}_s = h_s\dot{m}_s + m_s\dot{h}_s - m_s v\dot{P}_s - m_s P_s\dot{v} - \dot{m}_s P_s v \tag{9}$$

$$\dot{U}_s = h_s\dot{m}_s + m_s\dot{h}_s - V_s\dot{P}_s - P_s\dot{V}_s \tag{10}$$

With equations (5), (6), and (10), the energy balance equation (4) can be rewritten as:

$$h_s\dot{m}_s + m_s\dot{h}_s - V_s\dot{P}_s = \dot{m}_s h_{in} + k_{as}S_{as}(T_{ext} - T_s) \tag{11}$$

Due to using the perfect gas, $\dot{h}_s$ can be expressed as:

$$\dot{h}_s = c_p\dot{T}_s = \frac{\gamma R}{\gamma - 1}\dot{T}_s \tag{12}$$

where γ is the specific heat ratio and c_p is the constant-pressure specific heat capacity. Substituting equation (12) into equation (11) yields:

$$\frac{\gamma m_s R}{\gamma - 1}\dot{T}_s - V_s\dot{P} = \dot{m}_s h_{in} - h_s\dot{m}_s + k_{as}S_{as}(T_{ext} - T_s) \tag{13}$$

Substituting equation (3) into equation (13) yields:

$$\left(\frac{\gamma m_s R}{\gamma - 1} - m_s R\right)\dot{T}_s = \dot{m}_s h_{in} - (h_s - RT_s)\dot{m}_s + k_{as}S_{as}(T_{ext} - T_s) - P_s\dot{V}_s \tag{14}$$

Substituting the expression of the enthalpy for perfect gas, $h_s = c_p T_s$, obtains

$$\dot{T}_s = \frac{\gamma - 1}{R m_s}\left[\dot{m}_s h_{in} - \frac{RT_s}{\gamma - 1}\dot{m}_s + k_{as}S_{as}(T_{ext} - T_s) - P_s\dot{V}_s\right] \tag{15}$$

Equation (15) indicates that the temperature variation is associated with four terms, including entering enthalpy, mass variation, heat exchange, and volume variation. The differential equations (3) and (15) fully define the two state variables, pressure and temperature.

The heat exchange term, $k_{as}S_{as}(T_{ext} - T_s)$, in equation (15) can be eliminated when a polytropic process is assumed. The changes in the airspring's volume and effective area are considered to be affected by the height change, which can be obtained experimentally. The force provided by the airspring can be expressed as:

$$F_s = (P - P_{atm})A_e + F_d \tag{16}$$

where F_d is the jounce or rebound force at the suspension travel limit, and A_e is the piston area for the airspring, when the airspring internal bumper is reached in jounce or the rebound limit is reached at full extension. The jounce and rebound limits are assumed to be stiff spring and stiff damper to prevent the airsprings from overextending in either direction. The airspring vertical stiffness can be obtained by differentiating equation (16):

$$K = \frac{dF_s}{dx} = A_e \frac{dP_s}{dx} + (P_s - P_{atm}) \frac{dA_e}{dx} = \frac{A_e \gamma P_s}{m_s} \frac{\dot{m}_s}{\dot{x}} + \frac{A_e(\gamma-1)k_{as}S_{as}}{V_s \dot{x}} \left(T_{ext} - \frac{V_s P_s}{R m_s}\right) - \frac{A_e \gamma P_s}{V_s} \frac{dV_s}{dx} + (P_s - P_{atm}) \frac{dA_e}{dx} \tag{17}$$

Equation (17) indicates that the airspring stiffness is affected by volume variation, heat transfer, and mass variation. Positive mass flow rate increases the stiffness while feeding air to the airspring, whereas negative mass flow rate by exhausting the airspring, decreases it.

3.2.2 Mathematic Equations of the Valve Model

In the modeling, the leveling valve in the pneumatic system, which is analogic to the resistor in the electric circuit, belongs to a resistive component, as shown in Figure 3-5. The flow characteristics of the leveling valve can be simulated by an orifice model with variable area. It is assumed that the orifice model always remains in an equilibrium state to immediately output airflow rate and enthalpy flow rate once it obtains the inputs of pressure and temperature.

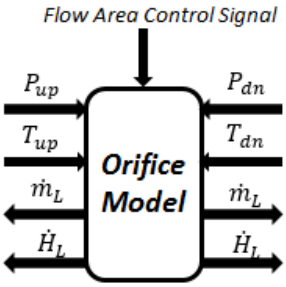

Figure 3-5. Diagram of external variables of the orifice model

To derive the flow equation for the orifice, it needs to start with the energy equation for an open system as [55]:

$$\Delta E = m_{Lin}h_{Lin} + \frac{1}{2}m_{Lin}{u_{Lin}}^2 + m_{Lin}gz_{Lin} + Q_{Lexc} - (m_{Lt}h_{Lt} + \frac{1}{2}m_{Lt}{u_{Lt}}^2 + m_{Lt}gz_{Lt} + W_{Lt}) \quad (18)$$

where

$m_{Lin}h_{Lin}$ is the enthalpy of inflow

$\frac{1}{2}m_{Lin}{u_{Lin}}^2$ is the flow-in kinetic energy of the inflow

$m_{Lin}gz_{Lin}$ is the potential energy of the inflow

Q_{Lexc} is the heat exchange

$m_{Lt}h_{Lt}$ is the enthalpy of outflow

$\frac{1}{2}m_{Lt}{u_{Lt}}^2$ is the flow-in kinetic energy of outflow

$m_{Lt}gz_{Lt}$ is the potential energy of outflow

W_{Lt} is the work supplied by the system

The air's potential energy is neglected because it is much smaller than the other factors. Here the state variable is considered to be independent of time ($\Delta E = 0$) and the inflow mass is equal to the outflow mass. For unit gas, equation (18) then becomes:

$$q_{Lexc} = h_{Lin} - h_{Lt} + \frac{1}{2}{u_{Lin}}^2 - \frac{1}{2}{u_{Lt}}^2 + w_{Lt} \quad (19)$$

Because there is no heat exchange and work supplied in the system, equation (19) can be simplified as:

$$h_{Lin} - h_{Lt} + \frac{1}{2}{u_{Lin}}^2 - \frac{1}{2}{u_{Lt}}^2 = 0 \quad (20)$$

Figure 3-6 shows the air exhaust of a large tank through a small orifice. It is assumed that P_{Lin}, T_{Lin} are constant. P_{Lt} and A_L are the pressure at the exhaust port and the flow area of the orifice, respectively, and P_b is the external pressure. By using $h = c_p T = \frac{\gamma R}{\gamma - 1} T$, equation (20) can be rewritten as:

$$\frac{\gamma R}{\gamma - 1} T_{Lin} - \frac{\gamma R}{\gamma - 1} T_{Lt} - \frac{{u_{Lt}}^2}{2} = 0 \tag{21}$$

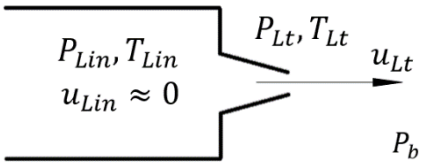

Figure 3-6. Schematic of air exhaust through a small orifice

Substituting the temperature of equation (21) with the perfect gas equation yields the expression of flow rate at the output port,

$$u_{Lt} = \sqrt{\frac{2\gamma}{\gamma - 1} \frac{P_{Lin}}{\rho_{Lin}} \left(1 - \frac{\rho_{Lin} P_{Lt}}{\rho_{Lt} P_{lin}}\right)} \tag{22}$$

With the assumption of isentropic flow, equation (22) can be written as:

$$u_{Lt} = \sqrt{\frac{2\gamma}{\gamma - 1} R T_{Lin} \left[1 - \left(\frac{P_{Lt}}{P_{Lin}}\right)^{\frac{\gamma - 1}{\gamma}}\right]} \tag{23}$$

The mass flow rate through the orifice can be computed as:

$$\dot{m}_{Lt} = \rho_{Lt} u_{Lt} A_L = \frac{\rho_{Lt}}{\rho_{Lin}} \rho_{Lin} A_L \sqrt{\frac{2\gamma}{\gamma - 1} R T_{Lin} \left[1 - \left(\frac{P_{Lt}}{P_{Lin}}\right)^{\frac{\gamma - 1}{\gamma}}\right]}$$

$$= P_{Lin} A_L \sqrt{\frac{2\gamma}{\gamma - 1} \frac{1}{R T_{Lin}} \left[\left(\frac{P_{Lt}}{P_{Lin}}\right)^{\frac{2}{\gamma}} - \left(\frac{P_{Lt}}{P_{Lin}}\right)^{\frac{\gamma + 1}{\gamma}}\right]} \tag{24}$$

If T_{Lin} , P_{Lin} are constant, it is found that $\dot{m}_{Lt}$ is a function of $\frac{P_{Lt}}{P_{Lin}}$. Solving the equation $\frac{d\dot{m}_{Lt}}{d(\frac{P_{Lt}}{P_{Lin}})} = 0$ obtains $\frac{P_{Lt}}{P_{Lin}} = \left(\frac{2}{\gamma+1}\right)^{\frac{\gamma}{\gamma-1}}$. This means that, while $\frac{P_{Lt}}{P_{Lin}} = \left(\frac{2}{\gamma+1}\right)^{\frac{\gamma}{\gamma-1}}$, the mass flow rate hit the maximum point. Substituting $\frac{P_{Lt}}{P_{Lin}} = \left(\frac{2}{\gamma+1}\right)^{\frac{\gamma}{\gamma-1}}$ into equation (24) yields:

$$\dot{m}_{Lt} = P_{Lin}A_L\sqrt{\frac{2\gamma}{RT_{Lin}(\gamma+1)}}\left(\frac{2}{\gamma+1}\right)^{\frac{1}{\gamma-1}} \tag{25}$$

If we decrease the external pressure P_b from $P_b = P_{Lt} = \left(\frac{2}{\gamma+1}\right)^{\frac{\gamma}{\gamma-1}} P_{Lin}$, there is no effect on the air flow through the orifice because the fluctuation caused by the pressure variation of P_b transmits at the sound speed, while the air is also flowing through the orifice in the sound speed. Therefore, the mass flow rate through an orifice is defined as a function of upstream pressure and downstream pressure and the flow area of the orifice, which can be expressed as [5]:

$$\dot{m}_{Lt} = A_L C_q P_{Lin}\sqrt{\frac{2\cdot\gamma}{R\cdot T_{Lin}(\gamma+1)}}\left(\frac{2}{\gamma+1}\right)^{\frac{1}{\gamma-1}} \qquad \left[\frac{p_{Lt}}{p_{Lin}} \le \left(\frac{2}{\gamma+1}\right)^{\frac{\gamma}{\gamma-1}}\right] \tag{26}$$

$$\dot{m}_{Lt} = A_L C_q P_{Lin}\sqrt{\frac{2\cdot\gamma}{R\cdot T_{Lin}(\gamma-1)}}\sqrt{\left(\frac{P_{Lt}}{P_{Lin}}\right)^{\frac{2}{\gamma}} - \left(\frac{P_{Lt}}{P_{Lin}}\right)^{\frac{\gamma+1}{\gamma}}} \qquad \left[\frac{p_{Lt}}{p_{Lin}} > \left(\frac{2}{\gamma+1}\right)^{\frac{\gamma}{\gamma-1}}\right] \tag{27}$$

Here, C_q is the flow coefficient, adjusting the theoretical result to be equal to the experiment. This adjustment includes the extra losses resulting from local friction, and the losses of kinetic energy. There are two approximations of C_q consisting of taking it as a constant value and assuming it as a polynomial function of the pressure ratio. The latter hypothesis is generally used for sharp-edge orifice, and the flow coefficient is the polynomial function of the pressure ratio as [56]:

$$C_q = \left[\left\{\left[\left(-1.6827\frac{P_{Lt}}{P_{Lin}} + 4.6\right)\frac{P_{Lt}}{P_{Lin}} - 3.9\right]\frac{P_{Lt}}{P_{Lin}} + 0.8415\right\}\frac{P_{Lt}}{P_{Lin}} - 0.1\right]\frac{P_{Lt}}{P_{Lin}} + 0.8414 \tag{28}$$

As given in equations (26) and (27), A_L is the geometric area of the orifice, which is considered to be the flow area in modeling the leveling valve. The value of the flow area is directly related to lever arm rotation caused by the suspension's deflection. The function of

the flow area with respect to suspension displacement can be obtained by experiments. The other output of the leveling valve model is the enthalpy flow rate expressed as follows:

$$\dot{H}_{Lt} = \dot{m}_{Lt} \cdot h_{Lin} \tag{29}$$

Additionally, the check valve is modeled by equations (26), (27), and (28). The flow area is a function of upstream and downstream pressure difference as follows:

$$\begin{cases} A_L = Flow\ area\ of\ the\ check\ valve & P_{Lin} - P_{Lt} - P_{crack} \geq 0 \\ A_L = 0 & P_{Lin} - P_{Lt} - P_{crack} < 0 \end{cases} \tag{30}$$

where P_{crack} is the cracking pressure, here settto be zero.

3.2.3 Mathematic Equations of the Pipe Model

The viscosity and the compressibility of the gas are the important factors influencing the fluid transient behavior in pipes. The dissipative effect can cause a pressure drop along the pipe. The effect of the compressibility of the gas results in an attenuation of the flow at the outlet of the pipe. In this model, the two effects are included by a manner of combining the resistant element (R) and the capacitive element (C). All three types of arrangements are shown in Figure 3-7, depending on the causality requirement of the pneumatic circuit.

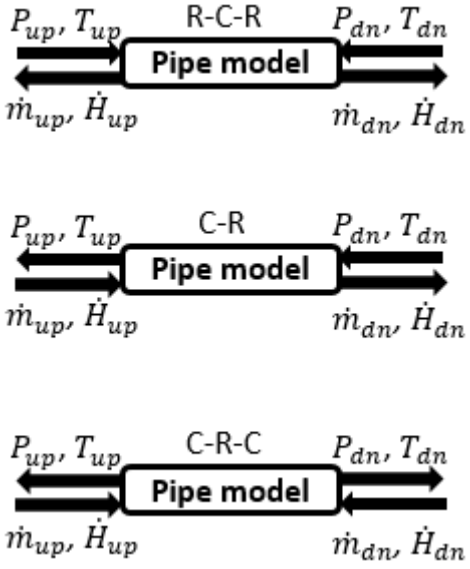

Figure 3-7. Diagram of external variables of the pipe model

For modeling the dissipative effect of the resistant element, the Darcy-Weisbach equation is employed to calculate the mean gas velocity from the pressure input for a straight pipe of a constant sectional area:

$$\mathrm{v} = \sqrt{\frac{2 \cdot D \cdot |\Delta P|}{l \cdot \rho \cdot ff}} \tag{31}$$

where ff is the friction factor, D is the inner diameter, and l is the length of flow segment. The Reynolds number is computed by:

$$Re = \frac{\mathrm{v} D}{v_p} \tag{32}$$

where v_p is the kinematic viscosity of the gas. When the flow is laminar ($\mathrm{Re} < 2500$), the friction factor ff can be computed as the following:

$$ff = \frac{64}{Re} \tag{33}$$

Extending the analysis for the wholly turbulent flow ($\mathrm{Re} \geq 2500$), the friction factor ff is extracted from the Nikuradse harp [57]$\mathrm{ff} = \frac{0.361}{\mathrm{Re}^{0.25}} = 0.361 \frac{\mathrm{v}}{\mathrm{vD}}^{0.25}$. During the transition phase between laminar flow and turbulent flow, the friction factor depends on both Reynolds number and relative roughness. The relative roughness is calculated by:

$$\mathrm{rr} = \frac{\Delta}{D} \tag{34}$$

Here, Δ is the absolute roughness which depends on the pipe material. With the value of the friction factor, the mass flow rate of the pipe resistant element in the round section is calculated according to an equivalent orifice model [56]:

$$\dot{m}_p = \pi \left(\frac{D}{2}\right)^2 \sqrt{\frac{D}{l \cdot ff}} P_{up} \sqrt{\frac{2 \cdot \gamma}{R \cdot T_{up} \cdot (\gamma + 1)}} \left(\frac{2}{\gamma + 1}\right)^{\frac{1}{\gamma - 1}} \qquad \left[\frac{p_{dn}}{p_{up}} \leq \left(\frac{2}{\gamma + 1}\right)^{\frac{\gamma}{\gamma - 1}}\right] \tag{35}$$

$$\dot{m}_p = \pi \left(\frac{D}{2}\right)^2 \sqrt{\frac{D}{l \cdot ff}} P_{up} \sqrt{\frac{2 \cdot \gamma}{R \cdot T_{up} \cdot (\gamma - 1)}} \sqrt{\left(\frac{P_{dn}}{P_{up}}\right)^{\frac{2}{\gamma}} - \left(\frac{P_{dn}}{P_{up}}\right)^{\frac{\gamma + 1}{\gamma}}} \qquad \left[\frac{p_{dn}}{p_{up}} > \left(\frac{2}{\gamma + 1}\right)^{\frac{\gamma}{\gamma - 1}}\right] \tag{36}$$

Due to the lack of data concerning thermal exchange, the capacitive element of the pipe is developed with polytropic law. Due to the fixed volume and ideal gas relation, equation (3) can be rewritten as follows:

$$\dot{P}_p = \frac{P_p}{T_p} \dot{T}_p + \frac{P_p}{m_p} \dot{m}_p \tag{37}$$

With the polytropic hypothesis and perfect gas law, we have:

$$P_p^{k-1} T_p^{k} = constant \quad (38)$$

k is the polytropic coefficient. By differentiating the previous equations, the temperature expression is obtained as:

$$\dot{T}_p = \frac{(k-1)T_p \dot{P}_p}{kP_p} \quad (39)$$

Substituting equation (39) into equation (37) yields the pressure derivative as:

$$\dot{P}_p = \frac{kP_p}{m_p} \dot{m}_p \quad (40)$$

3.2.4 Mathematic Equation of the Tee-junction Model

The Tee-junction model is idealized for no energy loss, which is functionally equal to the 0 junction in the bond graph, as shown in Figure 3-8. Pressure and temperature are fixed by port 2, which leads to

$$P_1 = P_3 = P_2, T_1 = T_3 = T_2 \quad (41)$$

Mass flow and enthalpy flow at port 2 are calculated by summing the flows through the other two ports as:

$$\dot{m}_2 = \dot{m}_1 + \dot{m}_3, \dot{H}_2 = \dot{H}_1 + \dot{H}_3 \quad (42)$$

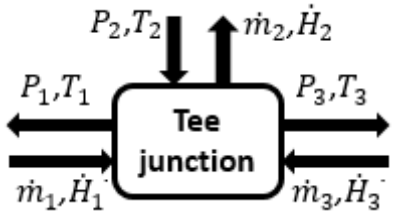

Figure 3-8. Diagram of external variables of the Tee-junction model

The air tank is considered to be a constant air supply, where pressure and temperature are ideally outputted at constant values regardless of inflow of air, as shown in Figure 3-9.

Figure 3-9. Diagram of external variables of pressure source model

Chapter 4 Modeling and Validation of the Pneumatic Suspension

This chapter is devoted to construct and analyze the non-linear analytical models of the pneumatic suspension component and system. The chapter provides an insight and deeper understanding of the pneumatic suspension dynamics to be investigated. The pneumatic suspension is broken down into components including airspring, leveling valve, and pipe, each of which is modeled by AMEsim according to mathematic equations developed in chapter 3. The airspring model is validated against the Simulink model and experimental data. The flow characteristics of the leveling valve are also verified by experimental results. The dissipative and compressive effects of the pipe model are examined by simulation. The pneumatic suspension system model is then established by aligning the verified component models. Truck rear-axles suspension tests are conducted to provide verification for pneumatic suspension system model. This chapter concludes that the developed pneumatic suspension model can be coupled with vehicle dynamics for the study and evaluation of the pneumatic suspension performance, which will be introduced in next chapter.

4.1 Introduction

Software named LMS Imagine.Lab AMEsim is used to perform the modeling of the pneumatic suspension. AMEsim is mechatronic simulation software that allows engineers to model, simulate, and analyze a multi-domain controlled system. It can provide an integrated simulation platform to accurately predict the multidisciplinary performance of intelligent systems. Numerous AMEsim physical domain libraries exist, such as fluids, thermodynamics, electrics, mechanics, and signal processing. As mentioned in the literature review in chapter 2, many researchers have utilized AMEsim to simulate the pneumatic suspension system since it possesses powerful and validated libraries filled with dedicated pneumatic models to allow engineers to easily create the pneumatic system model in reduced

time and to solve a more complex problem covering multiple physical domains. Several libraries of AMEsim, including mechanical, pneumatic, pneumatic component design, and signal processing are applied to the modeling work in this investigation.

4.2 Airspring Modeling Description

4.2.1 Development of the Airspring Model

There is no existing airspring model available in the pneumatic library of AMEsim. Many previous modelers [48, 52] simulated the pneumatic characteristics of the airspring by the pneumatic cylinder model in the AMEsim pneumatic library. Their models fail to accureately capture the non-linear characteristics of the airspring due to lack of assurance on the effective area change and the volume change.

In this section, a novel and advanced airspring model is developed in AMEsim as shown in Figure 4-1. This model is able to accurately capture effects of effective area variation and the volume change based on experimental data. Two lookup tables (function blocks) are included to interpolate the functions of effective area and volume relative to height. As shown in Figure 4-1, the proposed airspring model is comprised of three subsystems. The first subsystem is shown in the top purple frame. One purpose of the subsystem is to calculate the volume difference between a desired value in a lookup table (function block of airspring volume) and the pneumatic piston model with moving body, which is then sent to a normal pneumatic piston model. The other purpose of the subsystem model is to output the value of effective area by the other lookup table (function block of effective area) in order to calculate airspring force. The second subsystem consists of a pneumatic piston with moving body, a normal pneumatic piston, and a pneumatic chamber, as shown in the brown frame of Figure 4-1. The pneumatic piston with moving body can output volume variation resulting from the displacement excitations on the top and bottom of the airspring. Here, a normal pneumatic piston is added to compensate for the volume difference between the pneumatic piston with moving body and the desired value provided by the lookup table. The two pneumatic pistons separately feed the volume data to a

pneumatic chamber where the volumes of the two pneumatic pistons are added. At Port 2 of the pneumatic chamber connected to the leveling system, the mass flow rate and enthalpy flow are inputted. Based on the information of volume variation and flows, the pneumatic chamber model is in charge of calculating pressure and temperature using equations (3) and (15). The third subsystem is shown in the bottom orange frame of Figure 4-1. This subsystem is used to obtain the airspring force by multiplying the pressure and the effective area as given in equation (16). The airspring forces are equally and separately transmitted to the vehicle body (sprung mass) and axles (unsprung mass) through the mechanical connectors of the AMEsim mechanics library. An extra mechanical connector is used in order to reverse the sign of airspring forces transmitted to the sprung mass (vehicle body). An elastic double end-stop model with a set of stiff springs and dampers simulates the emergency rubber to prevent the airspring from overextending in either direction. The clearance at each port of the double end-stop model is defined according to the maximum allowable stroke of the airspring.

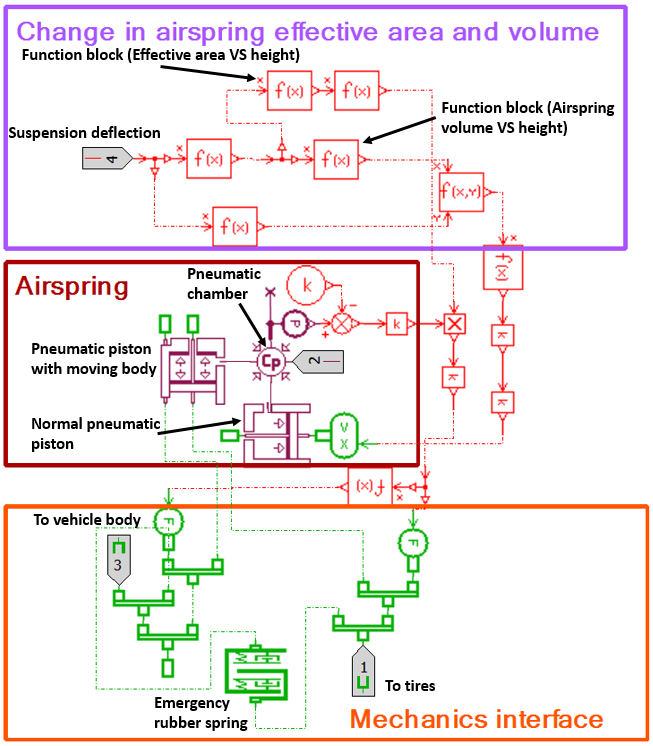

Figure 4-1. Model of airspring in AMEsim

4.2.2 Test-based Determinations of Effective Area Change and Volume Variation

The airspring on the semi-tractor is manufactured by Volvo (model number 556-24-3-110.) Due to proprietary considerations, the supplier does not provide any related information about the changes of effective area and volume that are necessary for modeling the airspring. Therefore, tests are carried out to determine and establish the needed relationship for these properties.

For the test of effective area variation, the truck airspring was fixed in a shock dynamometer (Roehrig EMA 2k dynamometer), which can create different axial excitation patterns, as shown in Figure 4-2. The airspring initially was set at 15 in. The test input was to compress the airspring from 15 to 8.5 in, while holding position for 12 s in 0.5-in increments. During the holding position, the airspring pressure was manually adjusted to test the required valve by means of a pressure control valve (leveling valve). A pressure sensor, which was calibrated by a high-accuracy pressure gauge (NIST-certificated), was mounted at the pneumatic port of the airspring to monitor pressure variations. The sensor outputs voltage data corresponding to the pressure, which consistently was collected and monitored by computer with QuickDAQ. A pancake load cell was used to record the airspring force. The test was performed at three constant pressures: 10 psi, 15 psi, and 20 psi. The maximum testing pressure cannot go over 20 psi for safety concerns, considering that the maximum force allowed by the Roehrig is 2000 lbf.

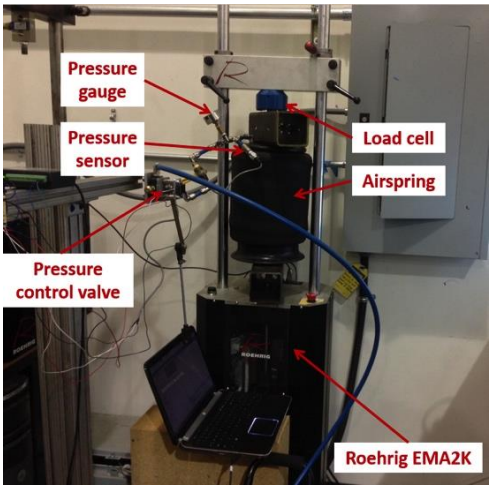

Figure 4-2. Test for airspring effective area

Figure 4-3 shows testing results of airspring force at different heights represented by markers fitted by a cubic trend line. The effective area is obtained by dividing the exerted force by the testing pressure. Figure 4-4 shows the change of effective area versus height at three different initial pressures. When the deflection changes around the design height (11 inches, which is measured on the tractor), the effective area is nearly independent of pressure. The function of the average cubic trend line is used for the airspring modeling, as expressed by:

$$A_e = -0.1263h^3 + 4.8003h^2 - 60.7041h + 323.9090 \quad (43)$$

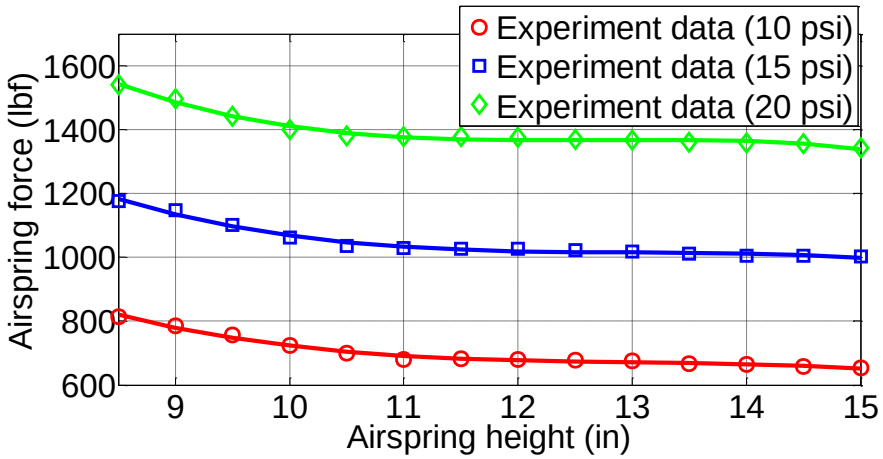

Figure 4-3. Experimental results of airspring force versus height for 10 psi, 15 psi, and 20 psi (airspring model: Volvo 556-24-3-110)

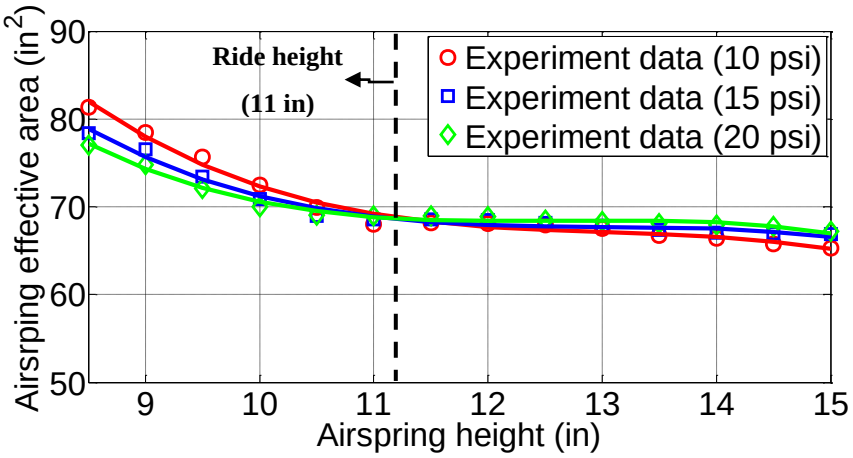

Figure 4-4. Experimental results of airspring effective area versus height for 10 psi, 15 psi, and 20 psi (airspring model: Volvo 556-24-3-110)

The effect of volume variation was explored by measuring the water-filled airspring at different heights while subjected to a static load. Firstly, as shown in Figure 4-5 (a), the airspring was stretched to 18 in height by the hoist and fully filled with water. The total consumption of water was recorded as 1074 in^3 (17600 ml). Subsequently, the airspring with water was placed on the test bench, as shown in Figure 4-5 (b). The lower end of the airspring was fixed on a steel plate, while the upper end was connected to the pallet only with a vertical degree of freedom.

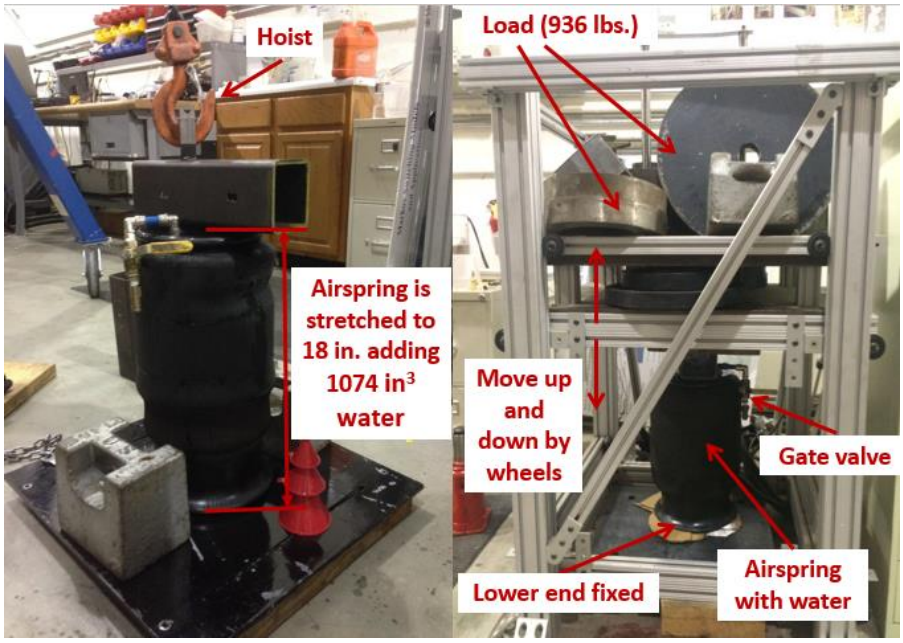

(a) (b)

Figure 4-5. Airspring volume testing: (a) fully filling the airspring with water and (b) measuring the airspring height sunject to a constant load

The testing bench allowed the 936-lbf force to act on the airspring vertically in order to make the rubber fully expand bellow for better estimation of the volume of the airspring. A certain amount of water was dumped out by opening the gate valve, while the airspring's height was measured under the static load, as shown in Figure 4-6 (a). The volume at the height was calculated based on the amount of water inside the bag. The process was repeated until the bumper of the airspring was touched. For safety concerns, a hydraulic jack needed to be placed underneath the pallet while discharging the water, as shown in Figure 4-6 (b). The process was repeated until the bumper of the airspring was touched.

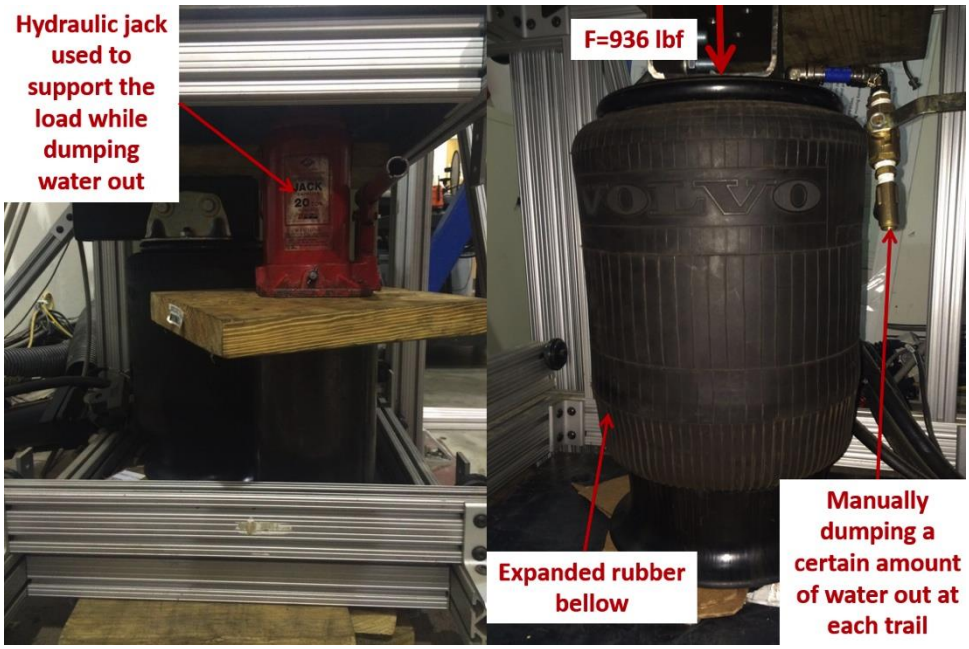

(a) (b)

Figure 4-6. Airspring volume testing: (a) hydraulic jack and (b) airspring

The results of the airspring volume testing are summarized in Table 4-1. About 30 in^3 (492 ml) of water is discharged from the airspring for each test. The airspring volume is calculated by subtracting the value of the previous test by the amount of discharged water.

Table 4-1. Test data of the airspring volume with different heights

Test #	Measured Water Discharge (in^3)	Calculated Airspring Volume (in^3)	Measured Airspring Height (in)	Test #	Measured Water Discharge (in^3)	Calculated Airspring Volume (in^3)	Measured Airspring Height (in)
1	0	1074.017	16.5	**12**	29.90161	734.7253	11.5
2	30.51185	1043.505	16	**13**	30.51185	704.2135	11
3	31.12209	1012.383	15.5	**14**	31.12209	673.0914	10.5
4	31.73232	980.6509	15	**15**	31.73232	641.3591	10.15
5	31.73232	948.9185	14.5	**16**	32.64768	608.7114	9.6
6	30.51185	918.4067	14	**17**	32.34256	576.3688	9.2
7	32.9528	885.4539	13.5	**18**	31.42721	544.9416	8.75
8	29.29138	856.1625	13.1	**19**	30.51185	514.4298	8.3
9	30.51185	825.6507	12.65	**20**	33.56304	480.8668	8
10	30.51185	795.1388	12.25	**21**	52.48038	428.3864	7.6
11	30.51185	764.627	11.75				

Figure 4-7 shows the curve of the airspring volume versus height obtained based on Table 4-1. The bumper is touched at 7.6 in. The volume changes more rapidly when the height is less than 8.3 in because the tapered bottom of the piston takes effect. Previous studies have indicated that the variation of the airspring volume is mainly dependent of airspring height rather than pressure. The fitting line plot is used to represent the volume variation in the airspring model:

$$V_s = -1.2077h^2 + 99.5938h - 241.0951 \quad (44)$$

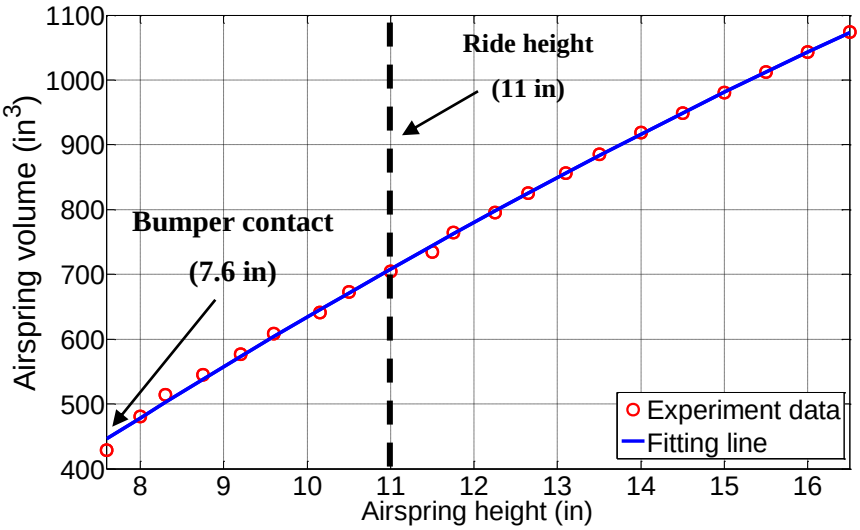

Figure 4-7. Experimental results of airspring volume versus height (airspring model: Volvo 556-24-3-110)

For the airsprings equipped on the trailer, they have different curves of effective area change and volume variation that can be determined by data provided by the manufacturer as shown in Figure A-1 and Figure A-2.

4.2.3 Validation of the Airspring Model with Simulink Model

A simulation "testing bench" is established in AMEsim, as depicted in Figure 4-8, to verify and analyze the dynamics of the airspring model. Inputting either displacement or force is allowed from the top of the airspring while the bottom is fixed. The perfect gas law is applied in the simulation. The parameters used in the simulation are shown in Table 4-2.

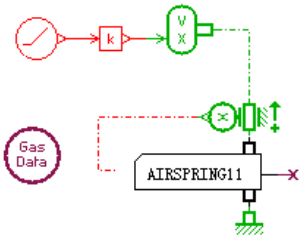

Figure 4-8. Model used for validation of the airspring model

Table 4-2. Parameters used in testing the airspring

Parameter	Value(English unit)	Value(SI unit)
Initial effective area of airspring, A_0	75 in^2	0.0484m^2
Initial height of airspring (tractor)	10.5 in	0.2667 m
Initial pressure of airspring	70 psi	482633 pa
Atmospheric pressure, Pa	14.7 psi	101300 pa
Initial temperature of airspring	68 F^0	293.15 K
External temperature T_{ext}	68 F^0	293.15 K
Gas constant R	287 J·K/kg	287 J·K/kg
Specific heat ratio γ	1.38	1.38

For verifying the AMEsim model, another airspring model is developed by using Matlab/Simulink based on equations (3) and (15), as shown in Figure 4-9.

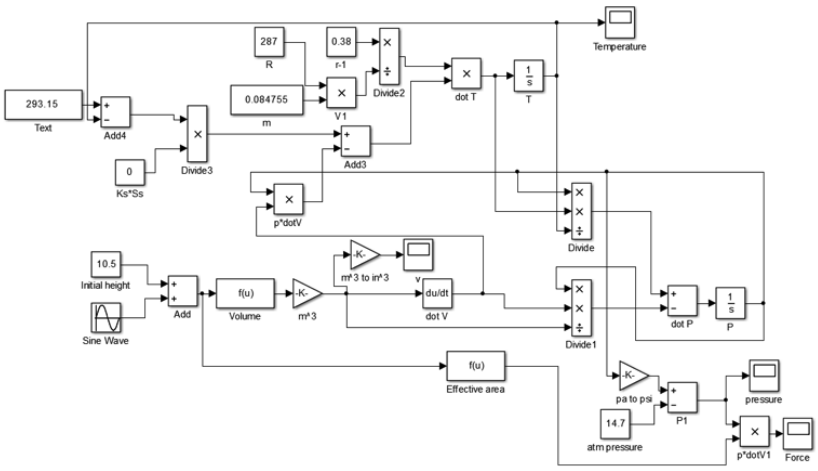

Figure 4-9. Airspring model in Matlab/Simulink

Figure 4-10 presents comparison results between the two airspring models for pressure, temperature, force, and volume submitted to a 0.25-Hz sinusoidal displacement excitation with an amplitude of 1 in. Good agreement is obtained between the two models, indicating that the non-linear characteristics of the airspring model in AMEsim are in line with equations (3) and (15).

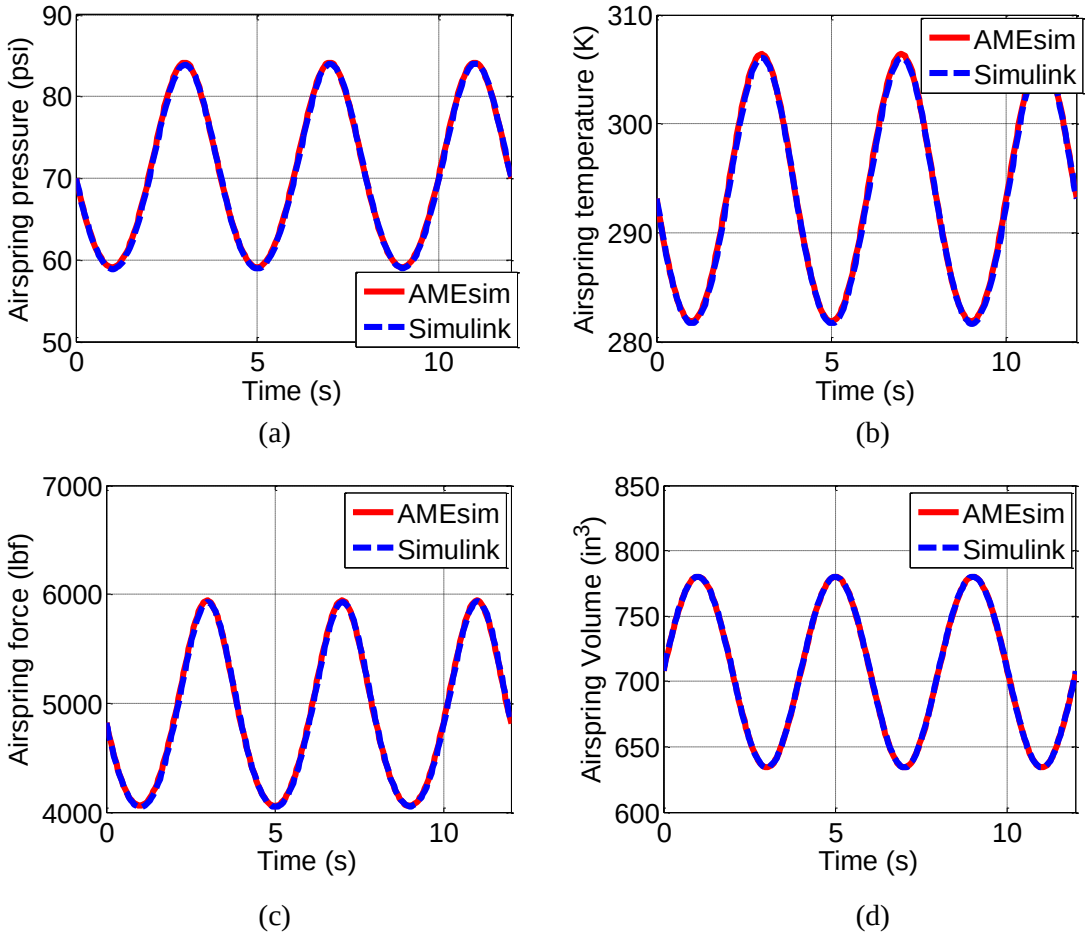

Figure 4-10. Comparison results of airspring pressure, temperature, force, and volume sujected to a 1-inch sinusoidal excitation at 0.25 Hz

4.2.4 Validation of the Airspring Model with Experimental Results

As shown in equation (15), the heat exchange between the pneumatic chambers (bellows and tanks) and the atmosphere is considered by the expression $k_{as}S_{as}(T_{ext} - T_s)$. The key point is to estimate the heat transfer coefficient $k_{as}S_{as}$. A null value of the heat transfer coefficient

corresponds to the adiabatic process, whereas an infinite value represents the isothermic process. In the present work, the area of thermal exchange is calculated from measured geometric data of the airspring, and the heat transfer coefficient is then adjusted through the comparison between simulation and experimental results. The heat transfer coefficient is finally set to be 2 W/K based on the experimental data.

Figure 4-11 shows the simulation and experiment results of airspring force versus the vertical displacement for a 1-inch sinusoidal motion excitation at 0.1 Hz, 0.5Hz, and 1 Hz. The 0.1 Hz and 1 Hz are shifted 200 lb. higher and lower than the actual value for better distinguishing the different data. The initial pressure of the airspring is 10 psi. The comparison between the simulated and the experimental results confirm the validity of the airspring model.

It can be observed from Figure 4-11 that the magnitude of the hysteresis in airspring force decreases as the frequency of the input increases from 0.1 Hz to 1 Hz. The variation of magnitude of the hysteresis can be explained by the following equation, which is derived by combining equations (3) and (15):

$$\dot{F}_s = \frac{\gamma A P_s}{m_s}\dot{m}_s + \frac{(\gamma-1)Ak_{as}S_{as}}{V_s}\left(T_{ext} - \frac{V_s P_s}{R m_s}\right) - \frac{\gamma P_s A}{V_s}\dot{V}_s + P_s\dot{A} \tag{45}$$

There is no air flow through the airspring during the test. When the sinusoidal vertical displacement, $x = xsin(2\pi ft)$, is applied to the airspring, only the second term, third term, and fourth term in equation (45) are considered, which yields:

$$\frac{dF_s}{dx} = \frac{(\gamma-1)Ak_{as}S_{as}}{x_0 2\pi ftcos(2\pi ft)V_s}\left(T_{ext} - \frac{V_s P_s}{R m_s}\right) - \frac{\gamma P_s A}{V_s}\frac{dV_s}{dx} + P_s\frac{dA}{dx} \tag{46}$$

where x_0 and f represent the magnitude and frequency of the sinusoidal displacement input. The equation clearly shows that the increase of the frequency reduces the effect of hysteresis resulting from the first term, which aligns with the simulation and experimental results.

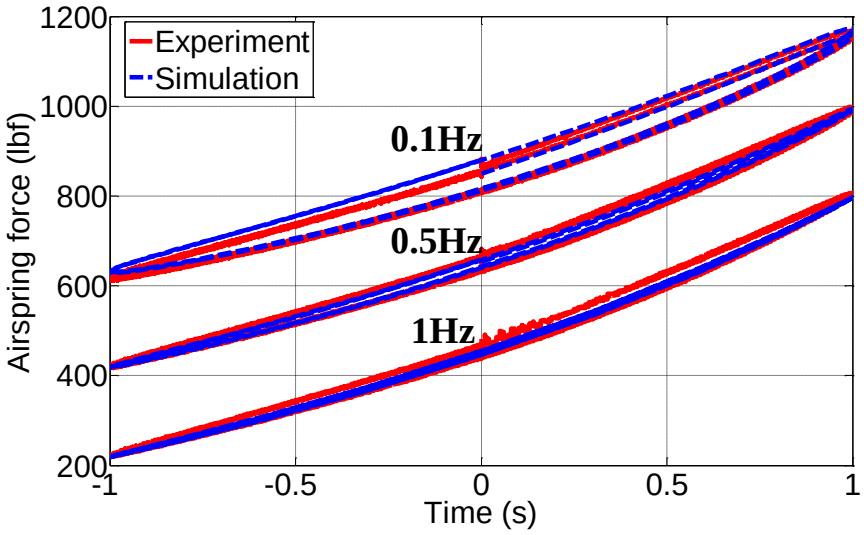

Figure 4-11. Force response for sinusoidal motion excitation at 0.1Hz, 0.5Hz, and 1Hz (the 0.1 Hz and 1 Hz are shown respectively 200 lbf higher and lower than actual values. Initial pressure is set to be 10 psi)

4.3 Valve Modeling Description

4.3.1 Model Development and Experimental Characterization for the Leveling Valve

The flow characteristics of the leveling valve are modeled by a 3-position, 3-port pneumatic valve in AMEsim, as illustrated in Figure 4-12. In this model, a second-order lag is implemented to calculate the movement of the spool:

$$\frac{y}{x} = \frac{k\omega^2}{\omega^2 + 2\zeta\omega s + s^2} \tag{47}$$

where y is the output from the second order lag, x is the input to the second order lag, k is the gain, ω is the natural frequency, and ζ is the damping ratio. Adjusting the natural frequency that is associated to response time of the leveling valve can simulate the delay characteristics of the valve. The deflating port T of the leveling valve is set at atmospheric pressure at all times.

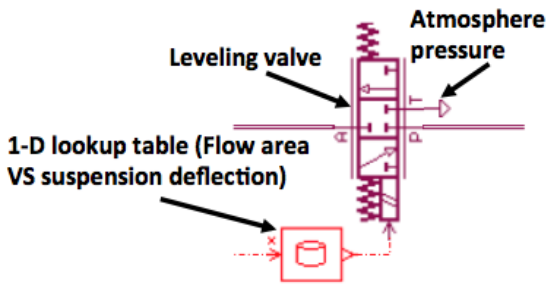

Figure 4-12. Leveling valve model in AMEsim

Figure 4-13 presents a typical arrangement of the leveling valve in the truck. The leveling valve adjusts the airspring pressure by sensing the deflection of the airspring. The flow characterization of the leveling valve defines how the suspension deflection affects the flow rate at a certain pressure difference.

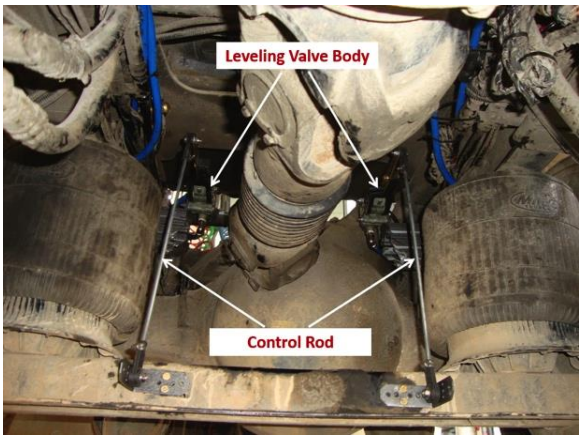

Figure 4-13. Mounting position of the leveling valve on the tractor

A test was designed and conducted [58] to determine the flow characteristics of the leveling valve that assists in establishing parameters for the leveling valve model. An alternative approach was proposed to measure the flow rate through the leveling valve without using flow meters that are expensive and designed for steady state measurement. The test employed a constant-volume air tank directly connected to the leveling valve. The flow rate across the leveling valve is developed by calculating the flow rate exiting the air tank as follows:

$$\dot{m} = \frac{V_r}{kRT_{ro}} \left(\frac{P_r}{P_{r0}}\right)^{\frac{1-k}{k}} \dot{P}_r \tag{48}$$

where P_r and V_r are the pressure and volume of the air tank, respectively, and k is the polytropic exponent of air. Equation (48) shows that the mass flow rate at the leveling valve depends on the rate of change and instantaneous pressure of the air tank. To measure the flow rate only needs a pressure sensor installed between the air tank and the leveling valve. Figure 4-14 shows the flow characterization experimental setup that consists of a 33-gallon air tank with a leveling valve connected. The downstream port of the leveling valve was exposed to the atmosphere. The shock dynamometer (Roehrig EMA 2k dynamometer) was used to provide an accurate displacement input to the control rod rotating the leveler arm of the leveling valve. All the pressure and rotation angle data of the leveler arm were then collected by a data acquisition module (Data Translation DT9816).

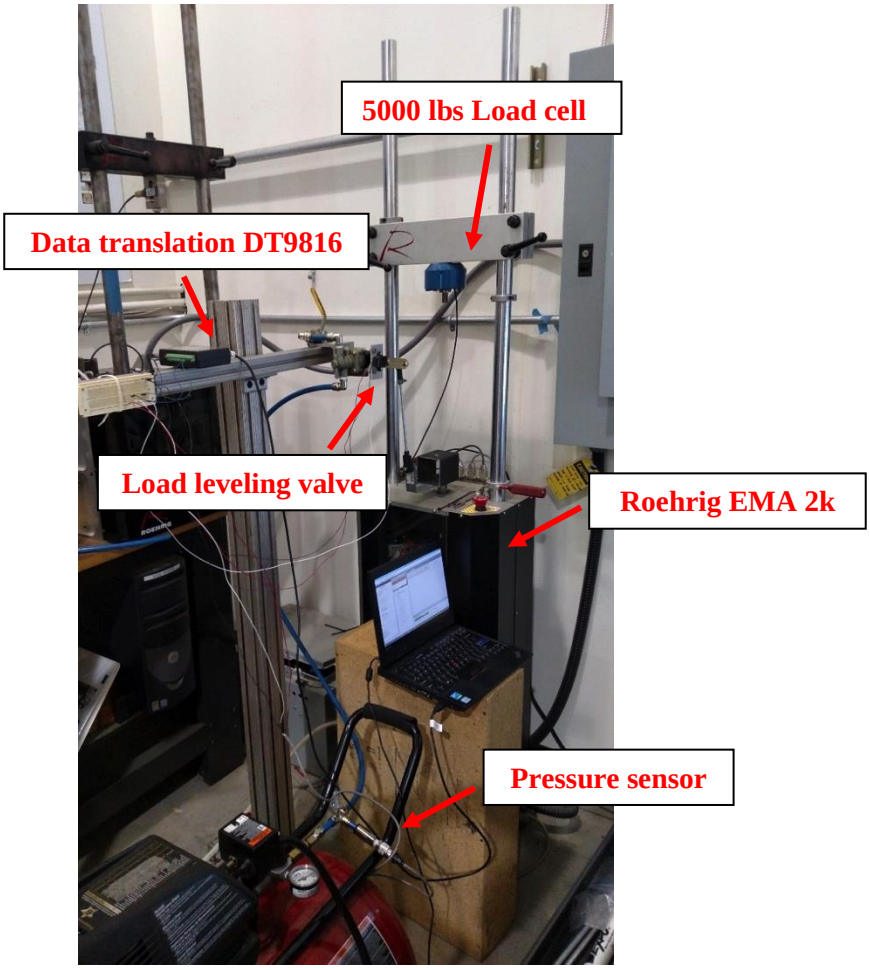

Figure 4-14. Test setup to determine the flow characterization of the leveling valve

A 1-D lookup table with input of the suspension deflection is interpolated to provide the control signal of the flow area for the leveling valve model depicted in Figure 4-15. The information for the lookup table is extracted from the testing results of the flow characterization of the leveling valve as shown in Figure 4-15.

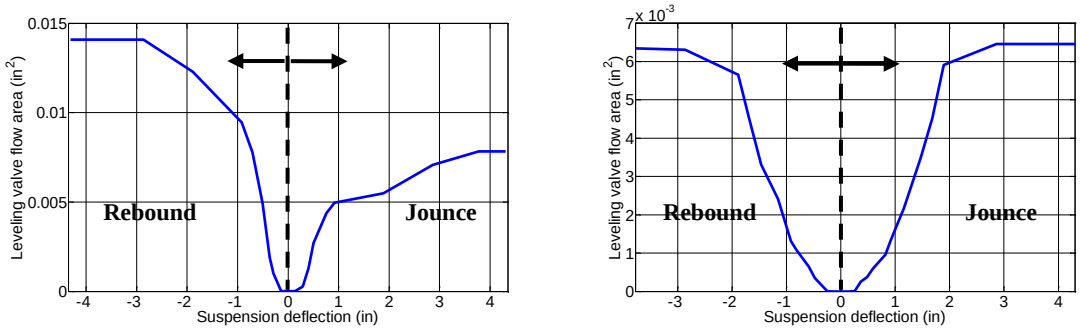

(a) (b)

Figure 4-15. Effect of the suspension deflection on the flow area of the leveling valve for (a) balanced suspension and (b) OE suspension

4.3.2 Validation of the Leveling Valve Model with Experimental Results

To verify the leveling valve model, a "testing bench" model is established as represented in Figure 4-16. Pressures of port P and port T are set to atmospheric pressure. To compare with testing results at different pressures, three different pressures, 36 psi, 50 psi, and 65 psi, are simulated at port A in sequence.

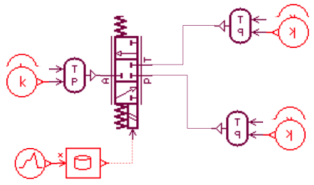

Figure 4-16. Model used for validation of the leveling valve model

Figure 4-17 shows the simulation and experiment results of the flow characteristics for leveling valves in balanced suspension (Hadley, model number: 500 series) and OE suspension (Barksdale, model number: 52321). It clearly indicates that the simulation results match the experimental data for the two types of leveling valves. In regard to the balanced

leveling valve (Hadley), the flow characteristics are non-linear and non-symmetrical for supplying and purging air. It possesses a narrow dead band (0.143 in). For the balanced leveling valve, there is a rapid change of flow rate for small suspension deflection (1 inch), which ends with a large flow rate, resulting in a larger flow zone. These characteristics allow the leveling valve to respond better to the vehicle pitch and roll dynamics. On the contrary, the OE leveling valve (Barksdale) offers a smaller flow zone (dead band =0.255in) and avoids the rapid change in flow rate for the small deflection to save gas. This type of leveling valve is typically designed to maintain the ride height for various loads, which is not desired to operate to help improve vehicle dynamics. A symmetric flow characteristic is observed for the OE leveling valve due to its symmetric inner structure for easier manufacturing. However, the balanced leveling is able to dump air out of the airsprings much faster.

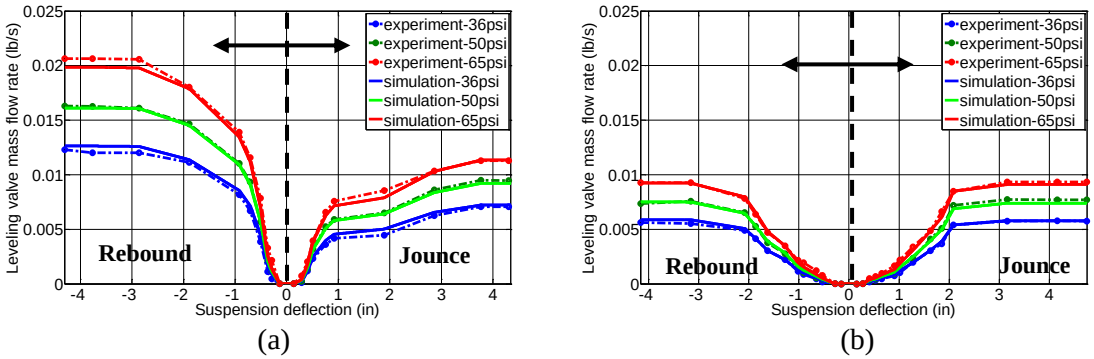

Figure 4-17. Effects of suspension deflection on mass flow rate for (a) leveling valve of balanced suspension and (b) leveling valve of OE suspension

4.3.3 Development of the Check Valve Model

A check valve is installed at the port of the tank to prevent the air at the airspring from flowing back to the tank. The pneumatic library in AMEsim provides a standard pneumatic check valve model. The flow rate through the check valve model adheres to equations (26) and (27), where the flow coefficient is computed using PERRY's polynomial equation (28). When the check valve opens and closes rapidly, many discontinuities will appear, resulting in a slow simulation run. To solve this problem, the hysteresis value of the valve model can be set to 0.0004. Figure 4-18 shows the simulation results of mass flow rate through the check

valve on the effect of downstream and upstream pressures. The flow area of the check is considered to be 0.155 in^2.

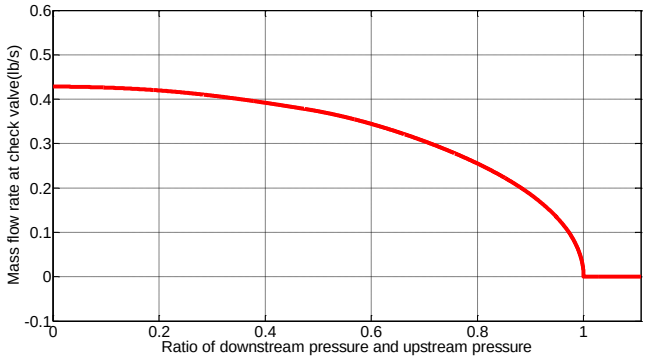

Figure 4-18. Mass flow rate as a function of the pressure ratio

4.4 Pipe Modeling Description

The transient behavior in pipes is influenced by the physical properties of gas, its compressibility and viscosity. Typically, the gas in the pipes can be assumed to be purely compressive, dissipative, inertial, or various combinations of the three, depending on whether they are all important or some of them dominate. In this investigation, the dissipative effect and compressive effect are considered in modeling pneumatic pipes.

4.4.1 Dissipative Effect of the Pipe Model

A pipe friction submodel (PNL00R) in the pneumatic library of AMEsim is used to simulate the pure dissipative effect while the air is flowing in a straight pipe. To verify the dissipative effect, a simulation "testing bench" for the submodel is established as shown in Figure 4-19. A pressure step and a constant temperature (293.15 K) are imposed at one end (port 1), and a 6-gallon rigid tank is connected at the other end (port 2). The absolute roughness for the nylon pipe is set to be 0.000118 in (0.000003 m).

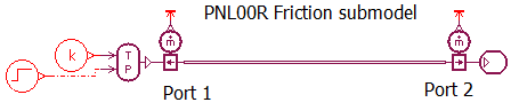

Figure 4-19. Model used for evaluating the effect of the pipe friction

The pipe friction submodel is a resistive element by which identical flows (mass flow rate and enthalpy flow rate) are provided at inlet and outlet. The energy flow is dissipated by the pressure loss that depends on the pipe diameter and pipe length according to equation (31). Figure 4-20 shows the evolution of pressure at the pipe outlet (equal to tank pressure) for different pipe diameters and lengths with a pressure step input at port 1 (dashed black line). As shown in Figure 4-20 (a), the increase in the diameter of the model contributes to the quicker pressure change, exhibiting a smaller pressure loss zone. Figure 4-20 (b) indicates that increasing the pipe length raises the pressure loss resisting the transient air. These simulation results are in line with the equations of chapter 3. The submodel with friction effect is then combined with the compressive element in next section to verify the AMEsim pipe model with both effects.

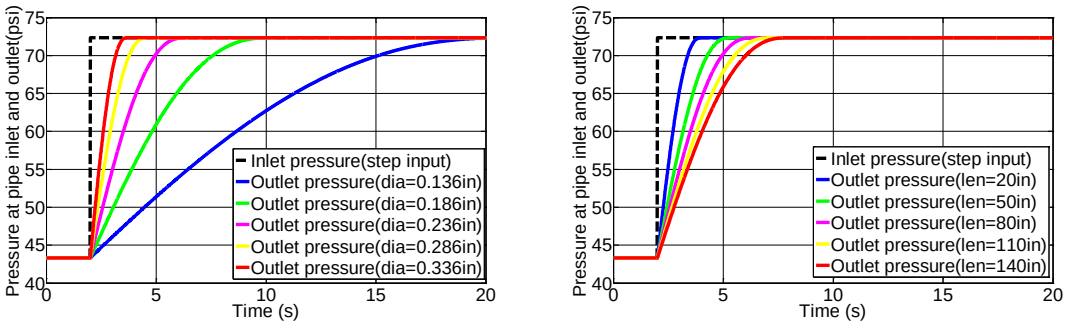

(a) (b)

Figure 4-20. Effect of different (a) pipe diameters and (b) pipe lengths on the pressure change at outlet

4.4.2 Combination of Dissipative and Compressive Effects

As mentioned previously, the lumped parameter pneumatic pipe model uses a combination of a friction submodel and a compressibility submodel. Three various combinations of the two submodels are shown in Figure 3-7 of Chapter 3, depending on the type of pneumatic components connected. If both ends of the pipe are connected with resistive components, the model PNL0003 in the pneumatic library of AMEsim will be used; if the components at both ends are attached to capacitive components, the model PNL0002 will be employed. If the pipe connects a resistive component to a capacitive component, model PNL0001 will be

used. The pneumatic pipe model must comply with the causality that a resistive element is always connected to a capacitive element.

The compressibility of the gas can be taken into account using either a polytropic model or a heat transfer model. This pipe model does not include the heat transfer due to lack of information regarding the heat transfer coefficient. To verify the original pipe model (PNL0001), a new model is developed by combining a pneumatic chamber model and a pure friction model (PNL00R), as shown in Figure 4-21 (a). The pneumatic chamber model has a fixed volume and follows polytropic law according to equations (37) and (40). The volume of the pneumatic chamber model is determined by multiplying pipe cross-section area and pipe length. To verify the original pipe model (PNL0001) with the developed model, a 6-gallon rigid tank is attached at port 2 with initial pressure of 43 psi, and a sinusoidal flow rate is inputted at port 1 with amplitude of 0.0088 lb/s at 0.25 Hz. Table 4-3 shows the parameters in the simulation.

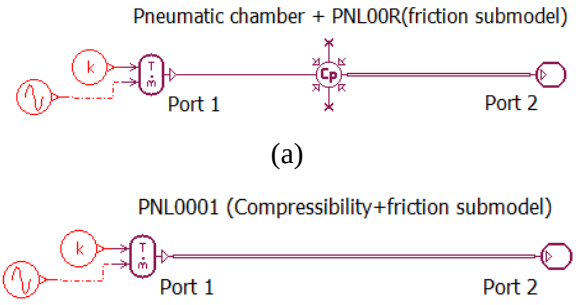

Figure 4-21. Pipe models (a) developed by coupling pneumatic chamber and friction submodel and (b) originally in the pneumatic library of AMEsim

Table 4-3. Parameters used in verifying the original pipe model

Parameter	Value(English unit)	Value(SI unit)
Polytropic constant	1.38	1.38
Diameter of pipe	0.4 in	0.01016 m
Pipe length	80 in	2.032 m
Pipe initial pressure	43.3 psi	298543 pa
Absolute roughness	0.000118 in	0.000003 m

As shown in Figure 4-22, the simulation results of the two models match perfectly for inlet and outlet pressures, outlet mass flow rate, and outlet temperature. Therefore, the pipe model (PNL0001) in the AMEsim pneumatic library is verified to include the effects of gas compressibility and friction and to combine them in a cascade manner.

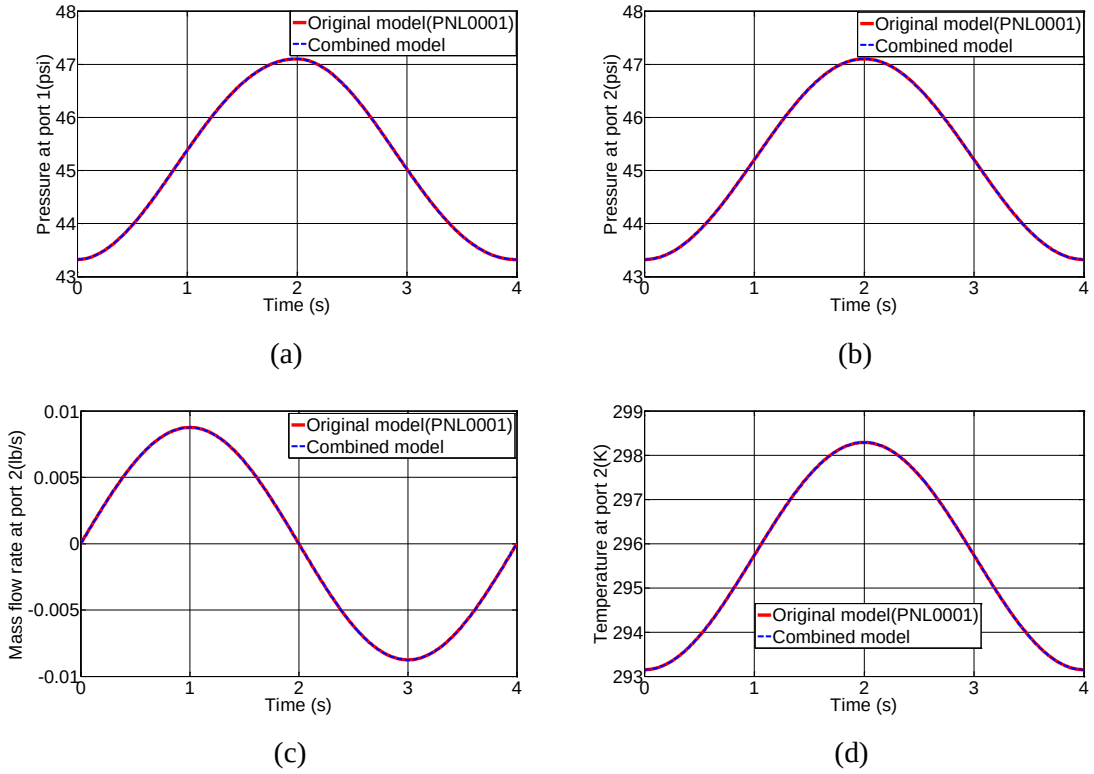

Figure 4-22. Simulation results comparison between the original pipe model (PNL0001) and the combined model : (a) pressure at port 1, (b) pressure at port 2, (c) mass flow rate at port 2, and (d) temperature at port 2

The compressibility of gas causes volume loss of the gas in the pipes. The mass flow rate at the outlet port is attenuated with respect to the mass flow rate at the inlet port. Figure 4-23 shows the effect of the compressibility of model PNL00R on the air outflow for different pipe length cases. There is more attenuation of the mass flow rate at the output port (port 2) as the length of the pipe increases. In other words, the energy loss due to the gas compressibility increases when the inner volume of the pipe increases.

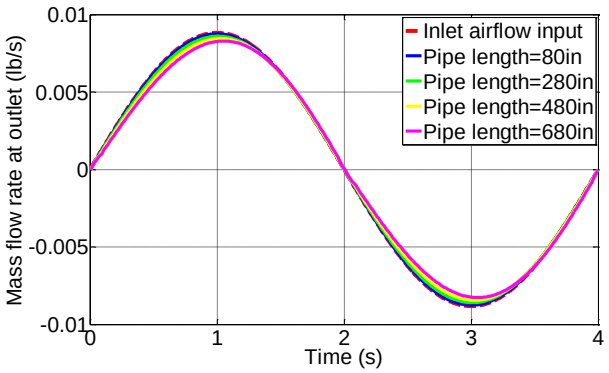

Figure 4-23. Effect of different pipe lengths on attenuating the mass flow rate at the outlet

4.5 Pneumatic Suspension Subsystem Modeling Description

By integrating the validated pneumatic components, a submodel of half-balanced pneumatic suspensions on rear tandem axles is created, as depicted in Figure 4-24. The green components represent the mechanical elements, while the purple components show the pneumatic elements.

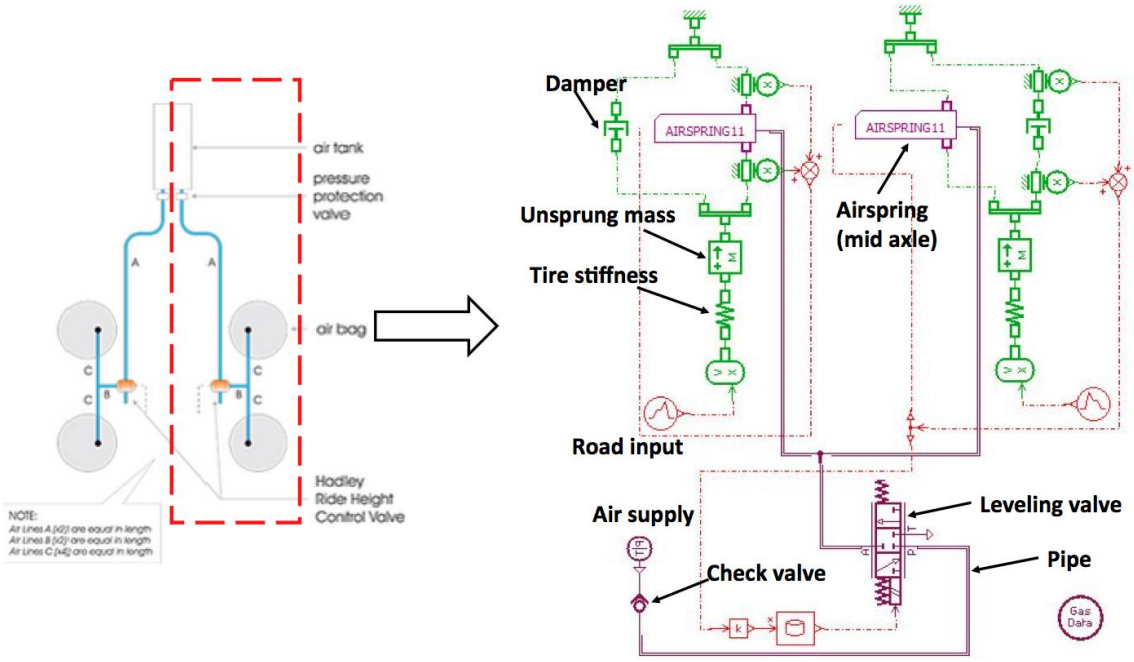

Figure 4-24. Model used for verifying one side of the balanced air suspensions

To test the subsystem model, a 3-in bump is encountered separately by the middle and rear wheels with the vehicle body grounded. The time for each wheel across the bump is 0.06s, and the time delay between the two axles for encountering the bump is 0.32s. The results are shown in Figure 4-25, Figure 4-26, and Figure 4-27. The leveling valve can be activated immediately for inflating when the deflection of the air suspension on the middle drive axle is over the dead band. As we can also see in Figure 4-25 (a) and Figure 4-26, in the short period after bumping the mid axle at 0.5 seconds, the pressure in the mid airspring increases while the mid airspring is compressed. At that moment, the pressure difference between the two interconnected airsprings and the operation of the leveling valve results in airflow into the rear airspring. This leads to a small increase in the displacement of the rear airspring with the rear wheel compressed, as shown in Figure 4-25 (b). According to equation (3), due to the airflow from the mid airspring and the leveling valve, the pressure in the rear airspring increases after 0.5 seconds, as depicted in Figure 4-26. Additionally, as soon as the excitation force disappears, the front-rear interconnected airsprings can quickly balance the pressure.

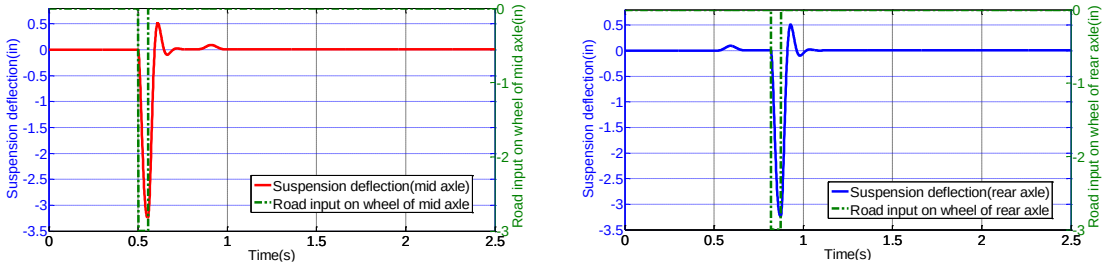

(a) (b)

Figure 4-25. Time trace of suspension deflection on middle axle (a) and rear axle (b) with a 3-inch bump input

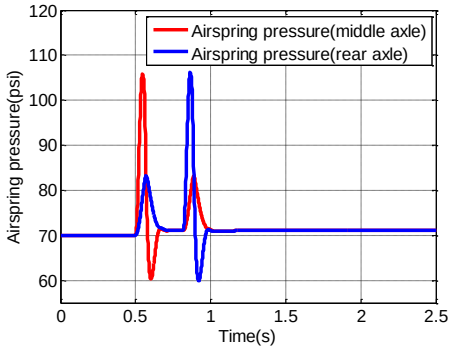

Figure 4-26. Time trace of airspring pressure

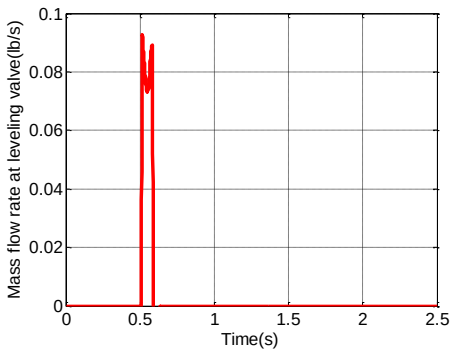

Figure 4-27. Time trace of mass flow rate at leveling valve

4.6 Pneumatic Suspension System Test and Model Validation

A truck rear-axles suspension test is designed and conducted to provide verification for the AMEsim-based pneumatic suspension system model. The test consisted of raising and lowering the truck by controlling one leveling valve to charge and discharge the airsprings on the tractor's rear drive axles as shown in Figure 4-28. The setup for the experiment is shown in Figure 4-29. To simulate the trailer vertical load, the vehicle was loaded by placing a stack of steel plates on the back of the truck where the fifth wheel normally resides. The additional weight consisted of a stack of 27 metal plates, 350 lb each, which was fixed to the truck frame by using four steel thread rods and nuts. With these modifications, the weight on the rear axles of the tractor was approximately 12000 lb. In addition, a three-port leveling valve used in the balanced suspension was employed. One port of the leveling valve connected airsprings on both sides by Tee-junctions and pipes. Another port went to the air supply, and the last port was for dumping air out as shown in Figure 4-28. As shown in the amplified picture on the lower right side of Figure 4-29, a servo motor was used to control the leveler arm movement that is consistently monitored by a rotary position sensor. The movement of the lever arm would introduce a pressure change and airspring height change which were detected by pressure transducers and string pots, respectively.

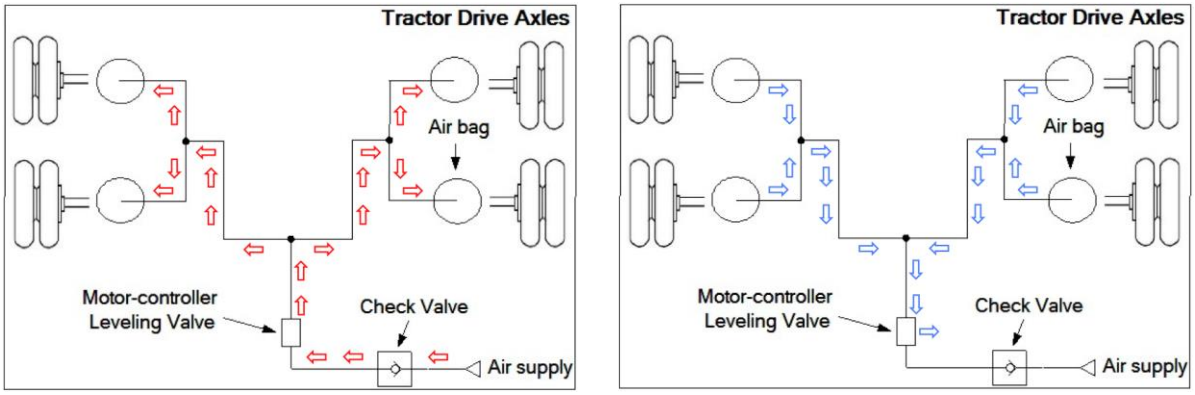

(a) (b)

Figure 4-28. Diagram of the test for (a) inflation process and (b) deflation process

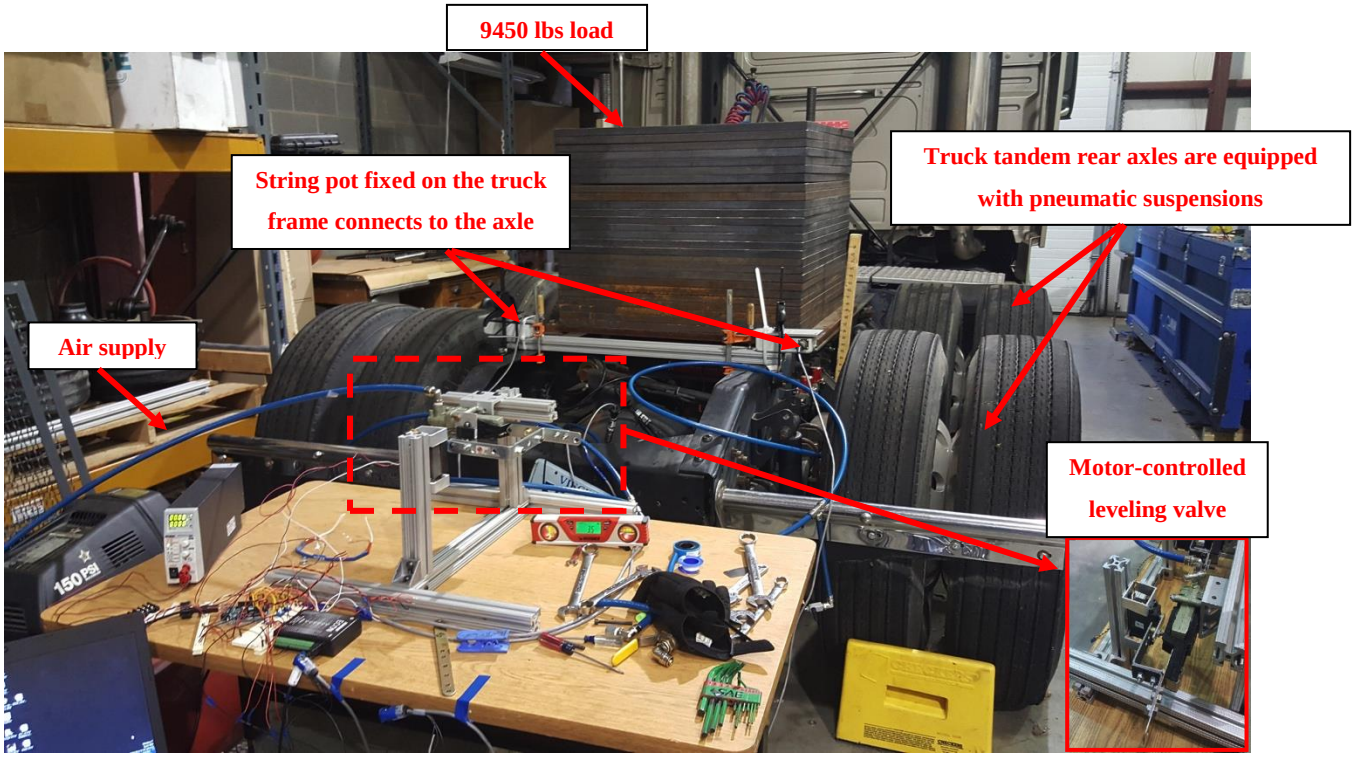

Figure 4-29. Test setup for the pneumatic suspension system on the truck tandem rear axles

Due to space limitations, the string pot was fixed on the frame, and the other end of the string was attached to the axle, sensing the axle travel with respect to the truck frame. The axle travel relative to the frame is not equal to suspension deflection considering their different locations on the trailer arm that moves about the pivoted end, as shown in Figure 4-30. It is

necessary to determine the relationship between the string pot data (axle travel relative to the vehicle body) and the airspring travel, as shown in Figure 4-31.

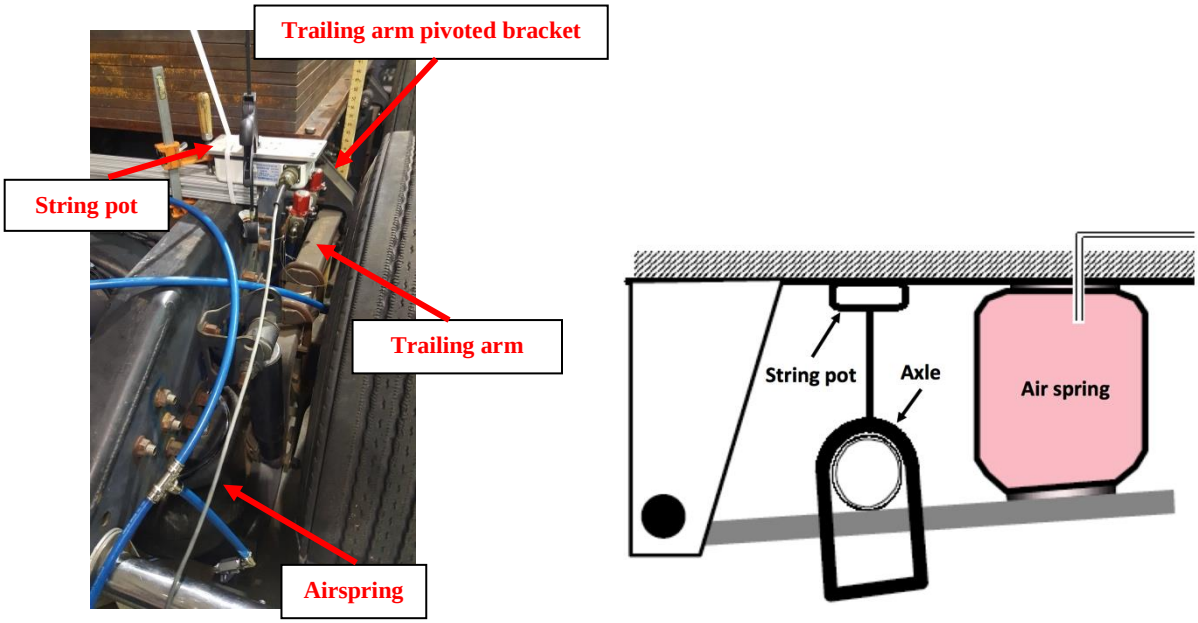

Figure 4-30. Installation of the string pot on one side of the bogie air suspension

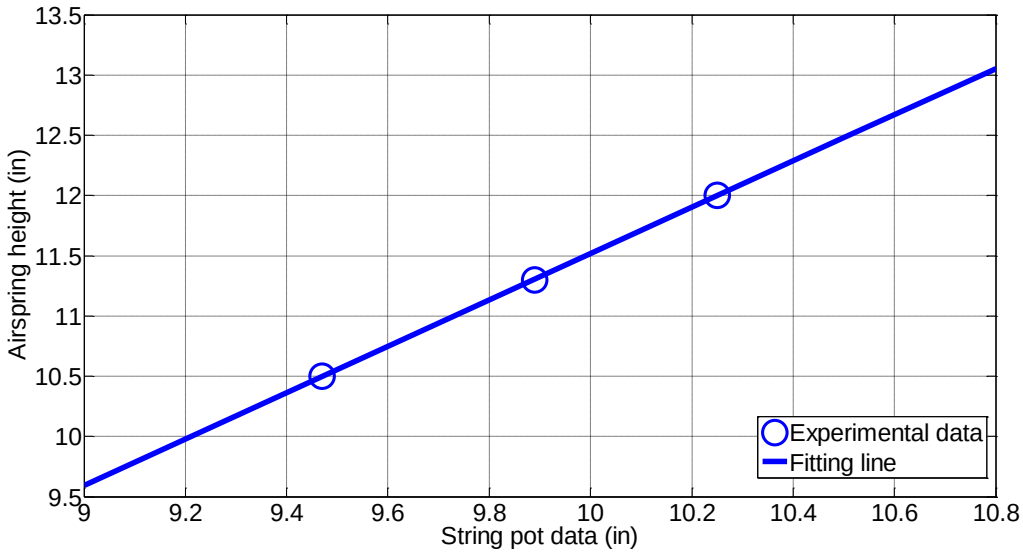

Figure 4-31. Relationship between airspring height and string pot data

[Airspring height=1.9226x(string pot)-7.7091]

A system model is programmed in AMEsim, as shown in Figure 4-32, for verifying the pneumatic suspension dynamics with experimental results. The model includes the testing

loaded truck dynamics in heave and pitch, and a pneumatic suspension system arranged identical to the testing setup. The test data of the leveler arm's rotation angle is applied to the model as an input for comparison purposes.

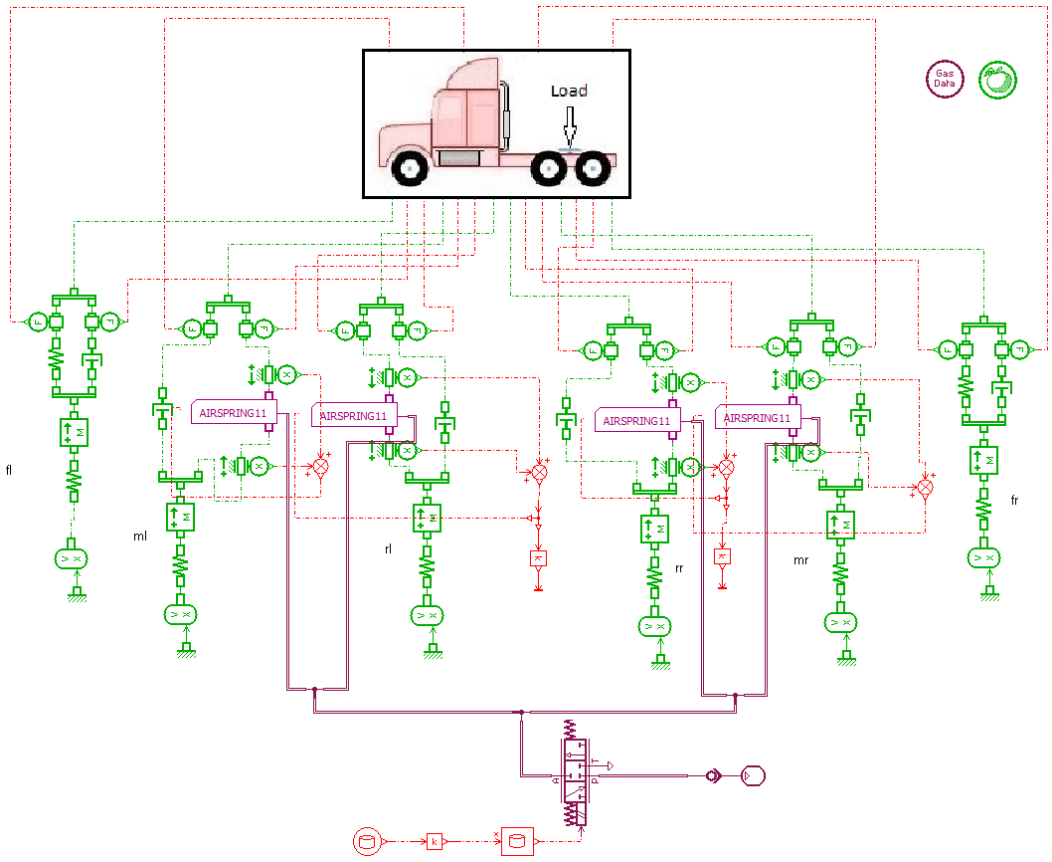

Figure 4-32. Model used for verifying the pneumatic suspension system with experiments

Figure 4-33 and Figure 4-34 show the comparison between the test results and the simulation results. Two tests were performed where the leveler arm was moved upward and downward separately by a servo motor. The data of the lever arm angle obtained by a rotary position sensor are presented in the top plot of each figure. As shown in the two bottom plots of Figure 4-33 and Figure 4-34, in terms of airspring pressure and airspring travel, the simulation results match the testing results very well. The pressure at the airspring ended with a different value compared to the initial value because of variation of airspring effective area, which is affected primarily by the airspring height. The testing results of airspring pressure and airspring travel are not perfectly equal from side to side due to the actual load that is distributed slightly non-uniformly.

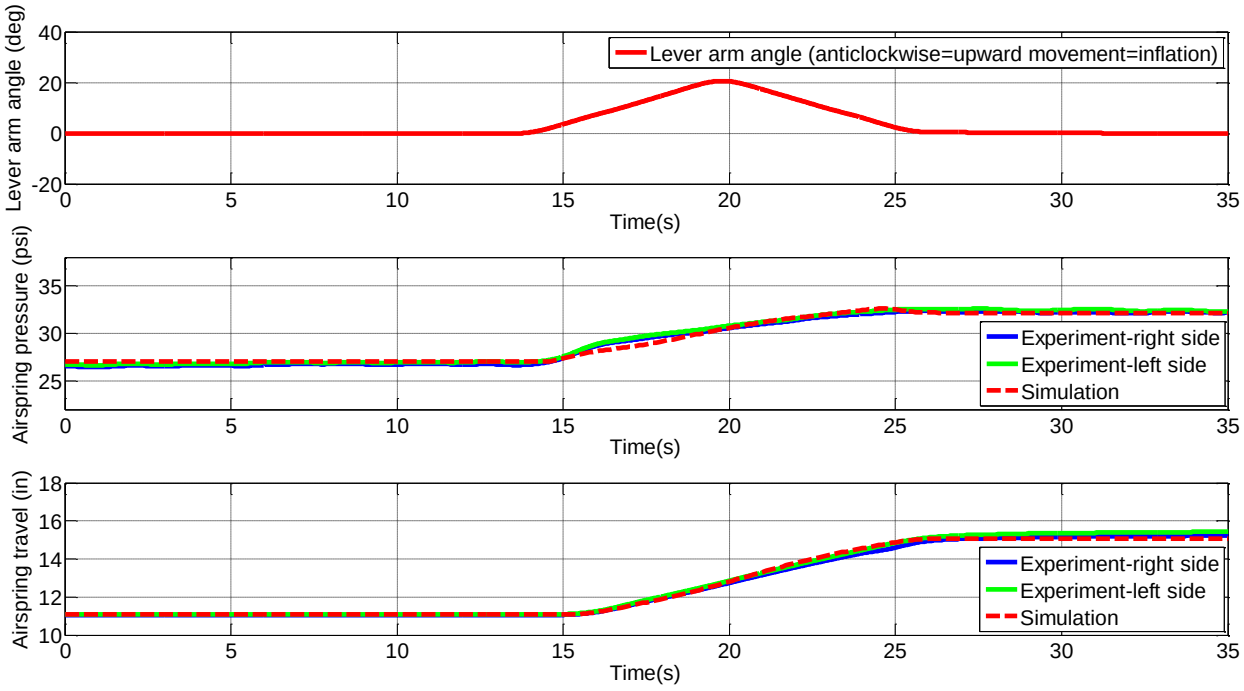

Figure 4-33. Comparison between simulation and experimental results for charging the airsprings by upward movement of the leveler arm

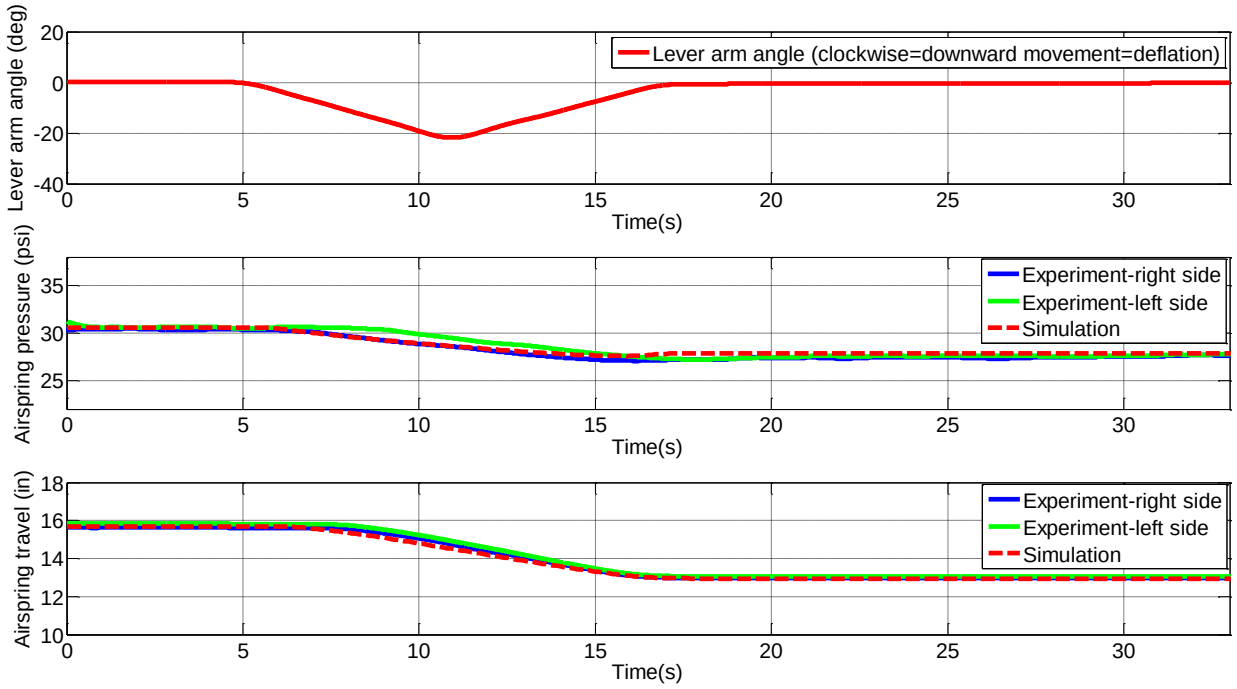

Figure 4-34. Comparison between simulation and experimental results for discharging the airsprings by downward movement of the leveler arm

Chapter 5 Simulation Study of a 9-DOF Truck Dynamic Model with Pneumatic Suspension Dynamics

This chapter provides a simulation evaluation of the effect of maintaining balanced airflow, both statically and dynamically, in heavy truck air suspensions on vehicle roll dynamics. The model includes a multi-domain evaluation of a 9-DOF truck's dynamics, combined with the pneumatic dynamics of the drive axle suspensions. The analysis is performed based on a detailed model of the balanced suspension's pneumatics, from the main reservoir to the airsprings, with two leveling valves, air hoses, and fittings. The suspension pneumatics is designed so that they are better able to respond to body motion in real time. Specifically, this chapter aims to better understand the airflow dynamics and how they couple with the vehicle dynamics. The pneumatic model is coupled with a roll-plane model of the truck to evaluate the effect of the pneumatic suspension dynamics on the body roll, as well as the force transmission to the sprung mass. The results of the study show that maintaining a balanced airflow through the suspensions improves the dynamic responsiveness of the suspension to steering, causing less body roll.

5.1 Truck Modeling Description

5.1.1 Development of a Truck Dynamic Model with 9 DOF

This chapter starts with developing a multi-body dynamic truck model with tandem rear axles. The schematic of the tri-axle truck model is shown in Figure 5-1. The truck model involves bounce z, pitch θ, and roll φ of sprung mass, and bounces of six unsprung masses. Here, tire damping is ignored. The stiffness of the airspring is variable due to the adjustment of the leveling valves.

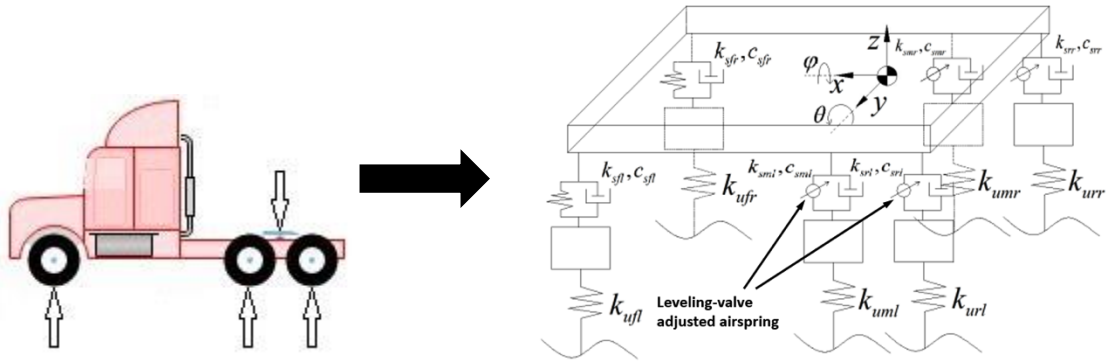

Figure 5-1. Truck multi-body dynamic model schematics

The truck multi-body dynamic model can be described by nine motion equations as follows:

The truck body vertical motion equation:

$$m\ddot{z} = k_{sfl}(z_{ufl} - z + a\theta - \frac{c}{2}\varphi) + c_{sfl}(\dot{z}_{ufl} - \dot{z} + a\dot{\theta} - \frac{c}{2}\dot{\varphi}) + k_{sfr}(z_{ufr} - z + a\theta + \frac{c}{2}\varphi) + c_{sfr}(\dot{z}_{ufr} - \dot{z} + a\dot{\theta} + \frac{c}{2}\dot{\varphi}) + (F_{sml} - F_0) + c_{sml}(\dot{z}_{uml} - \dot{z} - b_1\dot{\theta} - \frac{d}{2}\dot{\varphi}) + (F_{smr} - F_0) + c_{smr}(\dot{z}_{umr} - \dot{z} - b_1\dot{\theta} + \frac{d}{2}\dot{\varphi}) + (F_{srl} - F_0) + c_{srl}(\dot{z}_{url} - \dot{z} - b_2\dot{\theta} - \frac{d}{2}\dot{\varphi}) + (F_{srr} - F_0) + c_{srr}(\dot{z}_{urr} - \dot{z} - b_2\dot{\theta} + \frac{d}{2}\dot{\varphi}) \quad (49)$$

The truck body pitch moment equation:

$$I_\theta\ddot{\theta} = b_1[(F_{sml} - F_0) + c_{sml}(\dot{z}_{uml} - \dot{z} - b_1\dot{\theta} - \frac{d}{2}\dot{\varphi}) + (F_{smr} - F_0) + c_{smr}(\dot{z}_{umr} - \dot{z} - b_1\dot{\theta} + \frac{d}{2}\dot{\varphi})] + b_2[(F_{srl} - F_0) + c_{srl}(\dot{z}_{url} - \dot{z} - b_2\dot{\theta} - \frac{d}{2}\dot{\varphi}) + (F_{srr} - F_0) + c_{srr}(\dot{z}_{urr} - \dot{z} - b_2\dot{\theta} + \frac{d}{2}\dot{\varphi})] - a[k_{sfl}(z_{ufl} - z + a\theta - \frac{c}{2}\varphi) + c_{sfl}(\dot{z}_{ufl} - \dot{z} + a\dot{\theta} - \frac{c}{2}\dot{\varphi}) + k_{sfr}(z_{ufr} - z + a\theta + \frac{c}{2}\varphi) + c_{sfr}(\dot{z}_{ufr} - \dot{z} + a\dot{\theta} + \frac{c}{2}\dot{\varphi})] + mg\theta r_\theta \quad (50)$$

The truck body roll moment equation:

$$I_\varphi\ddot{\varphi} = \frac{d}{2}[(F_{sml} - F_0) + c_{sml}(\dot{z}_{uml} - \dot{z} - b_1\dot{\theta} - \frac{d}{2}\dot{\varphi}) + (F_{srl} - F_0) + c_{srl}(\dot{z}_{url} - \dot{z} - b_2\dot{\theta} - \frac{d}{2}\dot{\varphi})] - \frac{d}{2}[(F_{smr} - F_0) + c_{smr}(\dot{z}_{umr} - \dot{z} - b_1\dot{\theta} + \frac{d}{2}\dot{\varphi}) + (F_{srr} - F_0) + c_{srr}(\dot{z}_{urr} - \dot{z} - b_2\dot{\theta} + \frac{d}{2}\dot{\varphi}) + \frac{c}{2}[k_{sfl}(z_{ufl} - z + a\theta - \frac{c}{2}\varphi) + c_{sfl}(\dot{z}_{ufl} - \dot{z} + a\dot{\theta} - \frac{c}{2}\dot{\varphi})] - \frac{c}{2}[k_{sfr}(z_{ufr} - z + a\theta + \frac{c}{2}\varphi) + c_{sfr}(\dot{z}_{ufr} - \dot{z} + a\dot{\theta} + \frac{c}{2}\dot{\varphi})] - ma_y r_\varphi + mg\varphi r_\varphi \quad (51)$$

The tire vertical motion on the left side of the front axle:

$$m_{ufl}\ddot{z}_{ufl} = -z_{ufl}k_{ufl} - k_{sfl}(z_{ufl} - z + a\theta - \frac{c}{2}\varphi) - c_{sfl}(\dot{z}_{ufl} - \dot{z} + a\dot{\theta} - \frac{c}{2}\dot{\varphi}) \quad (52)$$

The tire vertical motion on the right side of the front axle:

$$m_{ufr}\ddot{z}_{ufr} = -z_{ufr}k_{ufr} - k_{sfr}(z_{ufr} - z + a\theta + \frac{c}{2}\varphi) - c_{sfr}(\dot{z}_{ufr} - \dot{z} + a\dot{\theta} + \frac{c}{2}\dot{\varphi}) \quad (53)$$

The tire vertical motion on the left side of the front drive axle:

$$m_{uml}\ddot{z}_{uml} = -z_{uml}k_{uml} - (F_{sml} - F_0) - c_{sml}(\dot{z}_{uml} - \dot{z} - b_1\dot{\theta} - \frac{d}{2}\dot{\varphi}) \quad (54)$$

The tire vertical motion on the right side of the front drive axle:

$$m_{umr}\ddot{z}_{umr} = -z_{umr}k_{umr} - (F_{smr} - F_0) - c_{smr}(\dot{z}_{umr} - \dot{z} - b_1\dot{\theta} + \frac{d}{2}\dot{\varphi}) \quad (55)$$

The tire vertical motion on the left side of the rear drive axle:

$$m_{url}\ddot{z}_{url} = -z_{url}k_{url} - (F_{srl} - F_0) - c_{srl}(\dot{z}_{url} - \dot{z} - b_2\dot{\theta} - \frac{d}{2}\dot{\varphi}) \quad (56)$$

The tire vertical motion on the right side of the rear drive axle:

$$m_{urr}\ddot{z}_{urr} = -z_{urr}k_{urr} - (F_{srr} - F_0) - c_{srr}(\dot{z}_{urr} - \dot{z} - b_2\dot{\theta} + \frac{d}{2}\dot{\varphi}) \quad (57)$$

Where $z, \theta, and\ \varphi$ represent the bounce, pitch, and roll of the sprung mass, m and m_{uij} are the sprung mass and the unsprung mass, and k_{sij} and k_{uij} mean the stiffness of the suspension and the wheels, respectively. z_{url} is the displacement of the unsprung mass, c_{sij} is the suspension damping coefficient and tire damping is ignored. I_θ and I_φ are the corresponding initial moments, and F_{sij} represents the airspring force at location "i" and "j". The subscript "*i*" denotes front "*f*", middle "*m*", or rear "*r*". The subscript "*j*" denotes left "*l*", or right "*r*".

According to the motion equations, a multi-body truck dynamic model is developed, as shown in Figure B-1 of Appendix B. This model is a pure vehicle dynamic model without including fluid dynamics of the pneumatic suspension, and rear drive axles are equipped with leaf springs instead of airsprings. The sprung mass dynamics (roll, pitch, and bounce) are modeled using the signal and control library (represented by the color red). The dynamics of suspensions and axles are simulated using components of the mechanical library (represented by the color green).

5.1.2 Validation of the Truck Dynamic Model with Simulink Model

A truck dynamic model is developed using Matlab/Simulink to verify the AMEsim model, as shown in Figure B-2. Corresponding parameters used in the simulation are listed in Table B-1. A 0.2g sinusoidal acceleration force at 0.5 Hz is applied to the two models for comparison purposes. The comparison results of vehicle roll angle, tire compression (1st axle), airspring force (2nd axle), and suspension deflection (3rd axle) are shown in Figure 5-2 (a)-(d). A perfect match between the AMEsim and Simulink models indicates that the AMEsim truck model can accurately describe truck dynamic behavior following the motion equations (49)-(57). In the next section, the verified AMEsim truck dynamic model will be intergrated with the pneumatic suspension model for this study.

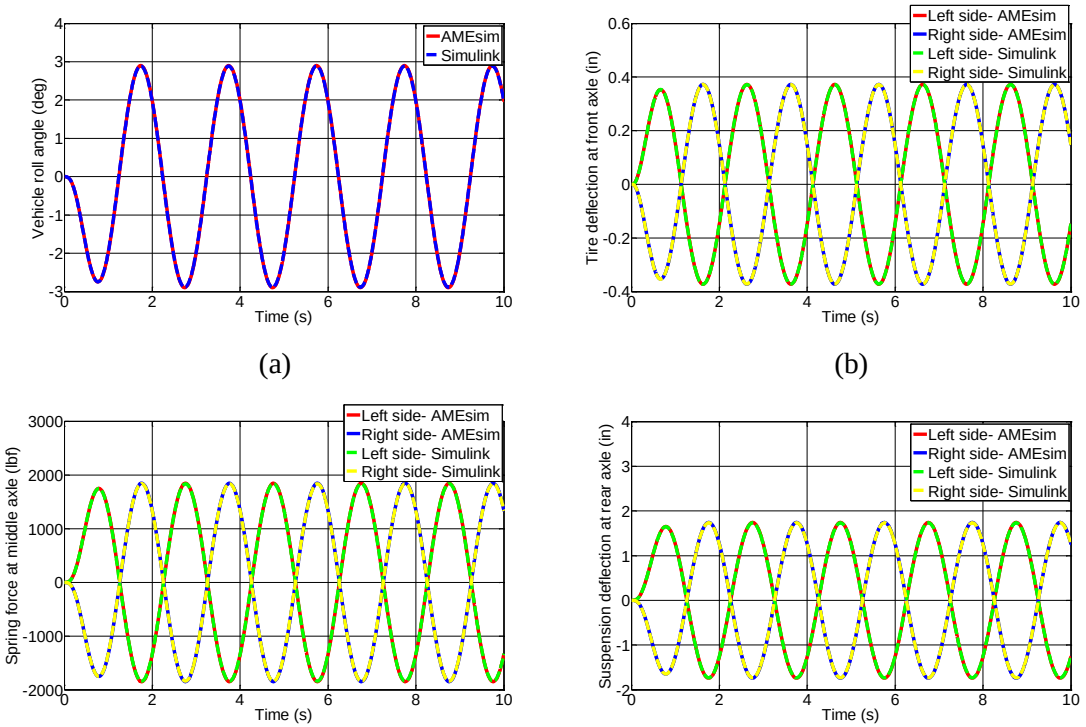

Figure 5-2. Truck multi-body dynamic model validation with Simulink model for a 0.2g sinusoidal lateral acceleration at 0.5 Hz

5.1.3 Integration with Pneumatic Suspension System

The integration is achieved by following the relationship as described in Figure 5-3. The air suspension model outputs spring force and damping force to the sprung mass model, while the sprung mass model feeds the air suspension model with suspension deflection. On the other side, the suspension deflection is sensed for determination of the leveling valve's flow rate. At the same moment, the air suspension model provides pressure data to the pneumatic pipe model to calculate the mass flow rate. The final aligned truck model with balanced suspensions is shown in Figure 5-4. The model with OE suspensions is shown in Figure B-3 of appendix B. Corresponding parameters used in simulating the multi-body truck model and the pneumatic suspension can be obtained in Table B-1 and Table B-2.

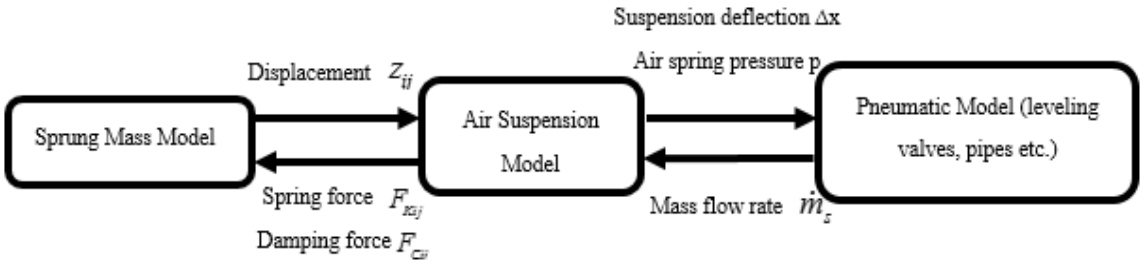

Figure 5-3. Relationship between the truck dynamic model and the pneumatic system model

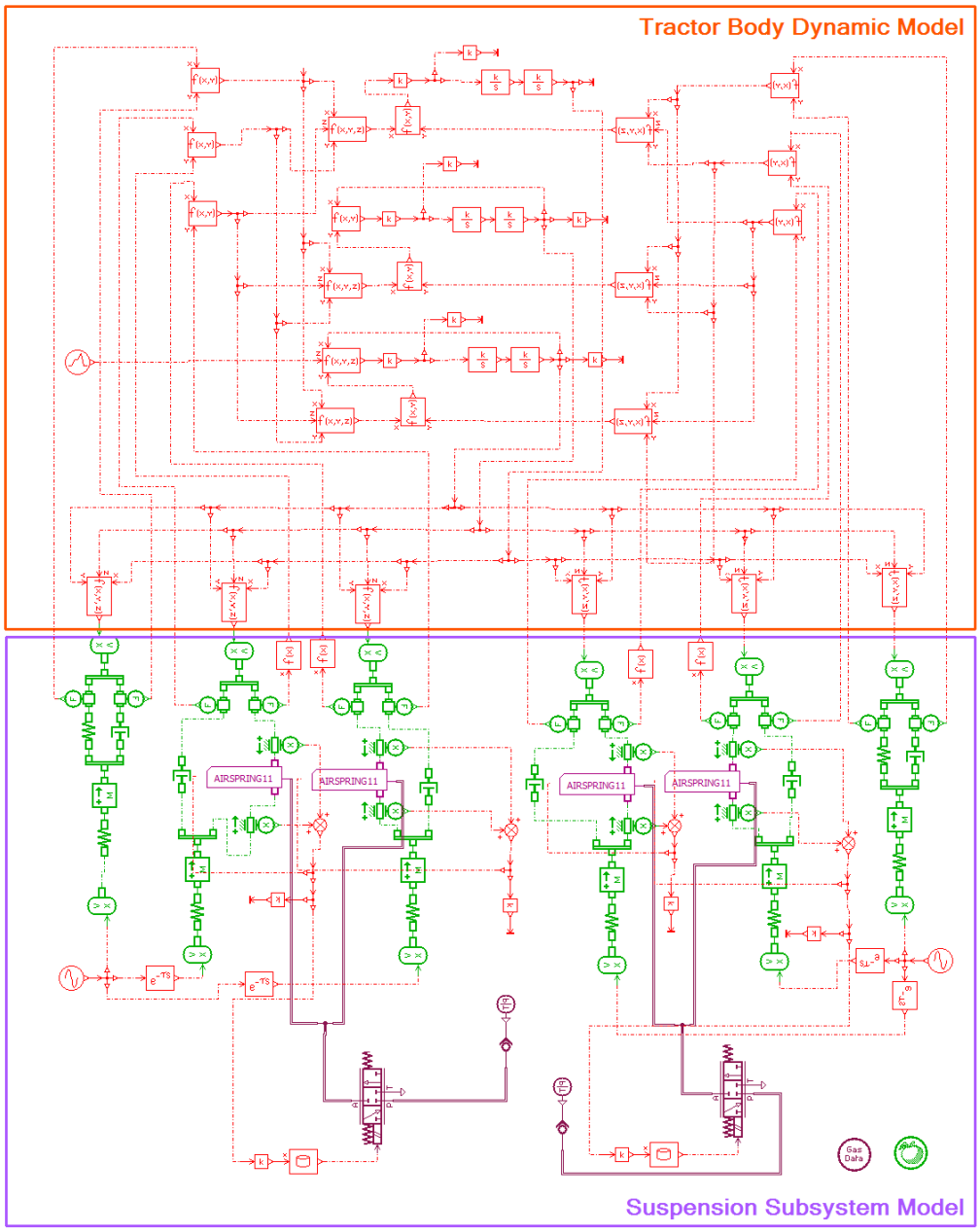

Figure 5-4. Aligned truck dynamic model with balanced pneumatic suspensions in AMEsim

5.2 Simulation Results

To assess the performance of the air suspensions, two different steering maneuvers, cornering and S-turn, are simulated. For the cornering maneuver, it is assumed that the truck enters a right turn for 5 seconds, and a square lateral acceleration is applied on the center of gravity

(CG) of the truck in the left direction, which is depicted in Figure 5-5 (a). Here, we take $\frac{V^2}{R} = 0.15g \frac{\mathrm{V}^2}{\mathrm{R}} = 0.15\mathrm{g}$, with V being the cornering speed of the vehicle and R being the curve radius. When the path is an 'S' curve, the lateral acceleration is approximated as a sinusoidal wave input, as shown in Figure 5-5 (b), whose magnitude and frequency are considered to be 0.15g and 0.14 Hz, respectively. In the simulation, the road is assumed to be perfectly smooth.

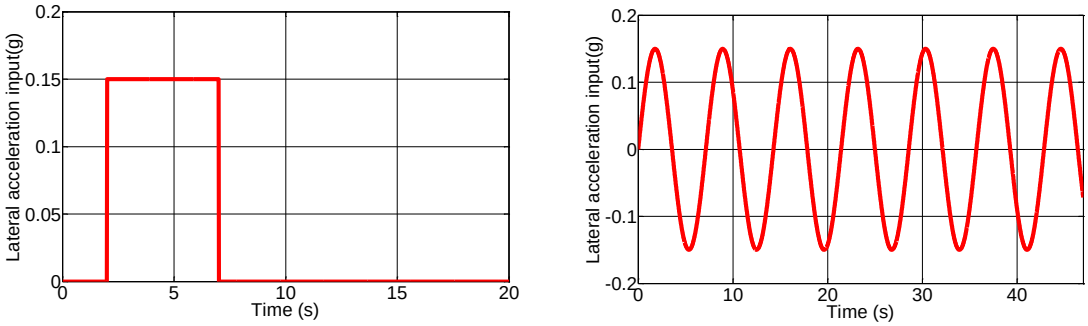

(a) (b)

Figure 5-5. Lateral acceleration for (a) right-hand turn and (b) an S-turn

The change in pressure of the airsprings on the driving axles obtained by the simulation is represented in Figure 5-6 (a)-(d). As can be seen by comparing with OE airsprings in Figure 5-6 (a) and (b), during cornering, higher pressure can be obtained in the balanced airsprings on the outer side, while simultaneously, there is lower pressure in the balanced airsprings on the inner side. The results indicate a larger difference of air pressure from side to side in balanced airsprings than in OE airsprings among driving axles. It is found from the simulation results of S-turns in Figure 5-6 (c) and (d) that the balanced airspring is able to retain the larger pressure difference from side to side in response to the body roll motion. The design of equal length pipes from the leveling valves to the airsprings in the balanced pneumatic arrangement allows two airsprings on either side to equally share air mass flow through the leveling valve. Consequently, the balanced airsprings are able to maintain equal pressure front and rear that doesn't happen in OE airsprings while the truck body is rolling, as shown in Figure 5-6 (a)-(d).

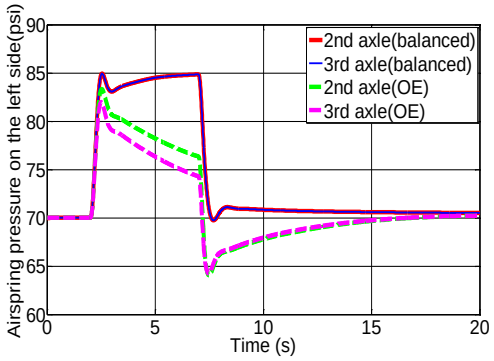

(a) Airspring pressure on left side (cornering)

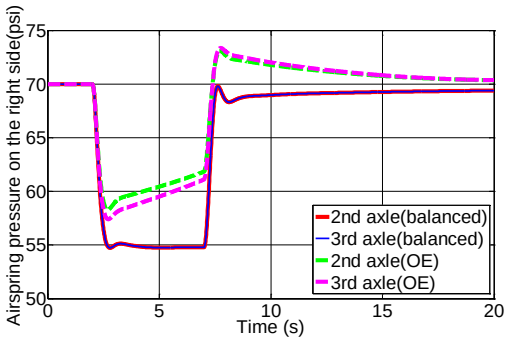

(b) Airspring pressure on right side (cornering)

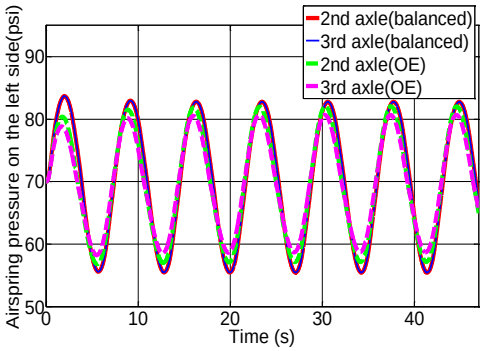

(a) Airspring pressure on left side (S-turn)

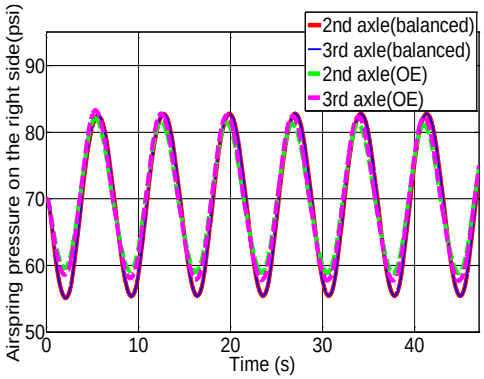

(b) Airspring pressure on right side (S-turn)

Figure 5-6. Time trace of airspring pressure on tandem driving axles and for right-hand cornering and an S-turn

It is observed in Figure 5-7 (a)-(d) that a larger restoring force is produced by the balanced airspring than the OE airspring to keep the suspension in balance. By comparing airspring forces on the right and left sides, it is found that the side-to-side force difference in the balanced airsprings is larger than in the OE airsprings to better resist the overturning moment of truck body roll. Furthermore, as we can see in Figure 5-7 (a)-(d), balanced air suspensions on either side of the driving axles can provide equal suspension force transmitted to the vehicle body and drive axles. However, for each side of the OE suspensions, uneven airspring forces are loaded upon the vehicle body and the axles/wheels' mechanics, resulting in more pitch angle and increased axle/wheel wear and tear.

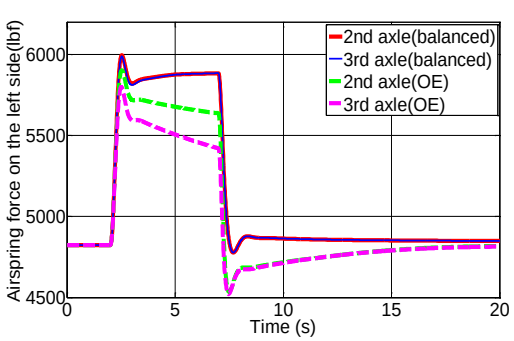

(a) Airspring force on left side (cornering)

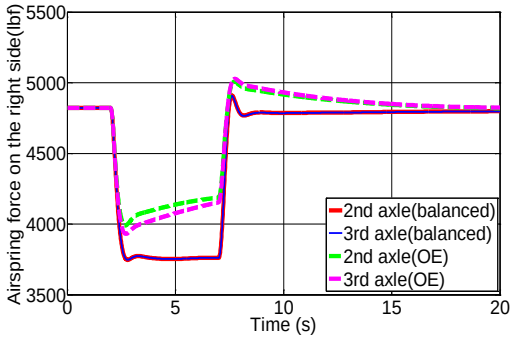

(b) Airspring force on right side (cornering)

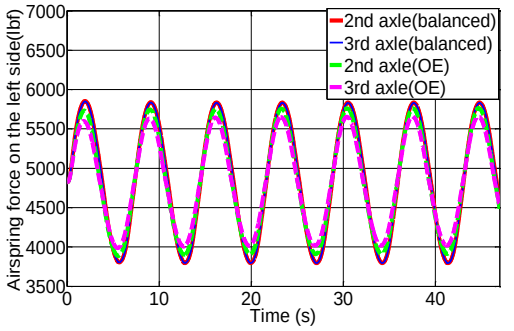

(c) Airspring force on left side (S-turn)

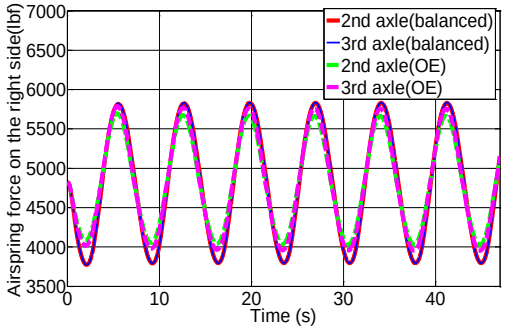

(d) Airspring force on right side (S-turn)

Figure 5-7. Time trace of airspring force on tandem driving axles for right-hand cornering and an S-turn

Suspension deflection on the driving axles and the mass flow rate at the leveling valves are shown, respectively, in Figure 5-8 (a)-(d). In comparison with the OE suspension, the balanced suspension has a small deflection and faster dynamic response to the load transfer. This implies that the balanced suspension has a higher bandwidth. Comparing the suspension deflection and flow rate at the leveling valve, Figure 5-9 (a) and (b) indicate that the leveling valves on opposite sides have opposition actions, with one adding air to the airsprings (on the jounce side) while the other one purges air (the rebound side) in response to the body roll. This results in the vehicle body returning to a leveled position more quickly, after it has been subjected to lateral forces (acceleration). The larger air hose diameters in the balanced pneumatic suspension result in less airflow resistance into or out of each airspring, better adjusting the air pressure in the airspring. Moreover, the lack of plumbing connection between the right and left airsprings plays an important role in maintaining the side-to-side balance forces. The leveling valve in the OE suspension provides unwanted adjustment of

airspring pressure on the sides opposite the leveling valve, although the small diameter of the pipes reduces the transient air pressure. As observed in Figure 5-8 (a)-(d), uneven and slow dynamic responsiveness of the OE air suspensions among the rear driving axles is obtained.

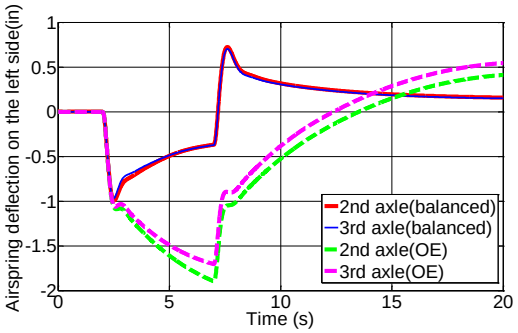

(a) Suspension deflection on left side (cornering)

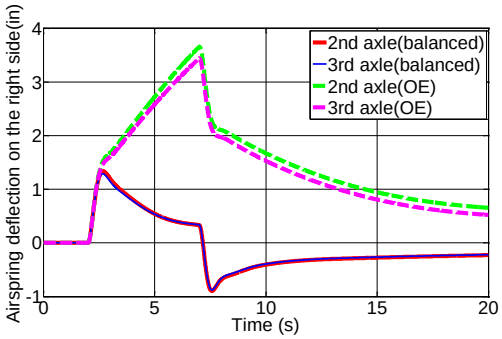

(b) Suspension deflection on right side (cornering)

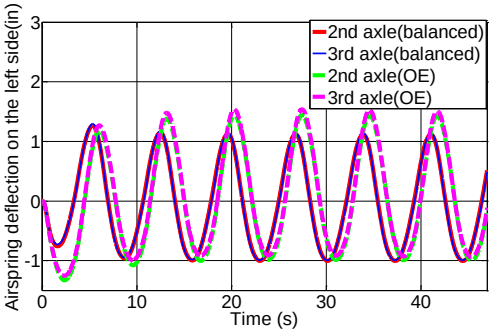

(c) Suspension deflection on left side (S-turn)

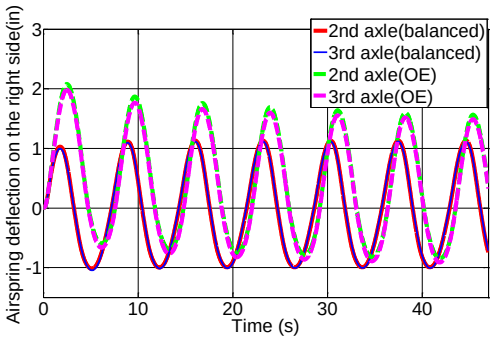

(d) Suspension deflection on right side (S-turn)

Figure 5-8. Time trace of suspension deflection on tandem rear axles for right-hand cornering and an S-turn

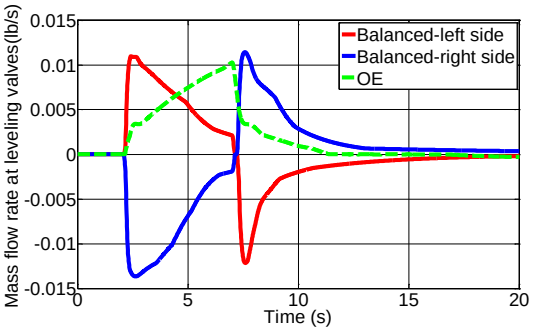

(a) Flow rate at leveling valve (cornering)

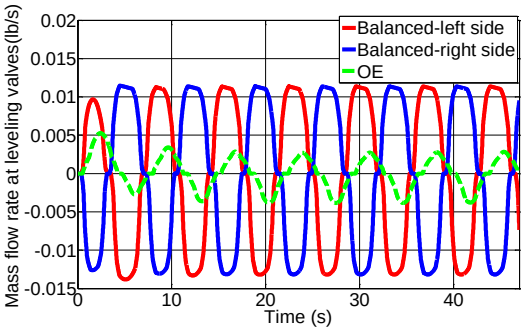

(b) Flow rate at leveling valve (S-turn)

Figure 5-9. Time trace of flow rate at leveling valves for cornering and S-turn

Figure 5-10 (a) illustrates that when the lateral force is applied, the roll angle reduces by the balanced suspension to a small value, balancing and keeping the truck body level. Additionally, the truck equipped with the balanced air suspension experiences a smaller maximum roll angle. When the lateral forces disappear after 7 seconds, as shown in Figure 5-10 (a), the balanced suspension enables the truck body to quickly return to the unrolled orientation with a shorter settling time than for the OE suspension. As shown in Figure 5-10 (c), in the S-turn, the balanced suspension results in a smaller roll angle as compared with the OE suspension. To the extent that the roll and pitch dynamic of the truck body couple, the balanced suspension results in less body pitch during the lateral maneuvers, as shown in Figure 5-10 (b) and (d).

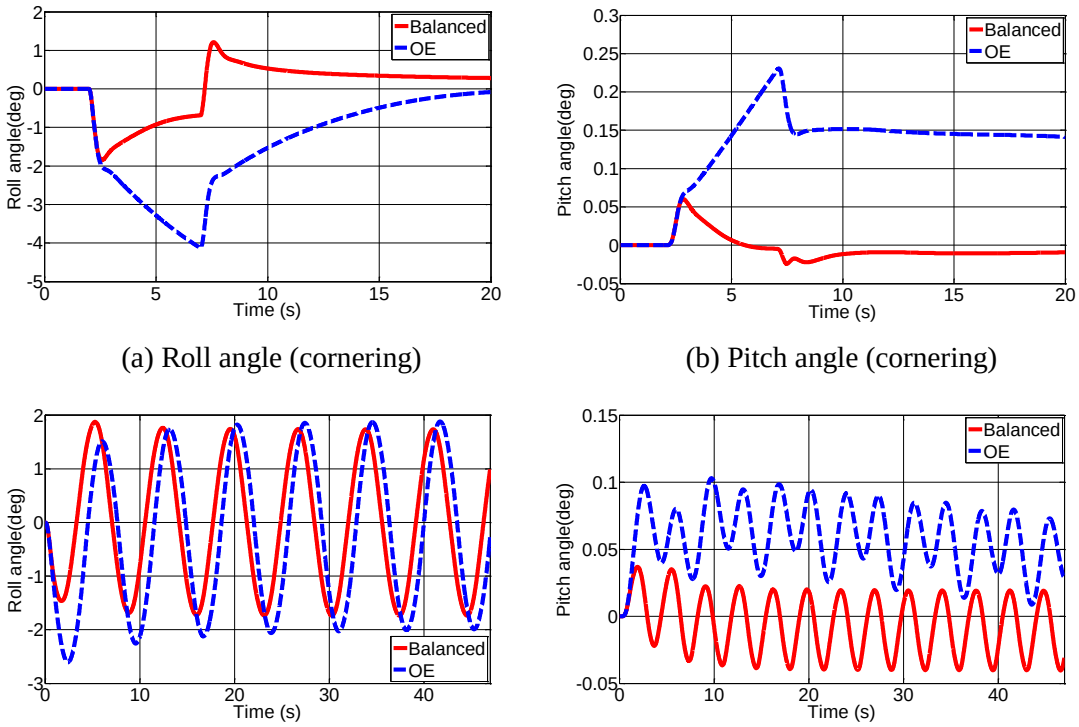

(a) Roll angle (cornering)

(b) Pitch angle (cornering)

(c) Roll angle (S-turn)

(d) Pitch angle (S-turn)

Figure 5-10. Time trace of roll angle and pitch angle for cornering and S-turn

5.3 Conclusions

In this chapter, the air suspension model coupled with truck multi-body dynamics has been developed and presented in detail. Based on the validated pneumatic components and suspension system models in chapter 4, the complete system model is employed to compare and analyze the performance of two air suspensions with different plumbing arrangements on the truck roll dynamics. The results of the simulation are summarized as follows:

(1) The leveling valves of the balanced suspensions can provide better adjustments to the body roll by charging the airsprings on the heavier side while dumping air out from the lighter side.

(2) When the dynamic load transfer is applied, higher and lower pressure in the balanced airsprings is obtained, respectively, on jounce and rebound than for the OE airspring. This contributes to the fact that the balanced suspensions are able to maintain a larger difference in pressure from side to side than the OE suspensions. Equal pressure is produced at the front and rear drive axles by the balanced suspension.

(3) In the steering maneuvers, compared with the OE air suspension, the balanced air suspension provides a larger restoring force to keep the suspension in the balance, contributing to a large anti-roll moment to resist the body roll motion.

(4) In cornering and S-turns, less suspension travel and quicker dynamic response are obtained for the balanced suspension compared with the OE suspension.

(5) During cornering and S-turns, lower roll and pitch angles are experienced by the truck with the balanced air suspensions, also providing a faster response of the body to the dynamic force changes.

Chapter 6 Achieving Pneumatic Anti-roll Bar through Suspension Balancing Control for a Semi-trailer Truck

This chapter proposes a novel anti-roll bar concept (balanced suspension) for heavy truck pneumatic suspensions through retrofitting conventional airspring suspensions such that they can resist body roll and provide additional roll stability to the vehicle. Anti-roll bars are commonly used in passenger vehicles to increase roll stiffness of the suspension, without increasing the vertical stiffness. The investigation suggests that the same can be accomplished in semi-trailer trucks by implementing two load-leveling valves and a symmetric plumbing circuit to achieve balanced side-to-side suspension forces. A multi-domain model that includes both the pneumatic details of the suspension and the dynamics of a semi-trailer truck is developed in a co-simulation environment and is used to extensively study the effect of the pneumatic anti-roll bar on vehicle dynamics. The simulation results indicate that, in comparison to conventional pneumatic suspensions, trucks with the proposed suspension experience better dynamic load sharing, more stable body roll, and better handling during steering maneuvers.

6.1 Simulation Dynamic Model

For evaluating the effect of the pneumatic anti-roll bar (balanced suspension) on the dynamics of the tractor and trailer combination, a co-simulation technique is applied to integrate the AMEsim pneumatic suspension model with a semi-trailer truck model in TruckSim. TruckSim is a simulation package specializing in the dynamic performance simulation of multi-axle commercial vehicles. It can provide a standard interface to Matlab/Simulink, allowing users to develop their self-designed components. This study employs a Class-8 semi-trailer truck model in TruckSim. Most parameters are defined based on the actual measurement of the vehicles, while some are based on the technical literature. If

the parameters, such as damper damping coefficient, and leaf spring stiffness, can't be determined, then the TruckSim default values are used. A list of all parameters used in the truck simulation can be found in Table C-1 of Appendix C.

6.1.1 Tractor Model

A 6×4 tractor unit model is developed in TruckSim, according to the tractor manufactured by Volvo, Model VN770, as shown in Figure 6-1. The tractor model has one steering axle with single tires, and two tandem rear axles with dual tires. The steering axle has leaf spring suspensions installed, whereas the tandem drive axles are equipped with air suspensions.

Figure 6-1. A 6x4 tractor model in TruckSim

6.1.2 53-ft Trailer Model

The dynamic characteristics of a 53-ft van trailer are modeled, as shown in Figure 6-2. The semi-trailer model does not have a front axle, but includes two axles at the rear, each with dual wheels. Both axles are equipped with pneumatic suspensions. In the simulation, the truck is simulated under three trailer load conditions: empty, half load, and full load, as illustrated in Table 6-1. The load is distributed uniformly.

Figure 6-2. A 53-ft semi-trailer truck model in TruckSim

Table 6-1. Three different load conditions

Case	Load weight	load distribution	Load CG height
Empty	Empty load (0 lbs)	Uniform	N/A
Half load	Half load (22525 lbs)	Uniform	106 in relative to ground
Full load	Full load (45049 lbs)	Uniform	106 in relative to ground

6.1.3 Fifth-wheel Coupling Model

The semi-trailer unit is attached to the semi-tractor unit with a fifth-wheel coupling. Figure 6-3 shows how this coupling is achieved by a fifth-wheel. The fifth-wheel is mounted on the rear of the tractor, and a kingpin (yellow component in Figure 6-3) is attached to the front of the semi-trailer. The fifth-wheel can transmit only the roll and pitch moments between the two units, but not the yaw moment.

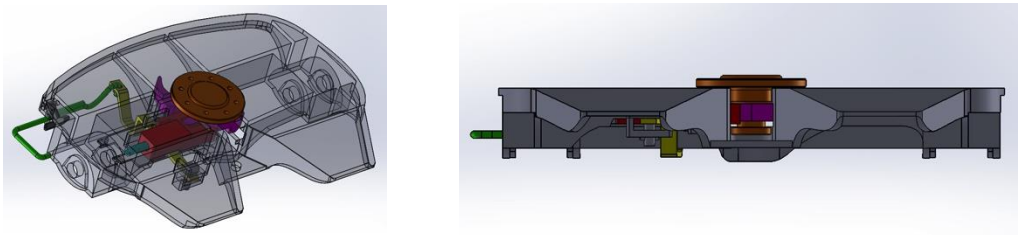

Figure 6-3. CAD model of fifth-wheel coupling

6.1.4 Pneumatic Suspension System Model

For the present study, four different pneumatic suspension systems are modeled: OE suspensions on both tractor and trailer (OE/OE), balanced suspensions on tractor and OE suspensions on trailer (Balanced/OE), OE suspensions on tractor and balanced suspensions on trailer (OE/Balanced), and balanced suspensions on both tractor and trailer (Balanced/Balanced), as shown, respectively, in Figure 6-4 (a)-(d). All of these pneumatic suspension systems are modeled by AMEsim, as shown in Figure C-1 of Appendix C. Corresponding parameters are listed in Table C-2.

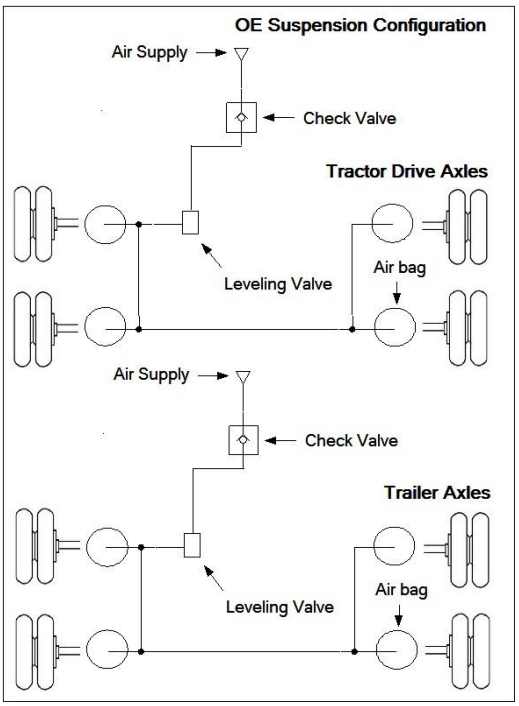

(a)

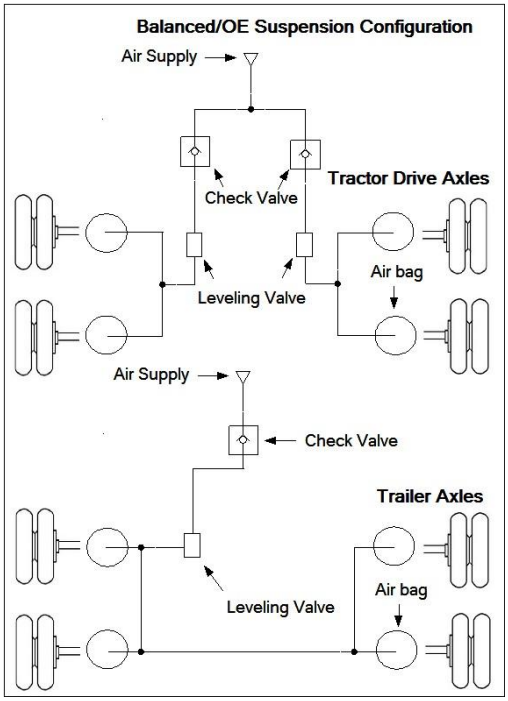

(b)

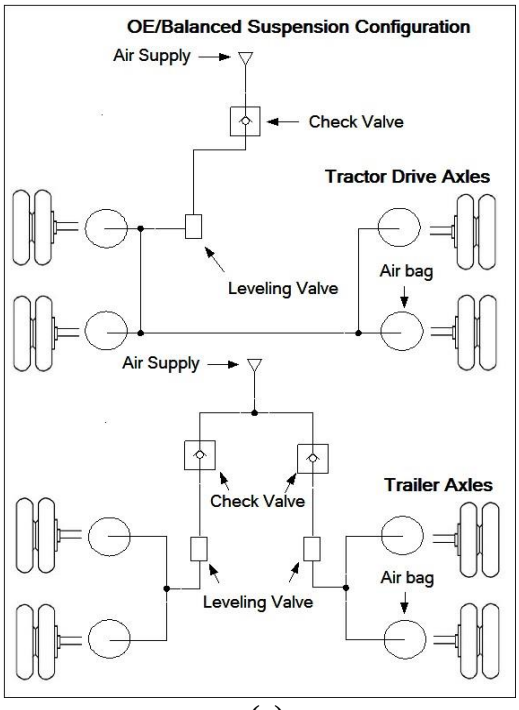

(c)

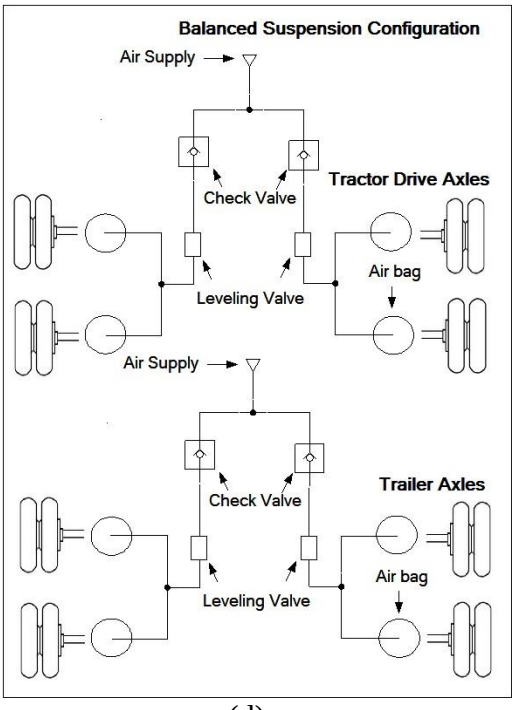

(d)

Figure 6-4. Plumbing configurations of heavy truck pneumatic suspensions: (a) OE/OE suspensions, (b) Balanced/OE suspensions, (c) OE/Balanced suspensions, and (d) Balanced / Balanced suspensions

6.1.5 Development of Co-simulation Environment

To integrate the semi-trailer truck dynamics with the airflow dynamics of the pneumatic suspension, a co-simulation environment is established by using three types of software, AMEsim, TruckSim, and Matlab/Simulink, as shown in Figure C-2 of Appendix C. Matlab/Simulink is used to provide a platform for the interconnection of the two dynamic models as two S-Function modules. To convert the AMEsim model into a Simulink module, a compiler (Microsoft Visual C++) is necessary. Furthermore, an environmental variable must be set in the computer to determine the installation direction of Matlab. The TruckSim model can be imported into the Simulink as a S-Function through a DLL file. This interaction must ensure that the airspring force provided by the pneumatic suspension model is sent to the truck model. Simultaneously, the suspension deflection is fed back into the pneumatic suspension model from the vehicle model, as depicted in Figure 6-5. The co-simulation needs a fixed time step set for Simulink, TruckSim, and AMEsim in order to ensure that the differential equations will be calculated from the same initial time at each step. Typically, the error tolerance has to be reduced appropriately to minimize the integration "noise" resulting from the amplified variation of some variables. However, too much reduction in the error tolerance can lead to an extremely slow calculation, which is undesirable.

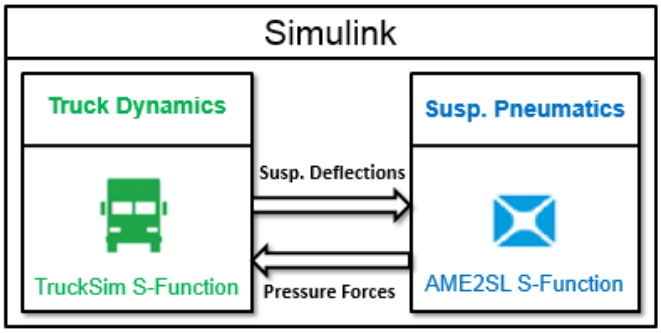

Figure 6-5. Co-simulation environment

6.2 Simulation Maneuvers

There are two types of maneuvering inputs in TruckSim: open-loop maneuvers and closed-loop maneuvers. The open-loop maneuver pre-defines the steering angle input, which is

independent of response of the vehicle and the driver. The closed-loop maneuver is based on a pre-defined path input so that the steering angle is computed with appreciated consideration of responses of the vehicle and driver. The present simulation adopts the latter type of maneuvering input, and the two maneuvers selected to be simulated are 1) single lane change, and 2) steady-state cornering.

(a) Single Lane Change

This test maneuver is conducted to determine the transient response of a vehicle when a sudden path change is applied. The simulation results are used to compare the transient roll control characteristics of the vehicle with different pneumatic suspension systems. The test procedure involves driving a truck from the initial lane to another parallel lane following a predetermined path, as shown in Figure 6-6.

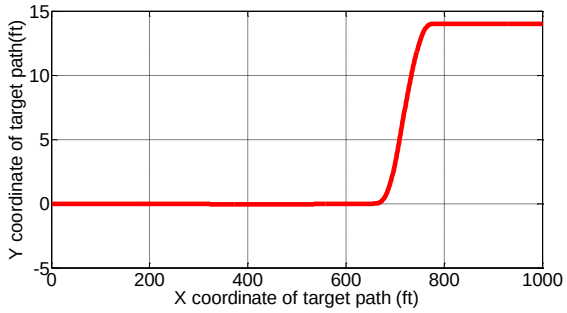

Figure 6-6. Target path for the single lane change maneuver

(b) Steady-state Cornering

In this test maneuver, the truck starts from a straight track and then enters a circular trajectory with a constant radius of 262.5 ft. The target path in global coordinates is shown in Figure 6-7. This maneuver is designed to evaluate the transient behavior (sprung mass roll) of the vehicle, and to qualify the steady-state cornering behavior of a vehicle.

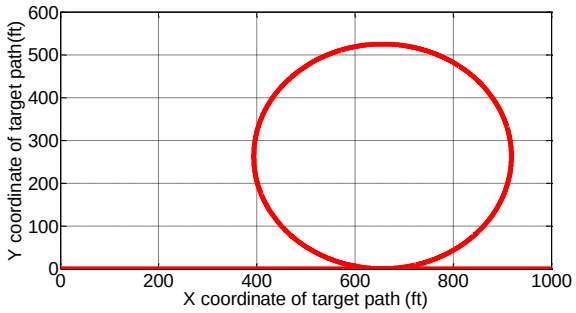

Figure 6-7. Target path for the single lane change maneuver

6.3 Simulation Results and Analysis

The simulation is performed with balanced suspensions and OE suspensions, respectively, on both tractor and trailer for a single lane change maneuver at 35 mph and steady state cornering at 28 mph. The simulation results of the two suspension control systems are compared to investigate how the balanced suspension system improves the dynamic roll behavior of the truck. Figure 6-8 illustrates the lateral acceleration results for tractor and trailer for the single lane change maneuver and the steady-state cornering maneuver.

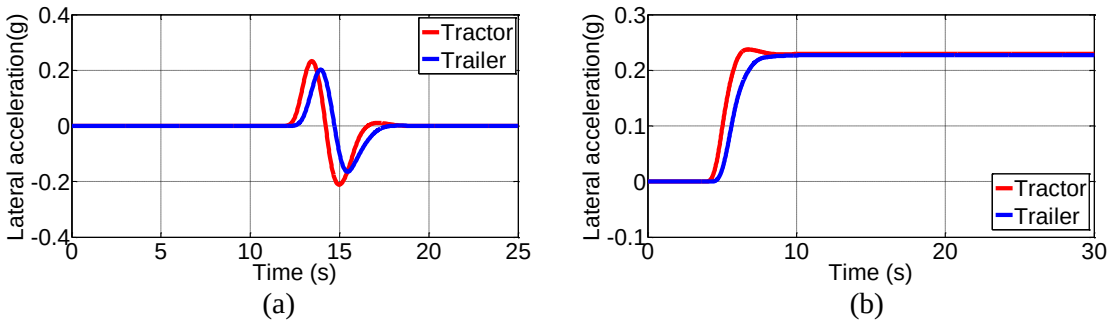

Figure 6-8. Simulation results of lateral accelerations on the tractor and trailer for (a) single lane change and (b) steady-state cornering

Figure 6-9 shows the body roll angles of the tractor and trailer during the steering maneuvers. Compared to the OE suspension, the balanced suspension contributes to smaller peak roll values. Peak-to-peak values of roll angles for the single lane change are reduced by nearly 8%, and the maximum roll angle during steady-state cornering is diminished by as much as 16.5%. The balanced suspension is capable of leveling the truck body during steady state cornering.

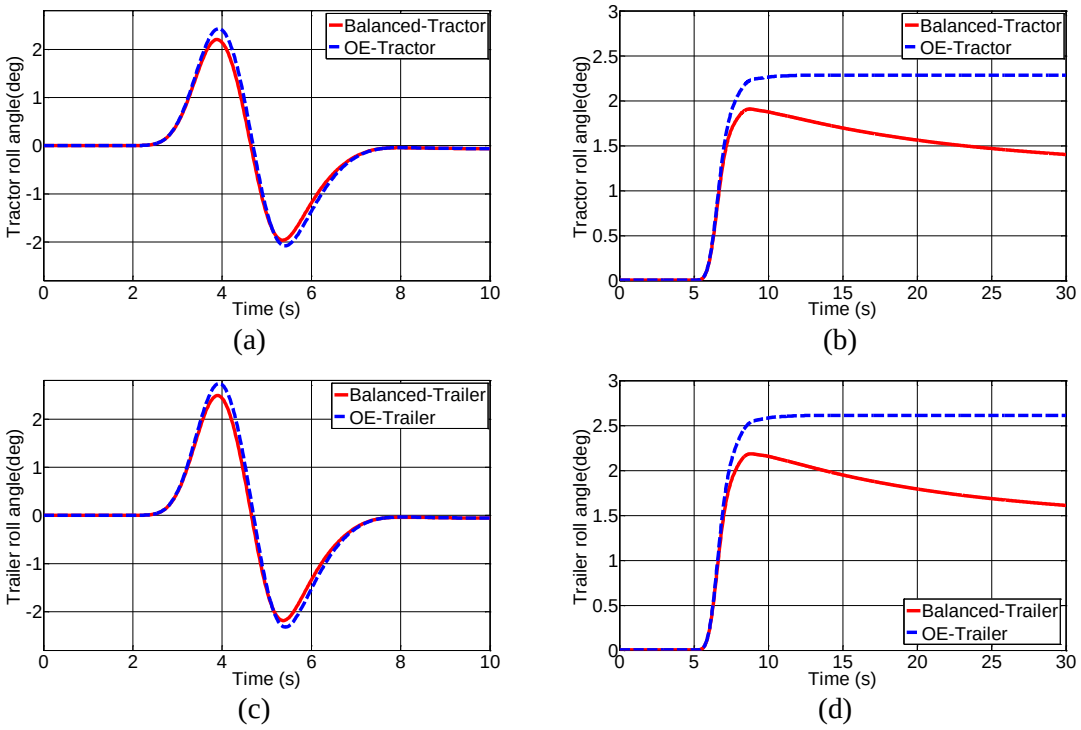

Figure 6-9. Simulation results of roll angles on the tractor and trailer for (a, c) single lane change and (b, d) steady-state cornering

The flow rate time responses plotted in Figure 6-10 reveal that in the balanced suspension, the airsprings on each side share an equal amount of airflow. Moreover, the balanced suspension allows the two leveling valves to operate in opposition, i.e. one airspring can be inflated, while the other one purges the air at the same flow rate in response to the body roll. Obviously, the leveling valves in the balanced arrangement also provide larger flow rates than the OE valves.

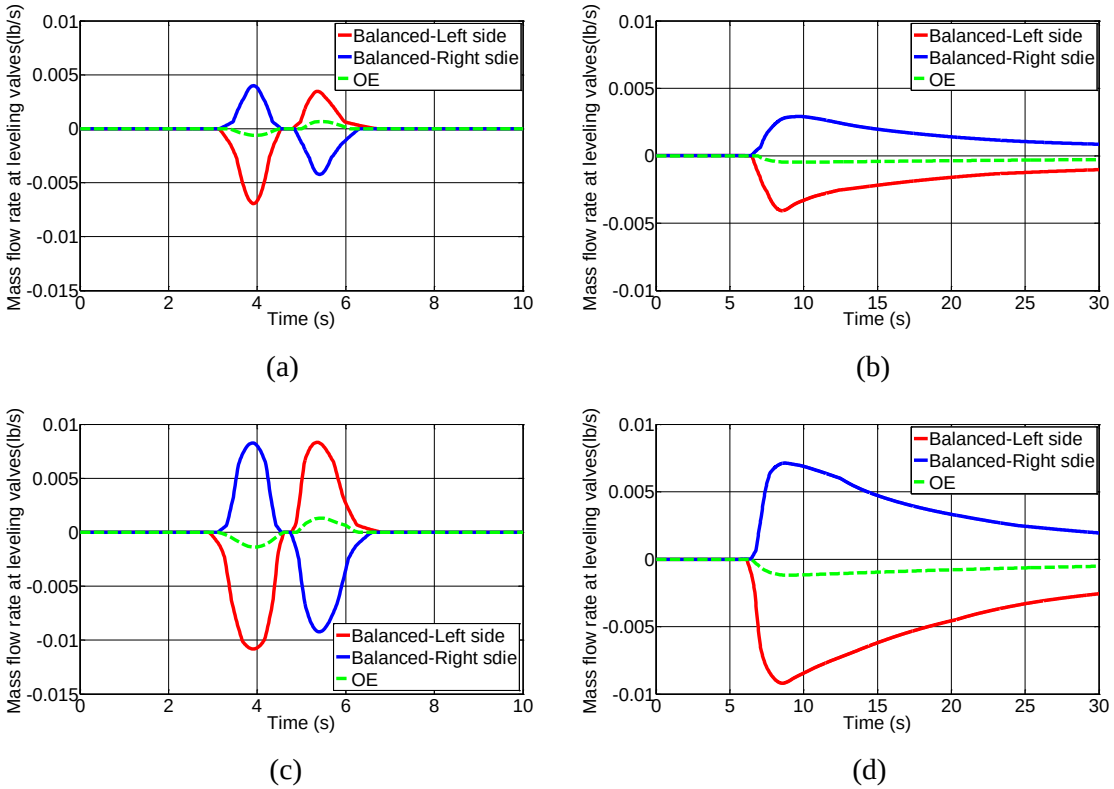

Figure 6-10. Simulation results of mass flow rate at the leveling valves on the tractor and trailer for (a, c) single lane change and (b, d) steady-state cornering

Figure 6-11 shows the trailer airspring pressure on the left and right sides for the two maneuvers. The same trend of pressure change is applied to the tractor airsprings. Balanced suspensions show considerably larger side-to-side pressure differences during steady state cornering. However, pressures for the OE suspensions are almost identical on both sides. Consequently, a larger restoring force is obtained for the balanced suspension from side to side to better control the body roll motion. During the single lane change maneuver, the balanced suspension minimizes the pressure variations between front and back, resulting in a better dynamic load sharing among the axles and pitch performance control. Nevertheless, for the OE suspension, the pressure of the airsprings is considerably more disorganized.

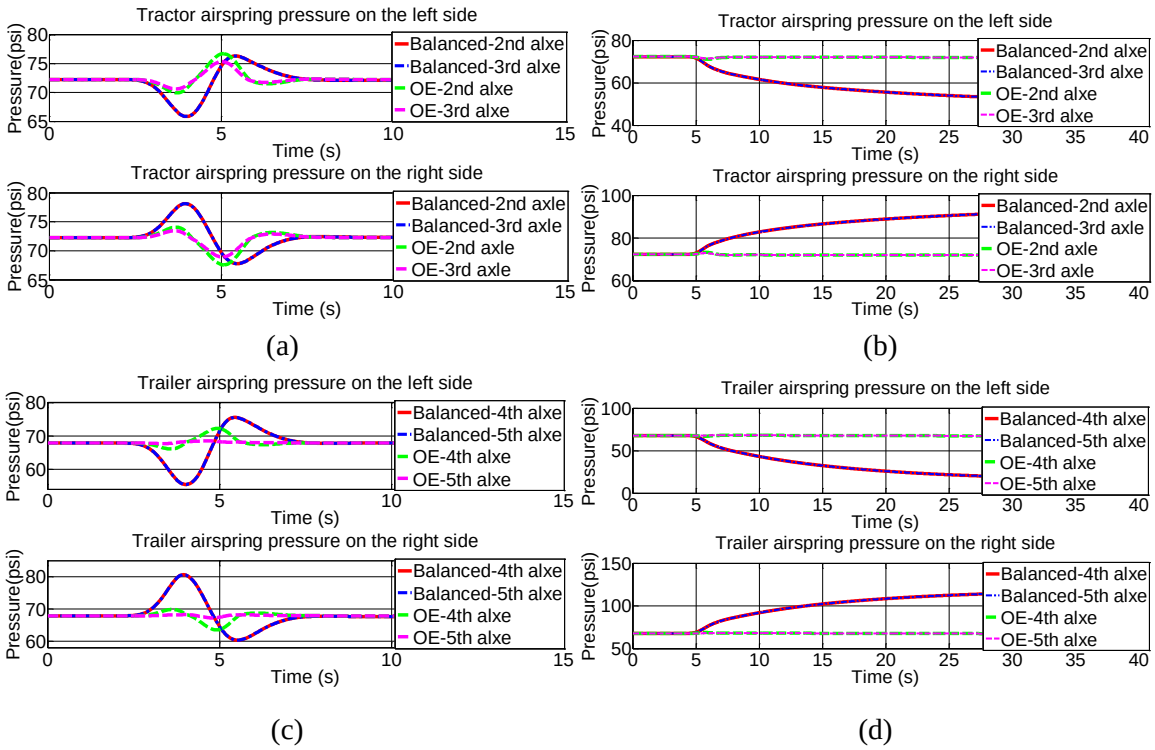

Figure 6-11. Simulation results of airspring pressures on the tractor and trailer for (a, c) single lane change and (b, d) steady-state cornering

Figure 6-12 illustrates the results of airspring anti-roll moment with respect to the roll angle for the two steering maneuvers. The balanced suspension provides greater anti-roll moments than the OE suspension for better resisting vehicle body roll. As shown in Figure 6-12 (a) and (c), the work done by the balanced suspension is positive with a clockwise hysteresis circle, while the OE suspension performs negative work with a counter-clockwise hysteresis circle. This implies that the OE suspension system dissipates energy by balancing pressure from side to side, whereas the balanced suspension system draws additional air energy to resist the roll motion, benefiting from the adjustment of the leveling valves. Narrowing the anti-roll moment circle (reducing the hysteresis effect) for the balanced suspension can reduce the air consumption and improve the roll stiffness.

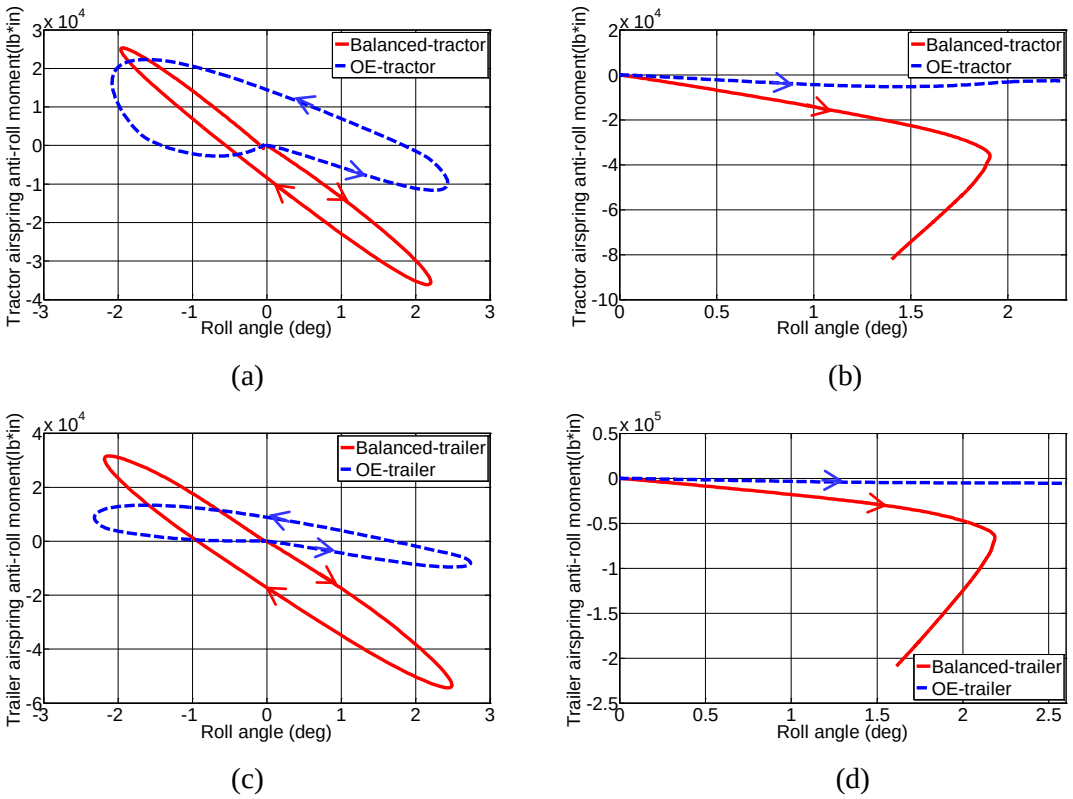

Figure 6-12. Simulation results of anti-roll moment versus roll angle on the tractor and trailer for (a, c) single lane change and (b, d) steady-state cornering

The roll stiffnesses of the balanced and OE suspensions are compared in Figure 6-13. The balanced suspension increases the roll stiffness as the roll angle increases, while the OE suspension maintains the original stiffness. Due to the adjustability of the roll stiffness, the balanced suspension can operate as an active anti-roll bar and improve the roll stability and the driver's handling of the vehicle.

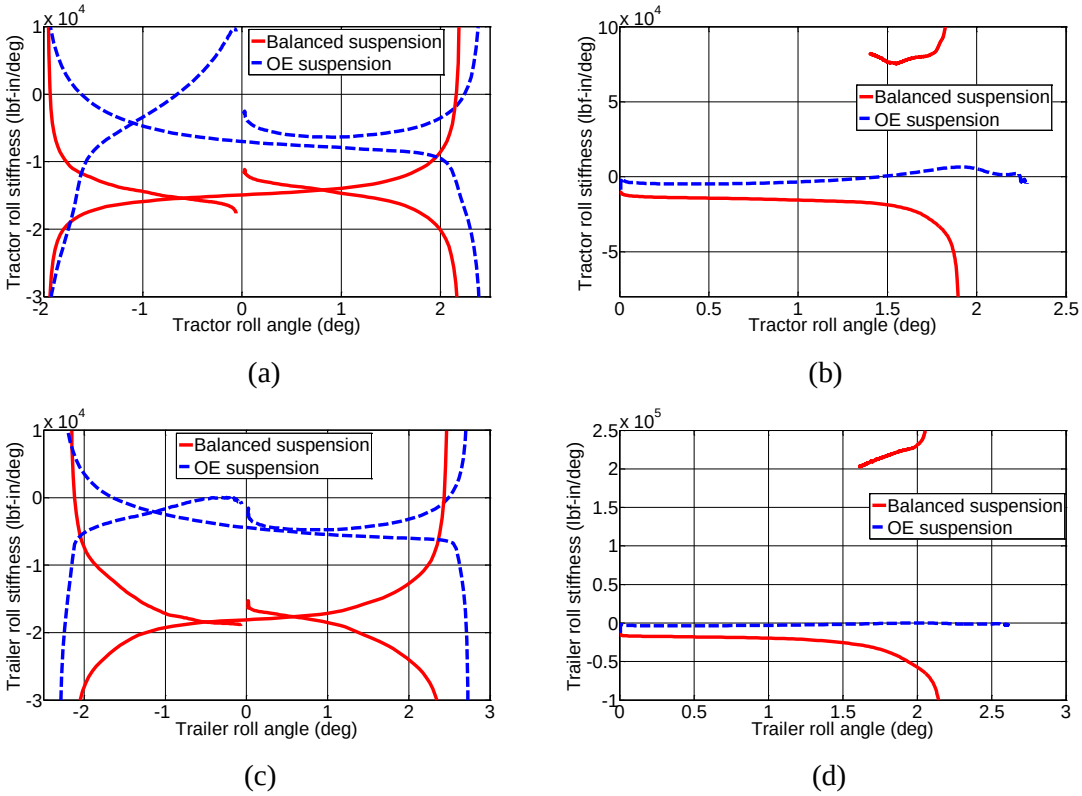

Figure 6-13. Simulation results of roll stiffness versus roll angle on the tractor and trailer for (a, c) single lane change and (b, d) steady-state cornering

6.4 Summary of Simulation Results

Eventually, extensive simulations are executed to further assess the performance of the balanced suspension system. Single lane change simulation is run under different load conditions and at different speeds to evaluate peak-to-peak values of the roll angle. Three load conditions considered are shown in Table 6-1. This simulation study includes two more suspension configurations: balanced suspensions on the tractor and OE suspensions on the trailer (balanced/OE), and OE suspensions on the tractor and balanced suspensions on the trailer (OE/balanced). Figure 6-14 (a-f) illustrate that the balanced suspension system results in a better body roll control in all study cases. Equipping the balanced suspension on both the tractor and trailer results in the lowest body roll. The truck with balanced suspensions only on the trailer performs better roll control compared to balanced suspensions only on the tractor.

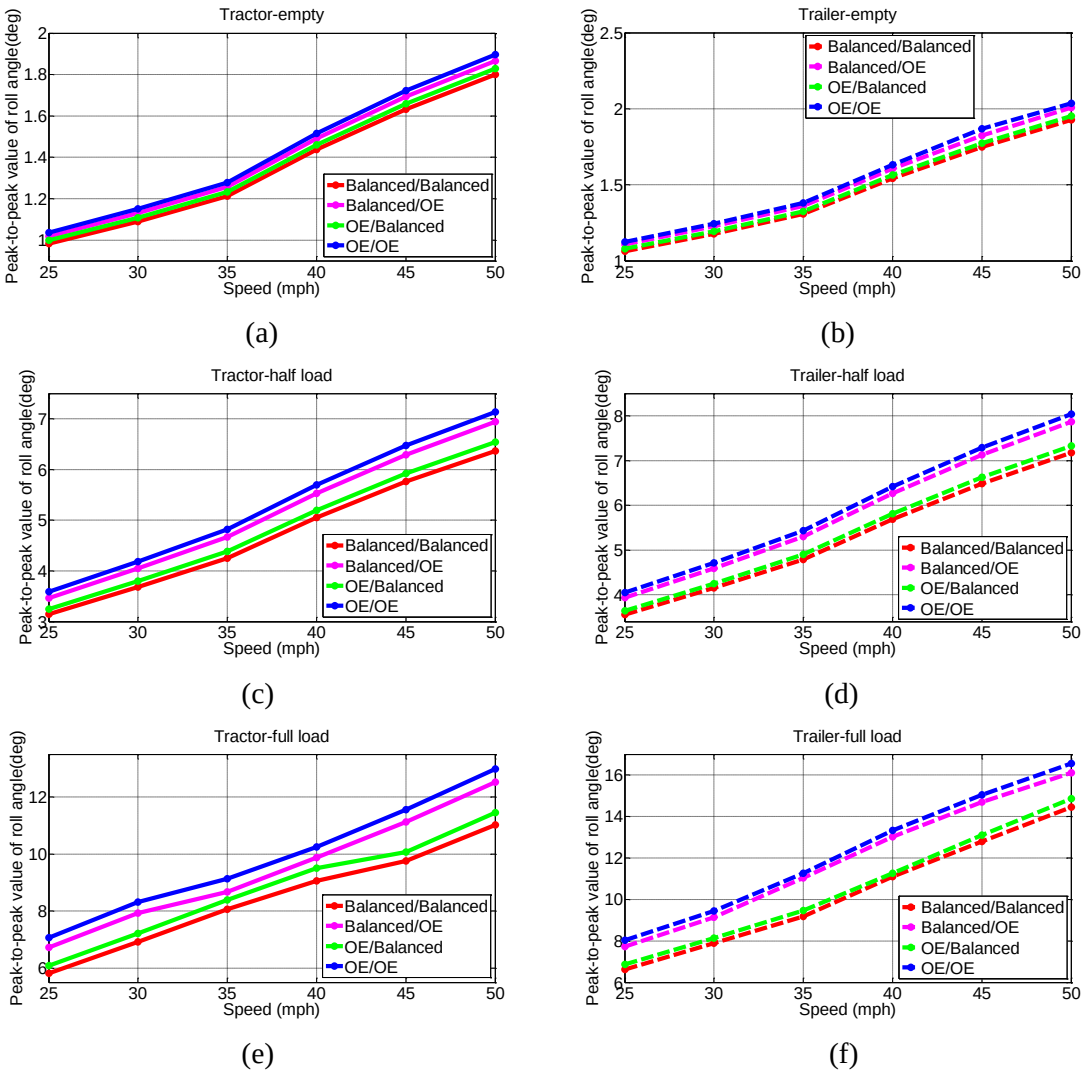

Figure 6-14. Summary of peak-to-peak value on the tractor and trailer for (a, b) empty, (c, d) half load, and (e, f) full load during the single lane change

Figure 6-15 shows the peak roll angle attained during the steady state cornering for all four different suspension control systems. The simulation results suggest that the balanced suspension control system is able to lower the peak roll angle in response to the steering maneuver. However, this phenomenon is not clearly apparent in the empty trailer case. Based on the reduction of the peak body roll, all four suspension control systems are ranked from the best to the worst: Balanced/Balanced, OE/Balanced, Balanced/OE, OE/OE.

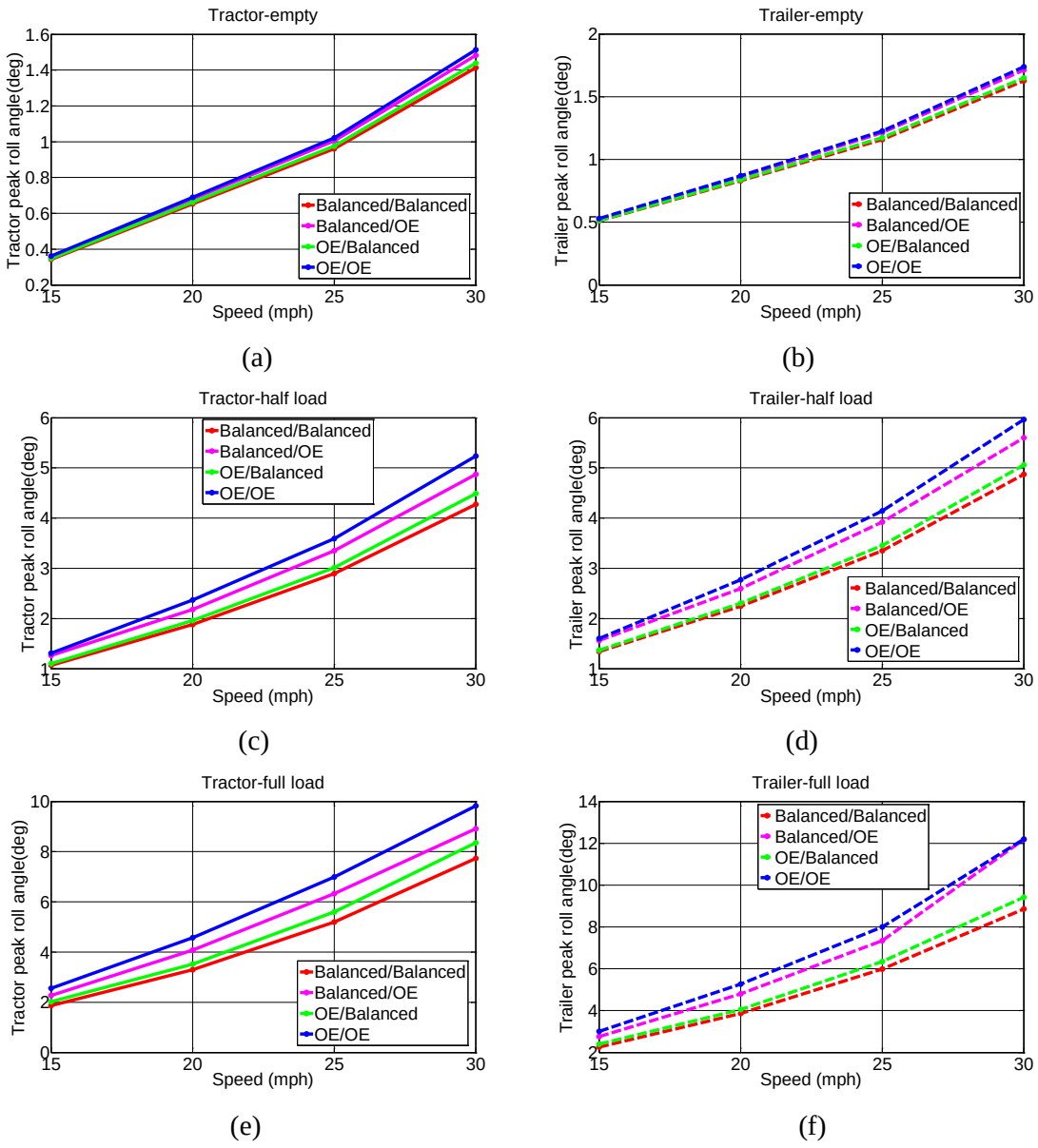

Figure 6-15. Summary of peak-to-peak value on the tractor and trailer for (a, b) empty, (c, d) half load, and (e, f) full load during steady-state cornering

6.5 Conclusion

In this chapter, a novel pneumatic anti-roll bar (balanced suspension) implemented by modifying the OE suspension is introduced and evaluated through an extensive set of simulations. A hybrid model is developed by coupling the pneumatic suspension model and

the full truck dynamic model in a co-simulation environment. The model is used to numerically investigate the effect of the balanced suspension on the roll dynamics of the articulated vehicle. The simulation results indicate that the proposed pneumatic suspension arrangement is capable of providing higher restoring force by regulating the air pressure and airflow in the airsprings. The truck with the modified suspension system serving as an active anti-roll bar exhibits lower body roll motion and less side-to-side sway, thereby improving the vehicle roll stability and handling.

Chapter 7 Failure Mode and Effects Analysis of Dual Leveling Valve Airspring Suspensions on Truck Dynamics

Failure mode and effect analysis are performed for the dual leveling valve pneumatic suspension to determine the effect of failures on truck dynamics using the model that couples the dynamics of detailed suspension pneumatics in AMEsim (commercial software) with a truck dynamics model in TruckSim. As differentiated from the single leveling valve suspension, the dual leveling valve suspension is designed with one leveling valve on each side to better maintain the balance of the vehicle body both statically and dynamically. A key element of the failure analysis is to determine how the body roll is affected if and when one or more components fail. By analyzing the function and composition of each component, a matrix is developed for failure modes and their effects. Relative to other components, the matrix assigns more failure modes to the leveling valve, such as getting stuck, bending of the control rod, and misalignment of the leveler arm. The pneumatic suspensions and their failure modes are modeled in AMEsim. The pneumatic suspension model is then integrated into TruckSim to study the consequences of the suspension failures on truck dynamics. The simulation analysis shows that the second leveling valve in a dual-valve arrangement brings a certain amount of failure redundancy to the system, in the same manner that when one side fails, the other side acts to compensate for the failure. Additionally, if the trailer is also equipped with dual leveling valves, such an arrangement will bring an additional stabilizing effect to the vehicle in case of a tractor suspension failure. There exists a reciprocal effect between the tractor and trailer failure: the trailer effet on stabilizing the tractor in case of suspension failure is reciprocated by the tractor in case such failures happen on the trailer suspension.

7.1 Introduction

Air suspensions are extensively used on highway semi-truck and -trailers to provide a softer ride and better handling [3]. In general, air suspensions require a load-leveling mechanism to

maintain the vehicle's intended ride height for widely varying loads that occur in loaded, unloaded, and bobtail operation conditions. Besides the leveling valve, air suspensions include regulator valves, air tanks, hoses, and fittings. These components can be put together in different configurations, which include employing one or two leveling valves. The schematic in Figure 7-1 (a) depicts a common plumbing configuration for a suspension with one leveling valve. We will refer to this configuration as "original equipment suspension (OE)." The primary advantages of using this configuration are lower cost and easier installation. This configuration, however, is not well-suited for controlling the roll and pitch dynamics of the truck [53]. Figure 7-1 (b) presents an alternative plumbing configuration with dual leveling valves and a symmetric pneumatic circuit on semi-truck rear tandem axles. This suspension configuration is also applied to the trailer's dual axles. We will refer to this configuration as "balanced suspension (BA)." The balanced suspension is able to provide a separate leveling control for each side through a balanced pressure and a well-regulated airflow [53]. The independent control yields a variable roll stiffness that increases with increasing body roll. Test data [5] have shown that a truck with the balanced suspension experiences less body roll and a faster return to leveled orientation during dynamic maneuvers, as compared with the OE suspension. The basic theory for the balanced suspension is that in response to the body roll, air pressure (airspring force) on the jounce side increases, while air pressure (airspring force) on the rebound side decreases, resulting in balanced suspension forces to perfectly level the truck body. The independent control configuration implies that even when one side fails, the other side still works as intended to maintain the balanced truck body. In addition, if either the tractor or trailer is encountering the suspension failure, the suspension on the other unit can still function to resist the truck body roll.

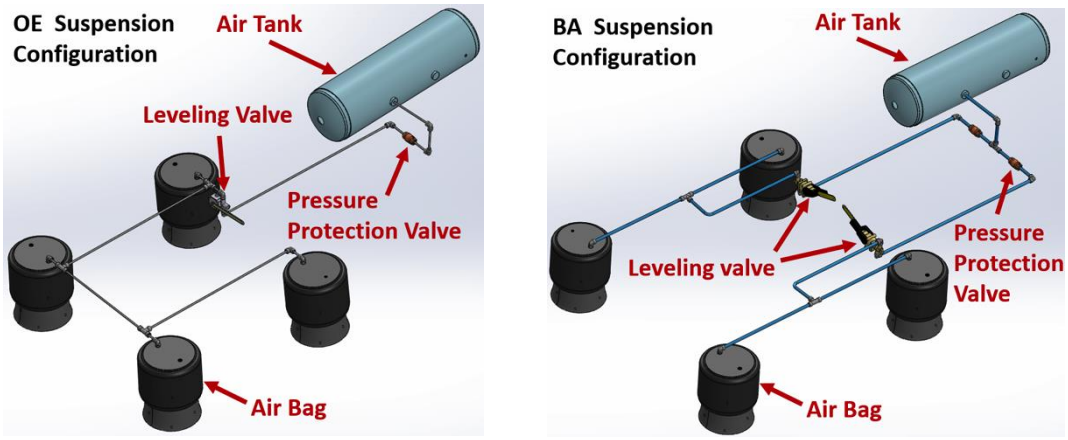

(a) (b)

Figure 7-1. (a) Original equipment (OE) and (b) balanced (BA) configurations on the semi-truck drive axles

In this chapter, failure mode and effect analysis for the pneumatic suspension system are studied. Specially, a multi-domain dynamic model is prepared. Simulations are conducted to investigate the effect of any pneumatic component failure on the suspension responsiveness and truck roll performance for the balanced suspension system. Primarily, the pneumatic suspension system is broken down into the component level to identify the potential failure of each component, including its causes and effects [59-62], resulting in establishing a failure mode and effect spreadsheet. Based on the spreadsheet, three representative failure modes are determined for the study, and are modeled separately in AMEsim. The pneumatic suspension model is then coupled with the single-trailer truck (WB-67) model in TruckSim. The combined model is used to investigate the performance of pneumatic suspensions on controlling the roll motion of the semi-trailer truck while one of the failures occurs. The simulation results for the failure cases are compared between the balanced suspension and the OE suspension through analyzing the mass flow rate at the leveling valve, the suspension dynamic response, and the vehicle body roll. The chapter concludes with a discussion of the simulation results.

7.2 Failure Cause and Effect Studies for a Semi-truck Pneumatic Suspension System

This section mainly includes recognizing various failure modes of the heavy truck pneumatic suspension and determining their effect. The pneumatic suspension system for heavy truck application consists of many components; therefore, it is necessary to identify the failure mode for each element/subsystem and categorize the various failure effects [59-64]. As shown in Figure 7-2, the balanced suspension components that are included in this analysis are:

- Leveling valves
- Air fittings (tee connector, elbow connector, etc.)
- Air hoses
- Regulator valves

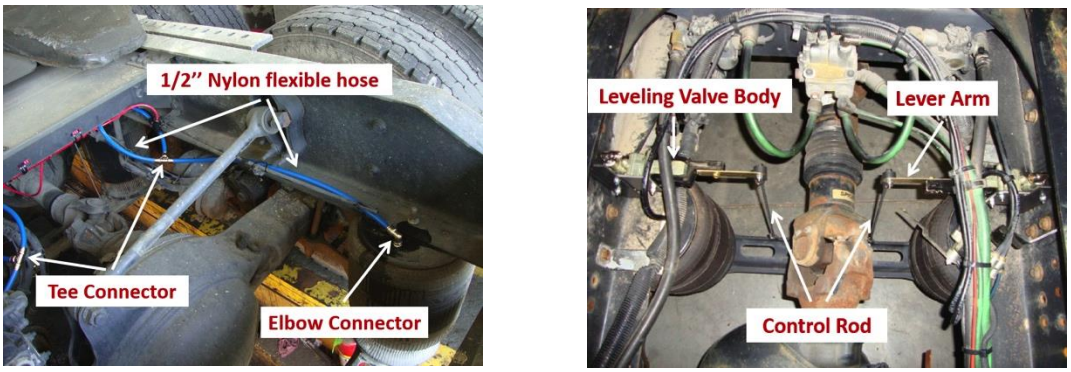

(a) (b)

Figure 7-2. Pneumatic suspension system: (a) air fitting and air hose, and (b) leveling valve

The potential failures of the components and their causes are determined as follows:

(1) Failure modes of the leveling valve: there are three different failure modes for the leveling valve:

- The valve clogs: The air impurities can cause the flow area of the leveling valve to become clogged (affects the inflation or the deflation or both). In the case of this failure, no air is even supplied into or dumped from the airsprings through the leveling valve.

- Control rod becomes detached: The failure takes place when the end of the rod disconnects from the lever arm or the vehicle axle, or the rod is broken. In this failure mode, the leveling valve completely loses the ability to sense the suspension deflection such that the leveling valve will stay closed at all times. Air mass in the airsprings on the affected side will remain unchanged until the failure is fixed.
- Control rod bends: The bending deformation of the control rod results in pulling down the lever arm to deflate the airsprings. This failure can result in a decrease of ride height and poor ride comfort. The same failure effect can also result from the bending of the bracket connecting the control rod and axle.

(2) Failure modes of the air fittings: The air fittings used for the balanced suspension include tee connectors, elbow connectors, and straight union connectors, among others. The failure mode of the air fittings is determined to be cracking due to excessive air pressure loading. Any such failure will result in an air leak at the point of failure.

(3) Failure modes of the air hoses: The failure of air hoses is considered to be a rupture, leading to system air leakage. Even though the air hoses are qualified for high-pressure application, the failure could happen due to fatigue and rotting. The leakages of air fittings and hoses can also be attributed to incorrect assembly procedure and poor installation that are, however, not considered to be the failure modes of the components.

(4) Failure modes of the regulator valve: The clogging can occur when the regulator valve is stuck due to a piece of debris jamming itself into the check valve. However, because the air from the air supply has been filtered and the flow area of the regulator valve is designed to be larger relative to the restrictor (leveling valve), the likelihood of this failure is very small. Therefore, the failure of the regulator is not considered in this investigation.

As shown in Table 7-1, a spreadsheet is established summarizing the failure modes and effects discussed. Since some failure modes cause identical failure effects, we will combine them for the failure effect evaluation via modeling and simulation. For example, suspension system air loss is considered as one study case, representing the related failure modes. In addition, multiple failure modes are assigned to the leveling valve. By classifying the failure effects as shown in Table 7-1, a total of three representative failure cases are identified:

- Fully-blocked leveling valve (no air flow)
- Control rod bending of the leveling valve
- Suspension system air loss

In the following sections, the effect of the representative failures for the balanced suspension on semi-trailer truck dynamics will be evaluated by using modeling and simulation.

Table 7-1. FMEA spreadsheet for the pneumatic suspension system

Part name	Failure mode	Failure effect
Leveling valve	The valve clogs	No air supplied to or dumped out of the airspring on the affected side (Note: The control rod detachment causes no air flow in and out of the airspring.)
	Control rod becomes detached	
	Control rod bends	Ride height on the affected side becomes lower
Push-to-connect Air fitting (elbow, straight, tee, etc.)	Mechanical rupture	Suspension system air loss
Flexible nylon hose	Rupture	

7.3 Pneumatic Suspension and Truck Dynamic Simulation Model

This section introduces how to model the three representative failures based on the pneumatic suspension developed in AMEsim, and the WB-67 truck dynamic model developed in TruckSim.

7.3.1 Modeling of Fully-blocked and Control Rod Bending of the Leveling Valve

In this simulation, the failure mode regarding the fully blocked leveling valve is modeled by setting the flow area to zero. While the control rod is bent, the straight-line distance from end

to end is reduced. The failure is simulated by shifting the flow characteristics of the leveling valve, as shown in Figure 7-3. The shift is directly proportional to the reduction of the rod's length due to bending. The failure considered in this paper is to shorten the rod length by 0.8 in.

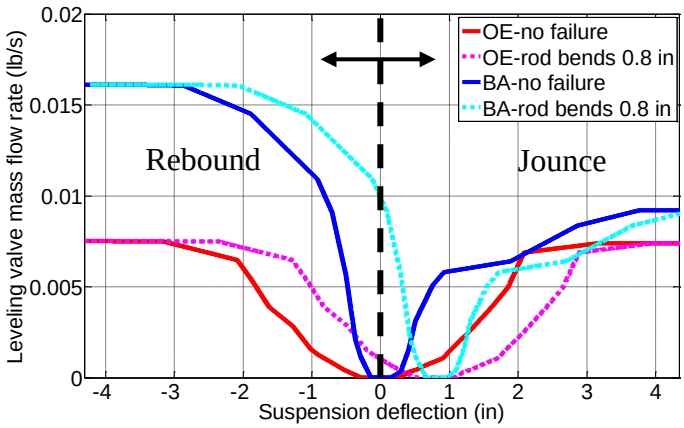

Figure 7-3. The effect of the control rod's bending on flow characteristics of the leveling valve

7.3.2 Modeling of Suspenison System Air Leak

Suspension system air leak is modeled by adding one port at the location of the failure, as shown in Figure 7-4. A pneumatic orifice model has been attached to the extra port such that the orifice flow area represents the size of the rupture. If the leak occurs between the air tank and leveling valve, the compressor can maintain the supply pressure to a specified value so that the system still functions well. If the air leakage takes place in any component between the leveling valve and airsprings, it will affect the inflation and deflation of the airspring, causing a system failure. The rupture area in the simulation is assumed to be 0.00775 in^2.

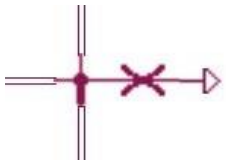

Figure 7-4. Pneumatic suspension air leak model in AMEsim

The three representative failure cases are modeled separately for the balanced (BA) suspension and the OE suspension on the tractor's tandem drive axles. The present

simulation focuses on the study of the suspension failure occurred only on the tractor drive axles. The simulation results on the tractor axles are also applicable to the trailer axles. Figure 7-5 shows which component in the suspension system fails for each failure case simulated in the study.

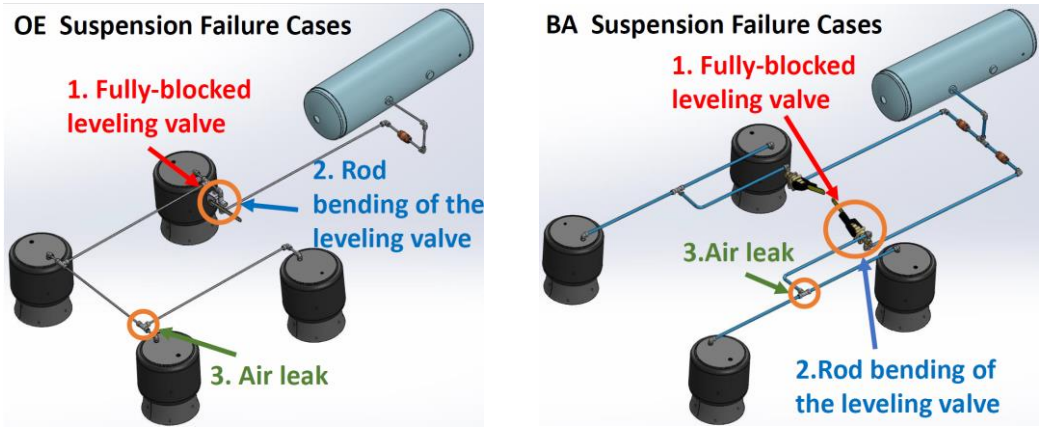

(a) (b)

Figure 7-5. Failure cases of (a) original equipment (OE) and (b) balanced (BA) suspension on the semi-truck drive axles

7.3.3 Full-truck Multi-body Dynamics Model Integration

The pneumatic suspension model developed in AMEsim is integrated into a WB-67 truck dynamic model in TruckSim by a co-simulation technique [13-15]. The tractor's tandem drive axles and the trailer's axles are equipped with pneumatic suspensions as shown in Figure 7-6. The integrated truck dynamic model is capable of simulating the effect of suspension fluid dynamics on truck roll performance. The parameters for the pneumatic suspension model and truck dynamic model are included in Table B-1 and Table B-2.

Figure 7-6. WB-67 semi-trailer truck model in TruckSim

7.4 Simulation Analysis of the Suspension Failures

7.4.1 Simulation Maneuver

A steady-state cornering maneuver is designed to evaluate the vehicle dynamic and steady cornering behavior of the vehicle when the suspension component fails. The test maneuver includes driving the truck at constant speed of 30 mph in a straight path of 1650 ft and then negotiating a circle track with a radius of 263 ft while subjected to a 0.23 g lateral acceleration, as shown in Figure 7-7. For some failure cases, the vehicle with balanced suspensions slightly inclines to the affected side (right side) in straight driving. A left-hand turn is more severe than a right-hand turn for the failed balanced suspension system, so the present simulation conducts the left-hand turn only.

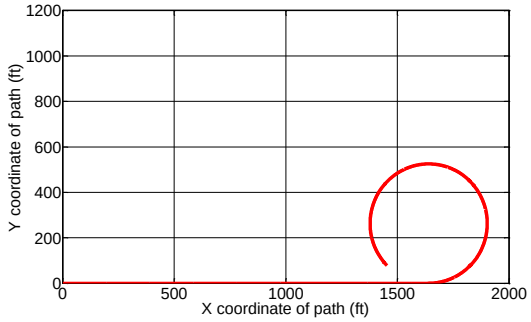

Figure 7-7. Path track for steady state cornering

7.4.2 Effect of Fully blocked Leveling Valve on the Truck's Roll Dynamics

In the following simulation results, "OE" represents the conventional suspension system, while the balanced suspension system is referred to as "BA." The front axle and rear axle on the tractor and trailer exhibit similar suspension dynamic response, and the results for the front axle (2^{nd} and 4^{th} axles) are represented in the following paragraphs

As shown in Figure 7-8 (a), there is no airflow through the disabled leveling valve on the tractor. For the balanced suspension, the valve on the unaffected side and the other two valves on the trailer still work to adjust the body roll. As observed in Figure 7-8 (b), for the failure case, the balanced suspension reduces the peak roll angle by 18% on the tractor and trailer in comparison to the OE suspension, and is still capable of returning the vehicle body to an unrolled position during steady state cornering.

As shown in the left plot of Figure 7-8 (c), by comparing to the OE suspension, the balanced suspension with one side failure provides a larger side-to-side airspring force to resist the vehicle roll motion, resulting from its separate plumbing configuration. The failure on the tractor does not provide any obvious impact on the unaffected side and balanced suspensions on the trailer, which exhibits a significantly large anti-roll suspension force. The left plot in Figure 7-8 (d) clearly indicates that the balanced suspension on the unaffected side (left side) can return to the neutral position due to leveling valve control on that side, whereas the suspension on the failure side performs the same as the OE suspension. On the trailer, as shown in the right plot of Figure 7-8 (d), the balanced suspension exhibits smaller suspension deflection than the OE suspension. By comparing the tractor and trailer for the OE suspension, it is found that the operation of the OE leveling valve gives rise to an unwanted change in ride height during cornering.

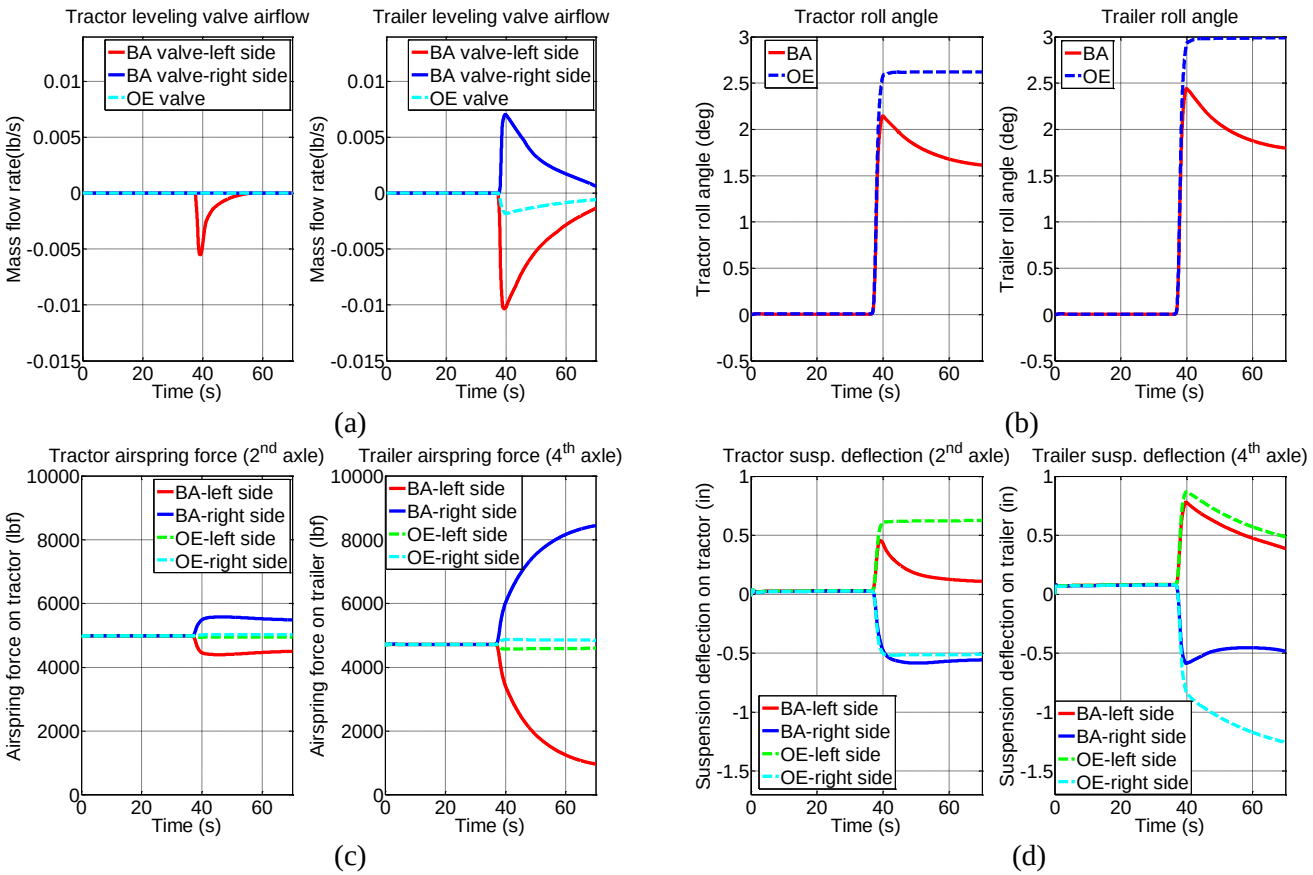

Figure 7-8. Simulation results for the failure case of the fully-blocked leveling valve: (a) mass flow rate at the leveling valve, (b) roll angle, (c) airspring force, and (d) suspension deflection

7.4.3 Effect of Control Rod Bending on the Truck's Roll Dynamics

In the simulation, the failure of control rod bending occurs at t=0s. At that moment, the lever arm rotates down and opens a purge valve to exhaust air from the airsprings, as shown in the left plot of Figure 7-9 (a). As a result, the vehicle ride height reduces by a specified amount to maintain airspring pressure required to support the load, as shown in the left plot of Figure 7-9 (d). The truck body with balanced suspension leans to the suspension failure side slightly, as shown in Figure 7-9 (b), because the leveling valves on the up and down sides tend to return their own suspension to different neutral positions. Note that the neutral positions change side-to-side due to the rod bending. During the cornering after t=37s in Figure 7-9 (a) and (c), the balanced leveling valves on the tractor almost do not provide adjustment. However, as shown in Figure 7-9 (c), the balanced suspension can keep larger airspring

forces from side-to-side on the trailer in response to the steering maneuver than the OE suspension. Figure 7-9 (b) suggests that, before the failure is corrected, the truck with the balanced suspension can drive more safely, experiencing less body roll. The simulation results show that even in the unlikely event that the suspension experiences a failure on both sides of the tractor (no air supply or dump out through airspring), the balanced suspension system on the trailer works to keep the truck body level.

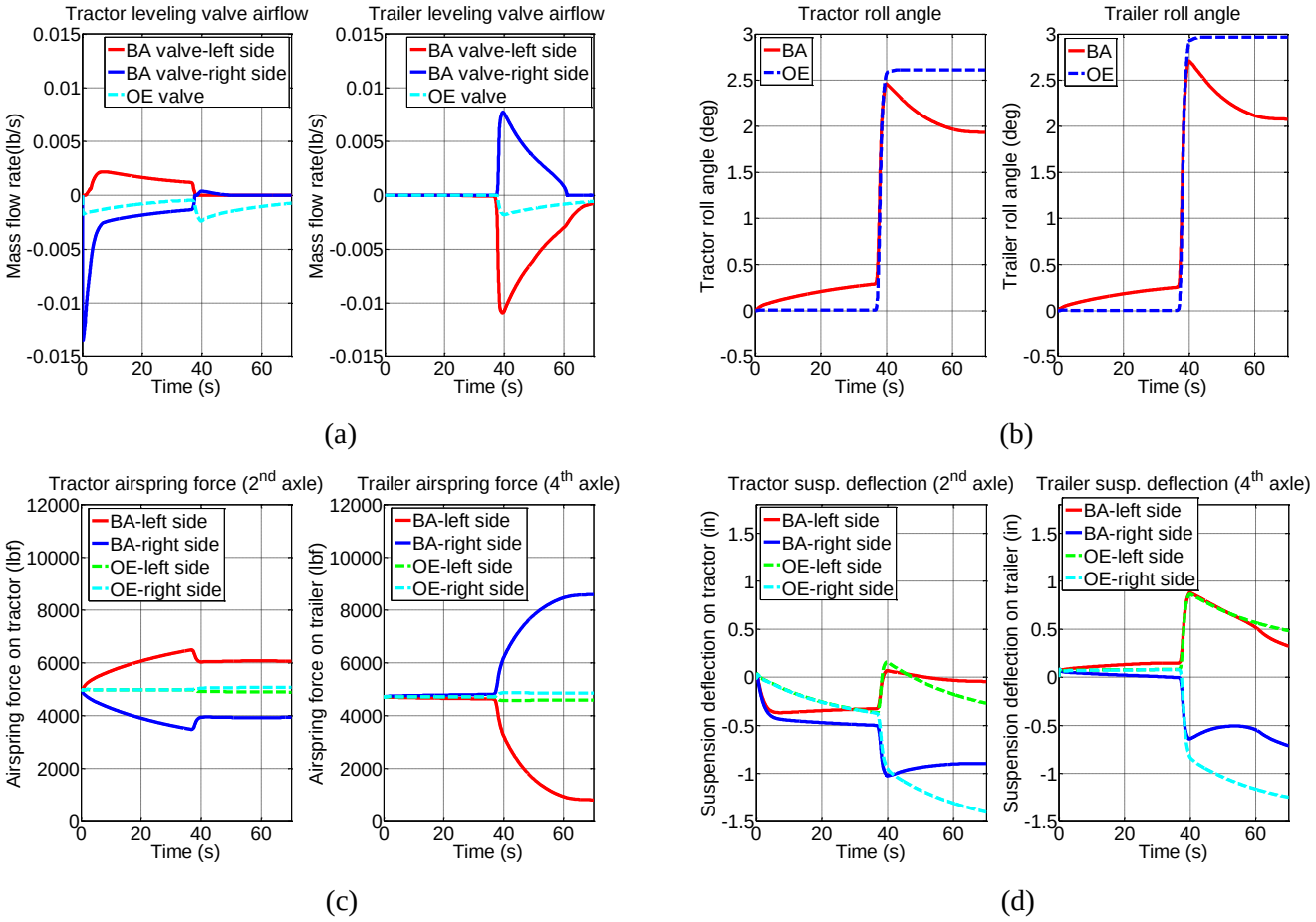

Figure 7-9. Simulation results for the failure of the control rod bending: (a) mass flow rate at the leveling valve, (b) roll angle, (c) airspring force, and (d) suspension deflection

7.4.4 Effect of Suspension System Air Loss on the Truck's Roll Dynamics

Figure 7-10 (a)-(d) illustrate the simulation results of the flow rate of the leveling valve and air leak, roll angle, airspring force, and suspension deflection for the failure of system air loss. As shown in Figure 7-10 (a) and (b), the failure causes a reduction of ride height on the tractor, while the leveling valve opens to compensate for the air loss. As shown in the left plot of Figure 7-10 (a), the air leak highly affects the adjustment of the leveling valve on the same side for the balanced suspension, but the other side valve can still work to maintain the desired height of the suspension. Consequently, similar to the failure case of rod bending, the truck with the balanced suspension slightly leans to the affected side in straight driving, as shown in Figure 7-10 (b). When the vehicle body is subjected to a lateral force, the truck with the balanced suspension exhibits a smaller roll angle compared to the truck with the OE suspension as shown in Figure 7-10 (b). Notably, the balanced suspension with failure still shows the ability to balance the vehicle body after t=40s. The left plot of Figure 7-10 (c) suggests that when the suspension leaks air on one side, the balanced suspension can still maintain a large force difference from side-to-side for controlling the body roll dynamics, which is not observed for the OE suspension. As shown in Figure 7-10 (d), OE suspension height significantly reduces by 1.7 in due to the failure, whereas the balanced suspensions shorten only by 0.5 in. The reduction in the airspring height increases vertical stiffness, leading to poor ride comfort.

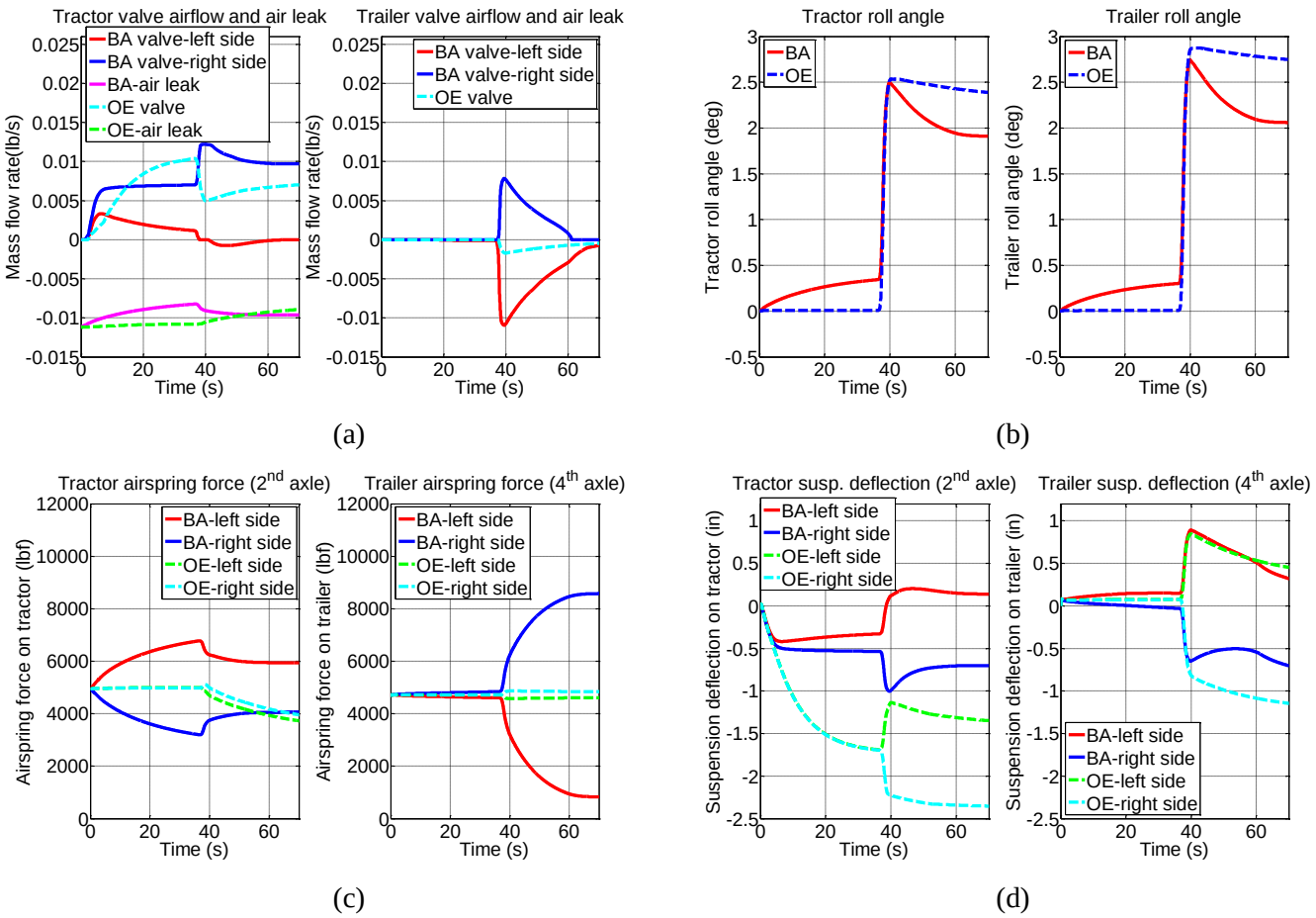

Figure 7-10. Simulation results for the failure case of air loss: (a) mass flow rate at the leveling valve and air leak, (b) roll angle, (c) airspring force, and (d) suspension deflection

7.5 Conclusion

A failure mode and effect analysis for the pneumatic suspensions on truck dynamics by modeling and simulation were provided, and the suspension potential failure modes and their effects were defined, as summarized in Table 7-1. Three representative failure cases were selected and modeled separately: fully-blocked leveling valve, control rod bending of the leveling valve, and air leak. A multi-domain model coupling the fluid dynamics of pneumatic suspensions and the dynamics of a semi-trailer truck was used to evaluate the control performance of the pneumatic suspension on roll dynamics of the truck combination if one of the failure cases occurs. The simulation results suggested that the failure on the side of the suspension has a minimal effect on the other side, due to failure redundancy offered by two

leveling valves. The unaffected side and the suspension system on the trailer still work to keep the truck body level. For the failure case of an air leak, the balanced suspension provided a better ability to maintain the ride height relative to suspensions with a single leveling valve (referred to as “OE suspension” in this study). Moreover, the OE suspension results in an unwanted ride height change during cornering. Specifically, a larger airspring force from side-to-side was obtained for the balanced suspension to resist the vehicle body roll motion for all failure cases. The truck with the balanced suspension exhibited less body roll angle than the OE suspension for the failure cases simulated. The simulation results showed that the failure of any part of the suspension pneumatic system would not disable the balanced suspension system. The unaffected side and the suspensions on the trailer, if failure occurs on the tractor, still work to keep the system functioning until the failure is corrected.

Chapter 8 Pneumatic Suspension Balancing Control for Improved Roll Dynamics of a Semi-trailer Truck Carrying non-uniform load

This chapter investigates the influence of a balanced suspension on the roll dynamics of a truck with non-uniform lateral load due to uneven loading or cargo shift (liquid sloshing) through computer simulation. Pneumatic suspensions are designed to provide balanced suspension forces from side to side for better vehicle roll dynamics in response to the lateral load shift that occurs statically and dynamically. The simulation analysis is based on the previously developed AMEsim-TruckSim model that combines the non-linear fluid dynamics of the suspension with the multi-body dynamics of the truck combination. The destabilizing impacts of fixed uneven load and liquid load shift occurring in the roll plane of a tank vehicle are characterized in the model and are studied separately. It is evident from the simulation that the balanced suspension is able to better withstand the non-uniform lateral load, thereby yielding significantly improved roll performance in comparison with conventional suspensions. Furthermore, the coupled tank-vehicle simulation platform could serve as an effective virtual design and simulation tool for pneumatic suspension development on partially-filled tank truck applications.

8.1 Introduction

The heavy truck typically provides poor roll stability and handling due to the fact that it transports larger cargo with a higher center of gravity (CG) compared to a passenger vehicle. Specifically, a non-uniform lateral load condition due to unbalanced loading or liquid sloshing gives rise to more overturning moments, further diminishing the controllability and the handling characteristics of the heavy truck. The uneven load condition makes the truck far more likely to be involved in rollover accidents [65]. According to a recent investigation conducted for the U.S. Department of Transportation [66], over 1300 cargo tank rollovers are

reported each year. The cargo tank rollover accounts for 31% of the fatalities related to rollovers of commercial vehicles. For shipments of hazardous materials, the associated fatalities, economic loss, and potential environment risks make the accidents more catastrophic. Therefore, it is a major concern for the truck users and manufacturers to improve safety for the truck carrying a non-uniform lateral load. The objective of this chapter is to explore the benefits of the balanced suspension on heavy trucks with non-uniform lateral loads using computer simulation.

Cargo weight is distributed unevenly from side to side due to either improper load distribution, or lateral movement of the load during the cornering (liquid sloshing). Both uneven load and liquid sloshing will be modeled and studied in order to better evaluate the performance of the balanced suspension in resisting overturning moments caused by the static and dynamic uneven load. The static uneven load constantly results in more weight on one side of the suspension with less weight on the other side, causing an inclination angle of vehicle body under normal straight driving conditions. As a result, during cornering, a larger destabilizing moment can be produced due to the sprung mass weight acting at a position that is more laterally offset from the center of the track resulting in a roll moment to one side. There is also an additional moment due the change in mass moment of intertie due to uneven load. The additional destabilizing moment increases as the condition of the uneven load becomes more severe. The body roll dynamics of the truck deteriorate more by the increased destabilizing moment. Apart from the static uneven load, the liquid sloshing encountered within a partially-filled tank during cornering increases the magnitude of the roll moment, leading to roll instability of the vehicle. The load shift due to the liquid sloshing is considered more complex to study than the static uneven load. A number of studies have investigated the influence of the liquid load shift on the dynamics response of the articulated tank vehicles by modeling and simulation. Ranganathan et al. [67] and Saeedi et al. [68] developed a quasi-dynamic roll plane model of a partially filled tank with cross-section and coupled with dynamic model of an articulated vehicle to analyze the stability of partially-filled tank vehicles. Ashtiani et al. [69] studied the effect of the transient fluid sloshing on a partly-filled B-train tanker under different steering maneuvers and filling conditions through computer simulations. Shangguan et al. [70] studied the effect of different cross-sections of the tank on

the directional dynamics of tank vehicle combinations by a TruckSim-Matlab model. In this investigation, a simulation platform is developed for the analysis of the balanced suspension performance on the lateral dynamics of a partially-filled tank vehicle under different filling conditions by integrating a quasi-dynamic model of a partially-filled tank to the previously developed AMEsim-TrukSim truck model.

8.2 Simulation Model

This section will study two cases of uneven load by simulating two types of truck: a semi-trailer truck with a lateral uneven load, and a partially filled tank truck with liquid cargo. The static uneven load model and the quasi-static fluid-sloshing model are presented separately in the following.

8.2.1 Uneven-loaded Semi-trailer Truck Model

A 5-axle, 53-ft semi-trailer truck is modeled to evaluate the performance of pneumatic suspensions under lateral uneven load condition. The uneven load condition is modeled in TruckSim by loading the trailer with two uniform square masses that possess different weights, as shown in Figure 8-1.

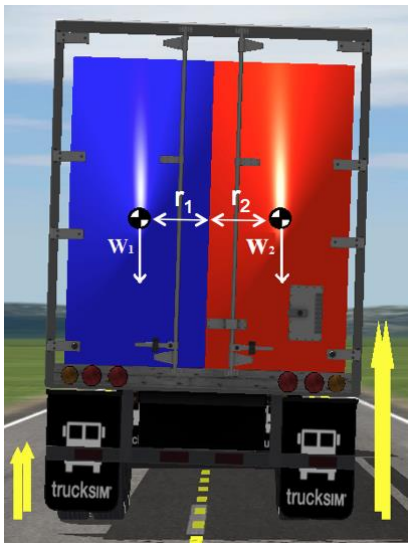

Figure 8-1. Back view of the truck model with lateral uneven load

The center of the combined masses is on the line connecting the two masses and is closer to the larger one. The offset of the center of the mass from the track center can be calculated given the weights of the two masses as follows:

$$r_{cm} = \frac{r_1 w_1 - r_2 w_2}{w_1 + w_2} \quad (58)$$

where $r_1 = r_2 = 24.68$ in is the distance from the of each mass center to the track center. As shown in equation (58), the lateral offset of the uneven load depends on the ratio between the weights of the two masses. The truck with three different lateral offsets of the load CG, i.e., 8 in, 15 in, and 25 in, is simulated and studied separately in the investigation.

8.2.2 Partially-filled Tank Truck Model

A 5-axle, 43-ft tank semi-truck is modeled. When the articulated tank vehicle is subjected to a tank roll and lateral acceleration, the CG movement and varying moment of inertia of the liquid cargo results in an increase in overturning (destabilizing) moment. Qualitatively, three additional destabilizing moments acting on the vehicle induced by sloshing cargo are:

- An additional moment due to the lateral acceleration imposed on the CG that moves in a vertical direction, resulting from the liquid sloshing;
- An additional moment due to the weight of the cargo acting at a position that laterally offsets from the center, caused by the liquid sloshing; and
- An additional moment due to change of mass moments of inertia of the deflected liquid cargo.

It is necessary to determine the movement of the liquid CG in the lateral and vertical axes and the moment of inertial change caused by the liquid sloshing in order to calculate the three additional moments. In this research, a quasi-steady-state model of the fluid sloshing within the tank is developed assuming a steady-state fluid flow condition. The tank with a circular cross-section is considered in the modeling. During the steering maneuver, the motion of the free surface of the liquid results in the shift of cargo CG and alters the roll moment of inertia [67]. The gradient of the free surface (α) in the partly-filled tank depends

on the lateral acceleration (A_l) imposed on the liquid and roll angle of the tank trailer (θ) as follows [70]:

$$\alpha = tan^{-1}\left(\frac{tan\theta + A_l}{1 - A_l tan\theta}\right) \quad (59)$$

Figure 8-2 depicts the gradient of the free surface in a roll plane representation of a partially-filled tank with circular cross-section.

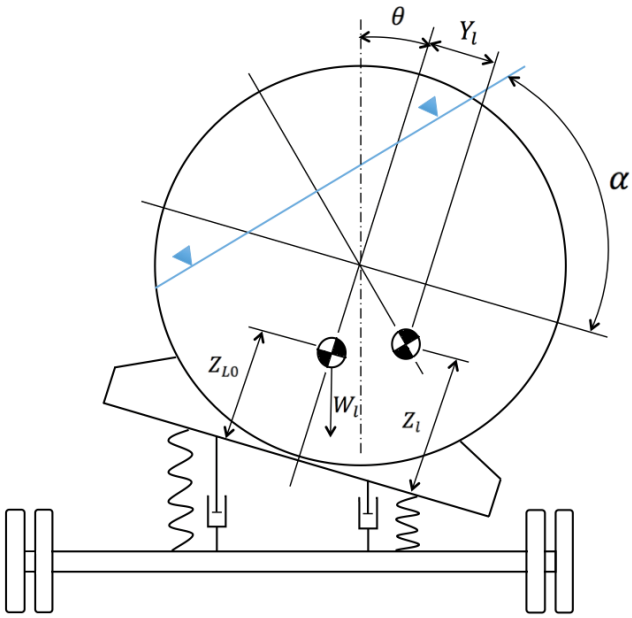

Figure 8-2. Roll plane representation of the partially-filled tank trailer

As shown in Figure 8-2, due to the lateral force, the liquid bulk CG moves according to the change of the gradient of the free surface. The instantaneous position of the CG is determined by the relative distance along the lateral (Y_l) and vertical (Z_l) axes [67]:

$$Z_l = R - (R - Z_{L0})cos\alpha \quad (60)$$

$$Y_l = (R - Z_{L0})sin\alpha \quad (61)$$

where R is the tank radius, and Z_{L0} is the height of the liquid CG without tank tilt. The extra overturning moment due to the liquid cargo shift can then be calculated as:

$$M_{xl} = W_l[A_l(Z_l cos\theta - Y_l sin\theta - Z_{l0} cos\theta) + (Z_l sin\theta + Y_l cos\theta - Z_{l0} sin\theta)] \quad (62)$$

where W_l is the load weight, and θ is the sprung mass roll angle. The motion of load results in a deflected shape of the liquid in the tank, changing the roll moment of inertia. By using the parallel axis theorem, the change in the roll moment of inertia with respect to a fixed roll center can be expressed as:

$$\Delta I_x = m_l({Y_l}^2 + {Z_l}^2 - {Z_{l0}}^2 + 2d_o Z_l - 2d_o Z_{l0}) \quad (63)$$

where m_l is the liquid mass and d_o is the distance from the initial position of the mass center to the roll center. Combining equations (62) and (63) yields the expression of the total additional overturning moment due to the cargo sloshing:

$$M_{xT} = M_{xl} - \ddot{\theta}\,\Delta I \quad (64)$$

The software TruckSim is applicable to the simulation of a fixed uneven load, however, it does not permit simulation of the influence of the liquid sloshing. As shown in Figure 8-3, a co-simulation scheme is developed to couple the quasi-static fluid-sloshing model with the AMEsim-TruckSim model. The quasi-static sloshing model neglects the contributions of transient fluid slosh. The proposed co-simulation model therefore is only suitable for steady-state response analyses. The quasi-static fluid-sloshing model is built up using Simulink, as shown in Figure D-1 of Appendix D. The details of the Simulink block for calculating the additional moment caused by the liquid load shifting are shown in Figure D-2 of Appendix D. Table 8-1 shows some parameters for the tank semi-trailer simulation.

Table 8-2 summarizes the simulation parameters for modeling three different filling volumes of liquid cargo in the tank (mass density = 0.03 lb/in). CAD models of static liquid cargos without tank roll are developed by SolidWorks, as illustrated in Figure D-3 of Appendix D, to determine liquid cargo properties necessary for the modeling.

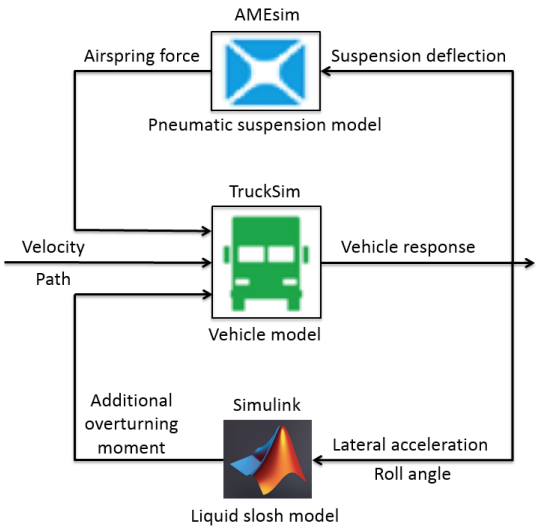

Figure 8-3. Co-simulation scheme for evaluating the effect of a pneumatic suspension on roll dynamics analysis of a partially-filled tank truck

Table 8-1. Tank semi-trailer simulation parameters [70]

Unit	Parameter	Value(English unit)	Value(SI unit)
Tank semi-trailer	Tare trailer mass (Sprung mass)	12900 lbs	5851.34 kg
	Vertical distance from kingpin to ground	50 in	1270 mm
	Distance from first trailer axle to kingpin	384.5 in	9766.3 mm
	Distance from second trailer axle to kingpin	439.5 in	11087.1 mm
	Track width of trailer axles	77.50 in	1968.5 mm
	Damping coefficient on trailer axles	2124.18 lb-s/ft	31.00 kN-s/m
	Lateral spacing between airsprings on trailer axles	39.37 in	1000.00 mm
	Lateral spacing between dampers on trailer axles	31.50 in	800.00 mm
	Vertical distance between tank bottom and axle	31.95 in	811.53 mm
	Longitudinal distance between CG and kingpin	255.91 in	6500 mm
	Roll mass moment of inertia	236354.39 lb ft^2	9960 kg m^2
	Yaw mass moment of inertia	4271275.04 lb ft^2	179992 kg m^2
	Pitch mass moment of inertia	4065865.04 lb ft^2	171336 kg m^2
	Tank diameter	38 in	11582.4 mm
	Tank length	43 ft	13106.4 mm

Table 8-2. Fluid cargo simulation parameters

Unit	Parameter	Value(English unit)	Value(SI unit)
30% fill volume of the tank	Liquid mass	16595.73 lbs	7527.70 kg
	Fluid level height to tank bottom	25.51 in	648 mm
	CG height to tank bottom	15.2 in	386.08 mm
	Roll mass moment of inertia	49432.46 lb ft^2	2083.09 kg m^2
	Yaw mass moment of inertia	3225142.9 lb ft^2	135907.88 kg m^2
	Pitch mass moment of inertia	3189395.82 lb ft^2	134401.49 kg m^2
60% fill volume of the tank	Liquid mass	33191.48 lbs	15055.4 kg
	Fluid level height to tank bottom	43.43 in	1103 mm
	CG height to tank bottom	24.73 in	628.142 mm
	Roll mass moment of inertia	134222.95 lb ft^2	5656.17 kg m^2
	Yaw mass moment of inertia	5928657.68 lb ft^2	249834.29 kg m^2
	Pitch mass moment of inertia	5864903.9 lb ft^2	247147.7 kg m^2
90% fill volume of the tank	Liquid mass	49787.21 lbs	22583.1 kg
	Fluid level height to tank bottom	63.27 in	1607 mm
	CG height to tank bottom	34.11 in	866.394 mm
	Roll mass moment of inertia	259630 lb ft^2	10940.84 kg m^2
	Yaw mass moment of inertia	8892067.44 lb ft^2	374712.7 kg m^2
	Pitch mass moment of inertia	8852452.34 lb ft^2	373043.32 kg m^2

8.3 Results and Discussion

Simulations are conducted to evaluate the pneumatic suspension performance on roll dynamic characteristics of the semi-trailer truck with lateral uneven load, and the partially-filled tank truck. Analyses are performed considering that the pneumatic suspensions are installed on tractor drive axles and trailer dual axles, while leaf springs are installed on the steering axle. A steady-state cornering maneuver is selected for the study. The roll dynamic performances of the truck with different pneumatic suspension systems are evaluated mainly in terms of roll angle and roll rate responses.

8.3.1 Effect of the Balanced Suspension on Roll Dynamics of the Truck with Lateral Uneven Load

The truck with lateral uneven load is simulated to negotiate a steady-state cornering (radius= 262.5 ft) at a constant forward speed of 20 mph, which is subjected to a 0.1 g lateral acceleration. In the simulation, the CG of the unven load is placed offset from the track center by 15 in. Figure 8-4 illustrates the comparison results of roll angle and roll rate responses between the balanced suspension (referred to as “BA”) and the original equipped suspension (referred to as “OE”). The truck with the balanced suspension experiences significant smaller roll angles and lower roll rates than with the OE suspension. Before t = 23s, when the truck runs straight, a lateral inclination appears on both the tractor and trailer bodies due to the uneven load. The inclination angle is smaller and constantly decreases for the balanced suspension, which is different from the OE suspension. In response to the dynamic steering after t = 23s, the balanced suspension obviously yields less peak roll angle on the tractor and trailer. Smaller peak roll rates are also exhibited for the balanced suspension, as shown in Figure 8-4 (b). Under steady-state steering, the balanced suspension has the ability to level the truck body, unlike the OE suspension. From the results, it is apparent that the balanced suspension can fight against the overturning moments caused by the uneven load distribution or cornering force, therefore tends to keep the truck leveled.

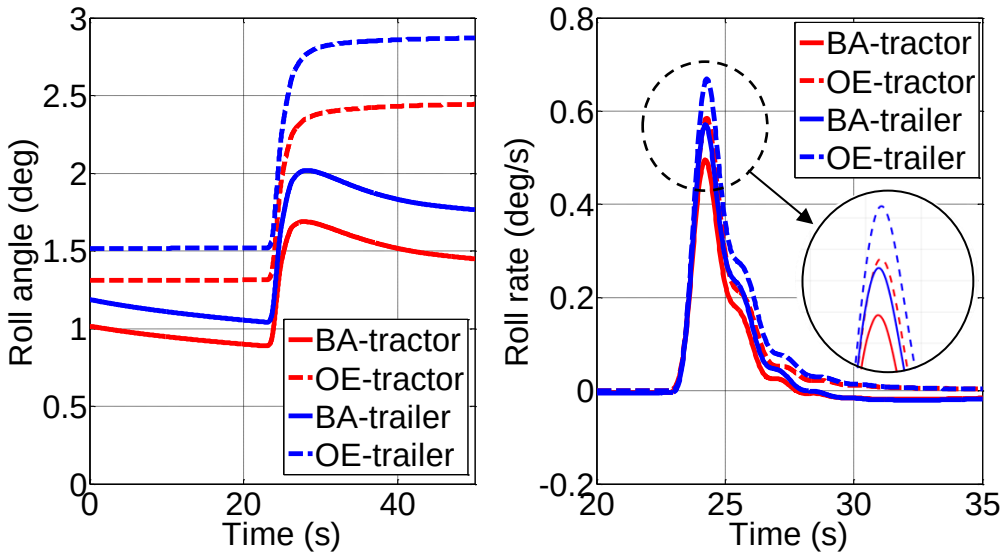

(a) (b)

Figure 8-4. Time trace of (a) roll angle and (b) roll rate responses of the semi-trailer truck with fixed unbalanced load (CG lateral offset of15 in) subjected to a 0.1 g lateral acceleration

Figure 8-5 compares peak roll angel and peak roll rate between the balanced and OE suspension for different lateral offsets of fixed uneven load. As shown in Figure 8-5 (a), the balanced suspension produces a notably smaller value of peak roll angel for the tractor and trailer for CG lateral offsets ranging from 8 in to 25 in. The reduction percentage ranges from approximately 23% to 37%. Specifically, the reduction percentage in peak roll angle between the two suspensions increases as the load's CG lateral offset increases, indicating that the balanced suspension can tune to be stiffer to resist the vehicle body roll when the unbalanced load condition becomes more severe. Figure 8-5 (b) shows a lower peak roll rate for the balanced suspension for all load cases. The roll rate for the OE suspension is nearly constant over all load conditions considered, whereas the peak roll tends to decrease for the balanced suspension. It is evident that the increasing uneven load more adversely affects the truck with the OE suspension than with the balanced suspension.

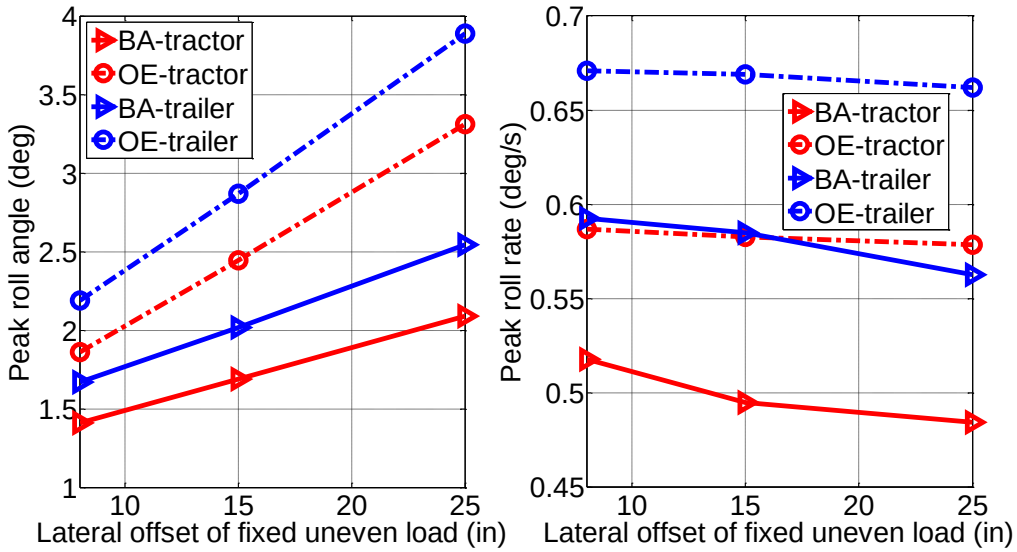

(a) (b)

Figure 8-5. Comparisons of (a) peak roll angle and (b) peak roll rate between the balanced and OE suspensions for various lateral offsets of uneven fixed load subjected to a 0.1 g lateral acceleration

8.3.2 Effect of the Balanced Suspension on Roll Dynamics of the Partially-filled Tank Truck

Figure 8-6 compares the dynamic roll performances of a 60%-volume filled tank truck in terms of roll angel and roll rate responses when subjected to a 0.14 g lateral acceleration. The roll angle as well as roll rate responses of the 60%-volume filled tank truck with the balanced suspension are improved by 18% and 14% compared with the OE suspension. The results in Figure 8-6 suggest that the balanced suspension would help enhance both static and dynamic roll motion of the partially-filled tank vehicle, intentionally maintaining the sprung mass upright to prevent the truck from rollover. As presented in Figure 8-7, a comparison of the peak roll angle and peak roll angle rate of the tractor and trailer indicates improved roll dynamics provided by the balanced suspension compared to the OE suspension, over the fill volume ranging from 30% to 90%. The improvement in the roll angle ranges from 14% to 19% with increasing fill volume. In addition, the increase in the tank volume fill negatively affects the vehicle roll dynamic response, leading to increases in the roll angle and roll rate.

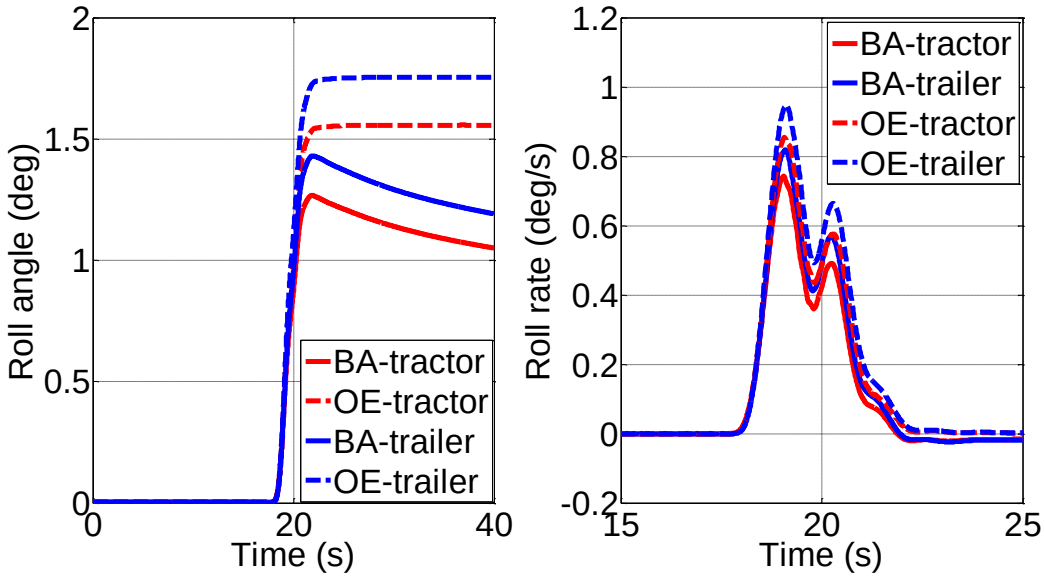

(a) (b)

Figure 8-6. Time trace of (a) roll angle and (b) roll rate responses of a 60%-volume filled tank truck subjected to a 0.14 g lateral acceleration

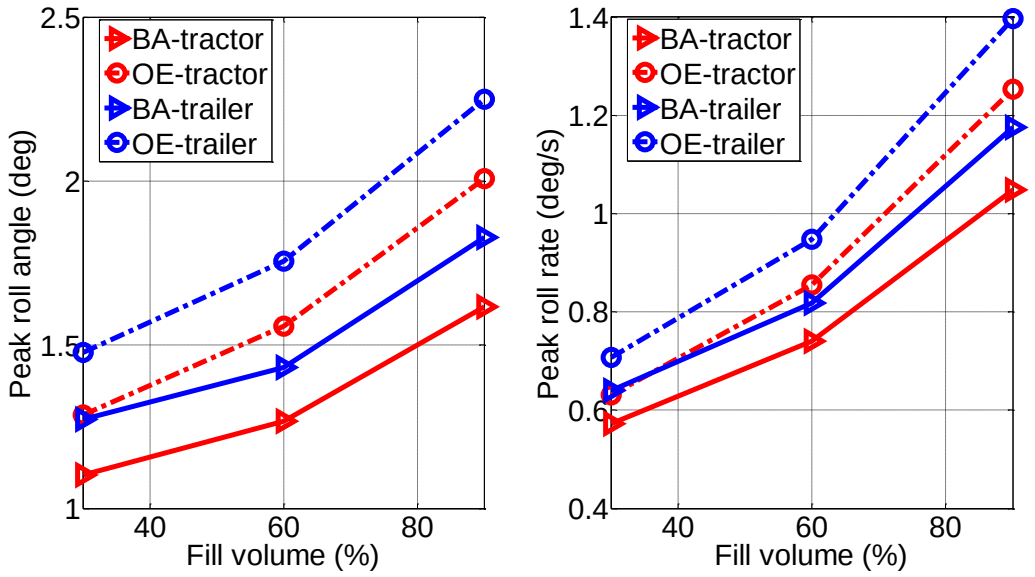

(a) (b)

Figure 8-7. Comparisons of (a) peak roll angle and (b) peak roll rate between the balanced and OE suspensions for various tank fills subjected to a 0.14 g lateral acceleration

Figure 8-8 illustrates the time-varying shift of the cargo mass center in the lateral and vertical directions of a 60%-volume filled tank subjected to a 0.14 g lateral acceleration. The tank with the balanced suspension yields a lower cargo mass center and smaller lateral load shift compared to the OE suspension. During steady-state cornering, this phenomenon increases due to the decreasing roll angle produced by the balanced suspension. Figure 8-9 compares maximum shifts of cargo mass center in the lateral and vertical directions between the balanced and OE suspensions for various tank fills considered. It can be seen that the maximum magnitudes of the lateral and vertical load shift for the balanced suspension are slightly smaller than those obtained for the OE suspension in the entire fill volume range. These are attributed to the effects of roll angle. From the results in Figure 8-9, it is apparent that decreasing the fill volume yields a greater load shift laterally and vertically.

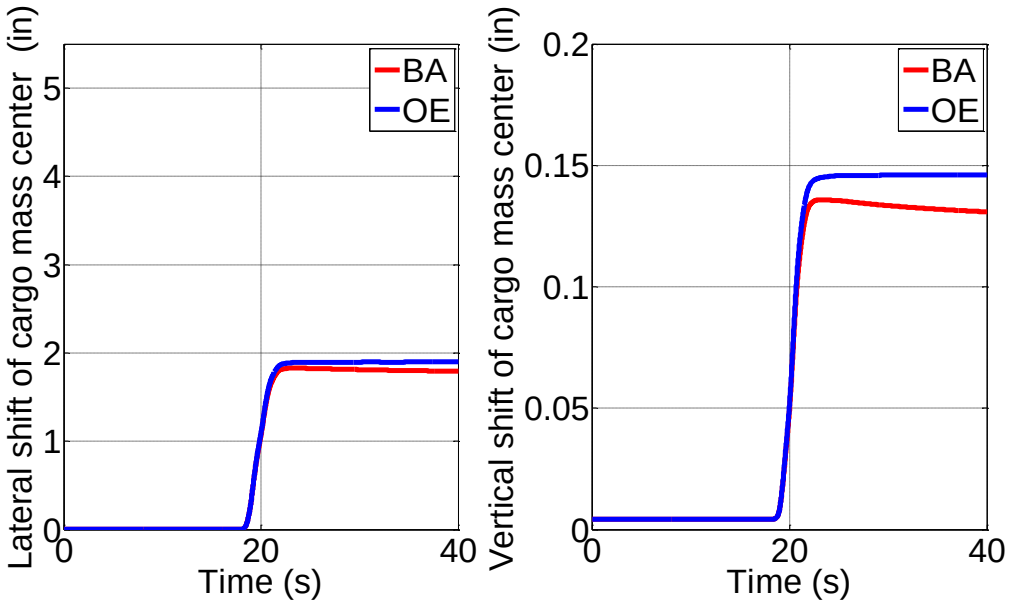

(a) (b)

Figure 8-8. Time trace of (a) lateral and (b) vertical variations of liquid cargo mass center of a 60%-volume filled tank subjected to a 0.14 g lateral acceleration

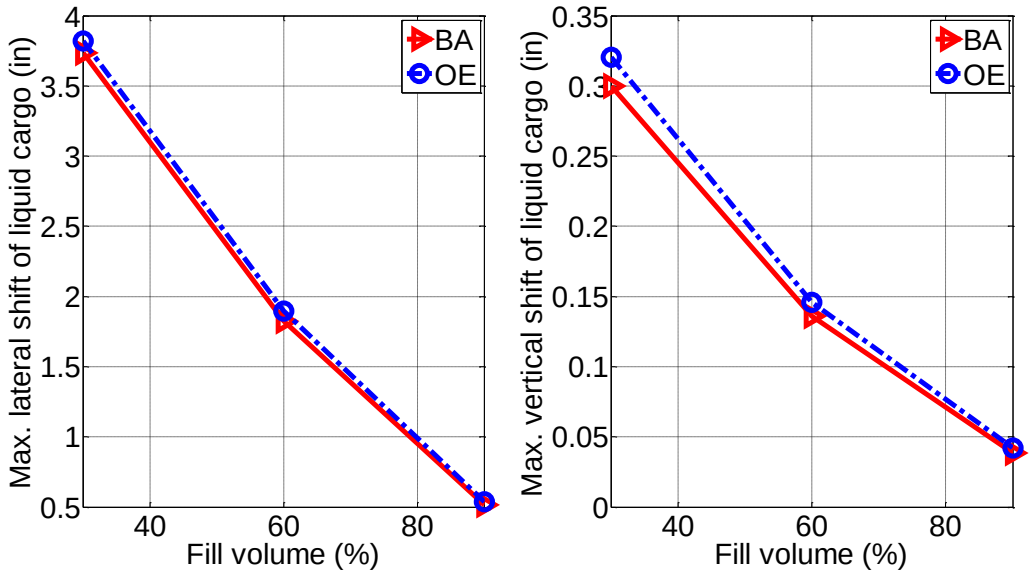

(a) (b)

Figure 8-9. Comparisons of maximum (a) lateral and (b) vertical shifts of liquid cargo mass center between the balanced and OE suspensions for various tank fills subjected to a 0.14 g lateral acceleration

Figure 8-10 (a) compares the relative overturning moment caused by the load shift for the balanced and OE suspensions considering a 60%-volume filled tank truck. Figure 8-10 (a) shows an overturning moment normalized with respect to the load weight, represented by the effective moment arm ($L_{effective} = M_{xl}/W_l$). This suggests that the tank with the balanced suspension yields a lower effective moment arm and thereby lower overturning moment in response to the steering maneuver. Specifically, a lower effective moment arm is also observed for the balanced suspension over the entire range of fill volumes, as shown in Figure 8-11 (a). Figure 8-10 (b) shows the variation in the roll mass moment of inertia (ΔI_x) of the deflected liquid cargo. The balanced suspension reduces the roll mass moment of inertia variation caused by the fluid sloshing. This is further proved by the results in Figure 8-11 (b) which show the maximum roll mass moment of inertia variation for the balanced and OE suspensions over fill volumes from 30% to 90%. As shown in equation (63), the roll mass moment of inertia change is directly related to the load shift so that the lower load shift contributes to lower ΔI_x for given fill volumes.

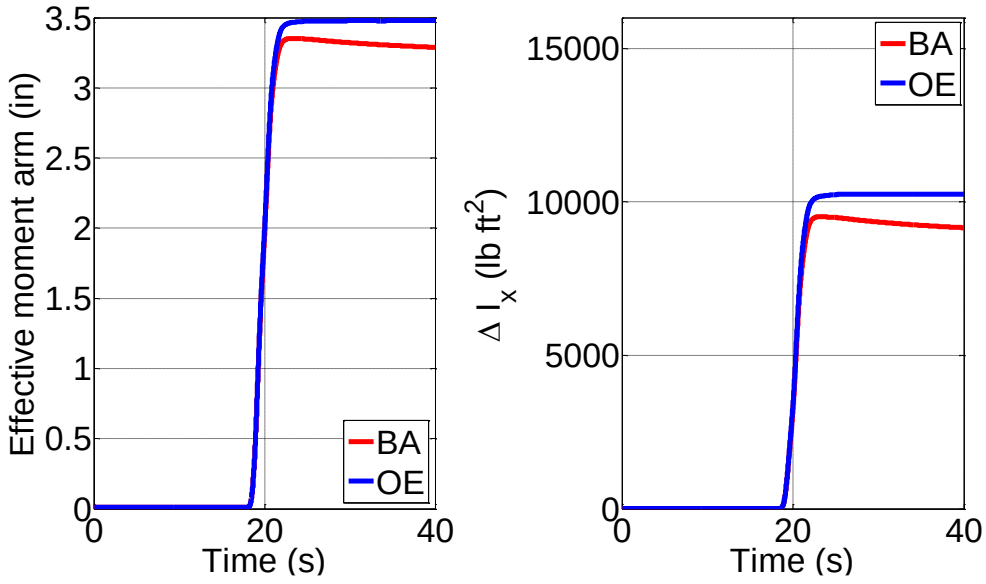

(a) (b)

Figure 8-10. Time trace of (a) effective moment arm and (b) roll mass moment of inertia change of a 60%-volume filled tank truck subjected to a 0.14 g lateral acceleration

Figure 8-10

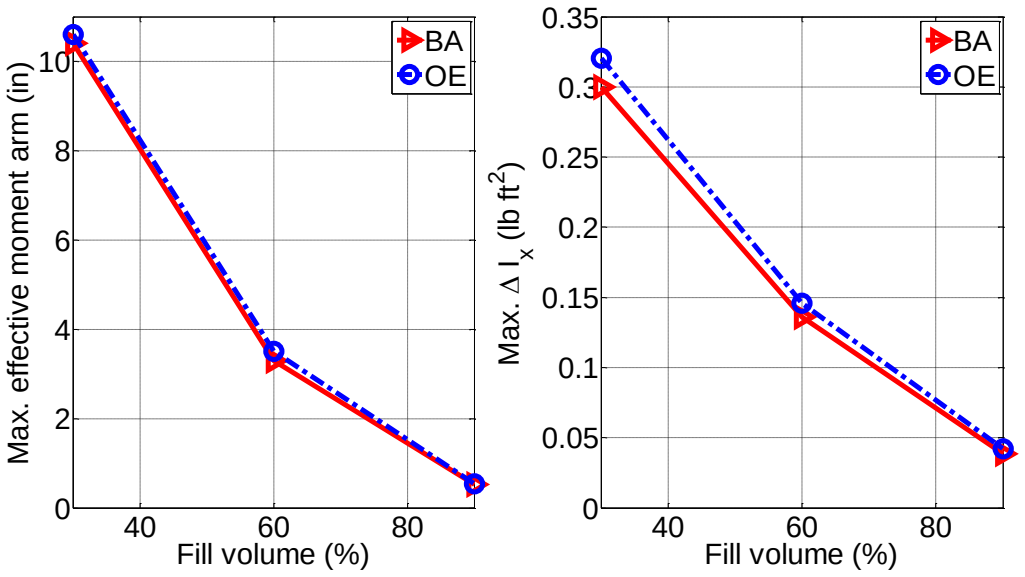

(a) (b)

Figure 8-11. Comparisons of (a) maximum effective moment arm and (b) maximum roll mass moment of inertia variation between the balanced and OE suspensions for various tank fills subjected to a 0.14 g lateral acceleration

Chapter 9 Summary and Future Work

This chapter will provide a summary of the work completed, draw some conclusions, and suggest future direction on the truck pneumatic suspension simulation study and design.

9.1 Summary

The goal of this project was to provide a simulation evaluation and design study of a novel pneumatic suspension (balanced suspension) for improved roll dynamics in heavy truck applications. The topic of the study is an innovative and new technique for which extremely limited information is available in the open literature. In addition, the investigation involves a multi-domain modeling and simulation, including highly non-linear fluid dynamics of a pneumatic suspension and complex multi-body dynamics of an articulated vehicle, which is very difficult to develop and debug successfully. To the author's best knowledge, there is no published work related to the modeling and simulation study of this sort of pneumatic suspension for heavy truck applications.

To achieve the goal of the project, the author began with an effort to derive mathematic equations of the pneumatic suspension system based on the principles of fluid dynamics and thermal dynamics. Next, a detailed development and in-depth analysis of the pneumatic suspension component and system modeling via computer software was realized. A number of experiments were designed and conducted to assist in determining some parameters necessary for the modeling and to validate the component and system models developed. A new truck dynamic model with 9 degrees of freedom was then developed coupled with detailed dynamics of a pneumatic suspension on rear tandem axles. The purpose of the model was to perform a parametric study in order to assess the influence of various suspension components on truck dynamics. On the other hand, the model allowed for a better understanding of how airflow dynamics couple with vehicle dynamics. Preliminary

simulation results have shown that maintaining a balanced airflow through the suspensions improves the dynamic responsiveness of the suspension to steering, causing less body roll.

To extend the study to a more detailed vehicle model (including the coupling effect between tractor and trailer), a hybrid model was established in a co-simulation platform. The model provided a practical simulation environment for the performance evaluation of a pneumatic suspension on tractor and trailer combination dynamics. Beyond assessing the suspension performance, the model was used to conduct a failure mode and effects analysis for the balanced suspension. Simulation results illustrated the benefits of applying the balanced suspension to the heavy truck, including leveling the truck sprung mass dynamically and statically, and better stabilizing the vehicle laterally in case of suspension failure compared to the conventional suspension. Finally, the effect of the balanced suspension on improving roll dynamics of trucks with non-uniform lateral load was evaluated via modeling and simulation. The evaluation was performed under the destabilizing impacts of fixed uneven load and liquid load shift occurring in the roll plane of a tank vehicle.

9.2 Future Work

This section discusses future work based on the knowledge accumulated thus far. Future work should primarily address the following:

- Determining the effect of balanced suspensions on ride comfort.
- Better understanding how the suspension can be used for other classes of vehicles.
    - Automobiles, buses, RV's, off-roading vehicles.
- Evaluating the effect of the suspension on operational efficiency of commercial vehicles, such as fuel economy and tire wear.

References

[1] Elsasser, D., Barickman, F., Albrecht, H., Church, J., Xu, G., Heitz, M., "Tractor Semitrailer Stability Objective Performance Test Research-Yaw Stability (part 1)," Accident Reconstruction Journal, vol. 24, no. 4, 2014.

[2] Cao, D., Song, X., and Ahmadian, M., "Editors' Perspectives: Road Vehicle Suspension Design, Dynamics, and Control," Vehicle System Dynamics 49, no. 1-2, pp. 3-28, 2001.

[3] Siqueira, D., Pugliese, L., Nogueira, F., Ramos, C. C., Herrmann, J. G., Sartori, S., Villiger, C., Paula, G. R., Fuhrken, F., Vargas, V. M., and Araujo, J. F., "Tractor Air Suspension Design and Tuning," No. 2002-01-3041.SAE Technical Paper, 2002.

[4] Cao, D., "Theoretical Analyses of Roll-and Pitch-Coupled Hydro-Pneumatic Strut Suspensions," Ph.D. dissertation, Concordia University Montreal, Quebec, Canada, 2008.

[5] Richardson, S., Sandvik, A., Jones, C., Josevski, N., Pok, P. W., Orton, T., "The Comparative Testing of a Single and Double Ride Height Control Valve Suspension Control Systems," 23rd International Technical Conference on the Enhanced Safety of Vehicles (ESV), no. 13-0292, 2013.

[6] Lambert, J., McLean, A., and Li., B., "Air Suspensions: Dynamic Performance," In Proceedings 8th International Symposium on Heavy Vehicle Weights and Dimensions, South Africa, 2007.

[7] Gillespie, T. D., "Fundamentals of vehicle dynamics," vol. 114. SAE Technical Paper, 1992.

[8] Cole, D. J., "Fundamental Issues in Suspension Design for Heavy Road Vehicles," Vehicle System Dynamics 35, no. 4-5, pp. 319-360, 2001.

[9] Cronjé, P. H., and Els, P. S., “Improving Off-Road Vehicle Handling Using an Active Anti-Roll Bar,” Journal of Terramechanics 47, no. 3, pp. 179-189, 2010.

[10] Bharane, P., Tanpure, K., Patil, A., and Kerkal, G., “Design, Analysis and Optimization of Anti-Roll Bar,” International Journal of Engineering Research and Applications 1, no. 4, pp. 137-140.

[11] Zulkarnain, N., Imaduddin, F., Zamzuri, H., and Mazlan. S. A., “Application of an Active Anti-Roll Bar System for Enhancing Vehicle Ride and Handling,” In Humanities, Science and Engineering (CHUSER), 2012 IEEE Colloquium on, pp. 260-265. IEEE, 2012.

[12] The History of Suspension, access at http://www.ycqcjs.com/news _detail/newsId=89. html

[13] Werminghausen, M., “Mercedes Air Suspension,” a report about legendary Mercedes Air Suspension from the 1960s.

[14] Hendrickson, “Understand Trailer Air Suspensions,” available at http://www.hendrickson-intl.com/CMSPages/GetFile.aspx?guid=7980b859-4512-4efa-8d6b-757d2d0c2fd5

[15] Wang, J., "Nonlinear Modeling and H-Infinity Model Reference Control of Pneumatic Suspension System," 2012.

[16] Lee, S. J., "Development and Analysis of an Air Spring Model," International Journal of Automotive Technology, vol. 11, no. 4, pp. 471-479, 2011.

[17] Goodyear, “Basic Principles of Air Springs,” available at https://www.mrostop.com/ pdfs/Goodyear-air-spring-catalog.pdf.

[18] Bao, W., "Research on the Modeling and Dynamic Simulation of the Air Suspension and Its Control System," Ph.D. dissertation, Huazhong University of Science and Technology, Wuhan, China, 2011.

[19] Quaglia, G., Sorli, M., "Air Suspension Dimensionless Analysis and Design Procedure," Vehicle System Dynamics, vol. 35, no. 6, pp. 443-475, 2001.

[20] Nieto, A. J., Morales, A. L., Gonzalez, A., Chicharro, J. M., Pintado, P., "An Analytical Model of Pneumatic Suspensions Based on an Experimental Characterization," Journal of Sound and Vibration, Vol. 313, 2008, pp. 290-307, doi: 10.1016/j.jsv.2007.11.027.

[21] HWH Online Technical School, "Introduction to Air Suspensions," access at http://www.hwhcorp.com/ml57000-014.html

[22] Nakajima, T., Shimokawa, Y., and Mizuno, M., "Air Suspension System Model Coupled with Leveling and Differential Pressure Valves for Railroad Vehicle Dynamics Simulation," Journal of Computational and Nonlinear Dynamics, vol. 9, no. 3, 2014.

[23] "Air Suspension System, Basic Training 15," available at http://inform.wabco-auto.com/intl/pdf/815/00/57/8150100573-15.pdf

[24] Kornhauser, A. A., Smith, J. L., "The Effects of Heat Transfer on Gas Spring Performance," Journal of Energy Resources Technology 115, no. 1, pp. 70-75. 1993.

[25] Docquier, N., Fisette, P., and Jeanmart, H., "Influence of Heat Transfer on Railway Pneumatic Suspension Dynamics," 21st International Symposium on Dynamics of Vehicles on Roads and Tracks (IAVSD'09), pp. 17-21, 2009.

[26] Hao, L., Jaecheon, L., "Model Development of Automotive Air Spring Based on Experimental Research," Measuring Technology and Mechatronics Automation (ICMTMA), 2011 Third International Conference , vol. 2, pp. 585-590, IEEE, 2011.

[27] Löcken, F., Welsch, M., "The Dynamic Characteristic and Hysteresis Effect of an Air Spring," International Journal of Applied Mechanics and Engineering, vol. 20, no. 1, pp. 127-145, 2015.

[28] Berg, M., "A Three-Dimensional Airspring Model with Friction and Orifice Damping," In the Dynamics of Vehicles on the Roads and on Tracks-Supplement to Vehicle System Dynamics, Volume 33. Proceedings of the 16th IAVSD Symposium Held in Pretoria, South Africa, August 30-September 3, 1999. 2000. 1.

[29] Berg, M., "A Non-Linear Rubber Spring Model for Rail Vehicle Dynamics Analysis," Vehicle System Dynamics, vol. 30, no. 3-4, pp. 197-212, 1998.

[30] Docquier, N., Fisette, P., and Jeanmart, H., "Multiphysic Modelling of Railway Vehicles Equipped with Pneumatic Suspensions," Vehicle System Dynamics, vol. 45, no. 6, pp. 505-524, 2007.

[31] Docquier, N., Fisette, P., and Jeanmart, H., "Model-based Evaluation of Railway Pneumatic Suspensions," Vehicle System Dynamics, vol. 46, no. S1, pp. 481-493, 2008.

[32] Sayyaadi, H., Shokouhi. N., "Improvement of Passengers Ride Comfort in Rail Vehicles Equipped with Air Springs," World Acad Sci Eng Technol 53, pp: 827-833, 2009.

[33] Chang, F., and Lu. Z. H., "Dynamic Model of an Air Spring and Integration into a Vehicle Dynamics Model," Proceedings of the Institution of Mechanical Engineers, Part D: Journal of Automobile Engineering 222, no. 10, pp. 1813-1825, 2008.

[34] Lee, H. W., Kim, S. H., Huh, H., Kim, J. Y., and Jeong, S. G., "Finite Element Analysis of Diaphragm-Type Air Springs with Fiber-Reinforced Rubber Composites," Journal of Composite Materials 37, no. 14, pp. 1261-1274, 2003.

[35] Liu, H., Zhuang, D., Lin, Y., Wang, W., Zhang, F., Zhang, W., and Liu, F., “A Study on Nonlinear Stiffness Characteristic of Air Spring for a Bus,” SAE Technical Paper, no. 2002-01-3092, 2002.

[36] Yin, Z. H., Khajepour, A., Cao, D., Ebrahimi, B., and Guo. K., "A New Pneumatic Suspension System with Independent Stiffness and Ride Height Tuning Capabilities," Vehicle System Dynamics, vol. 50, no. 12, pp. 1735-1746, 2012.

[37] Nieto, A. J., Morales A. L., Chicharro, J. M., and Pintado, P., "An Adaptive Pneumatic Suspension System for Improving Ride Comfort and Handling," Journal of Vibration and Control: 1077546314539717, 2014.

[38] Robinson, W. D., Kelkar, A. G., and Vogel, J. M., "Modeling and Identification of a Pneumatic Air Spring-Valve-Accumulator System for Semi-Active Suspension Control," In ASME 2012 5th Annual Dynamic Systems and Control Conference joint with the JSME 2012 11th Motion and Vibration Conference, pp. 691-700, 2012.

[39] Robinson, W. D., "A Pneumatic Semi-Active Control Methodology for Vibration Control of Air Spring Based Suspension Systems," 2012.

[40] Porumamilla, H., Kelkar, A. G., and Vogel. J. M., "Modeling and Verification of an Innovative Active Pneumatic Vibration Isolation System," Journal of Dynamic Systems, Measurement, and Control 130, no. 3, 2008.

[41] Deo, H., Suh, N. P., "Pneumatic Suspension System with Independent Control of Damping, Stiffness and Ride-Height," In Proceedings of ICAD2006, 4th International Conference on Axiomatic Design, Firenze, pp. 1-6. 2006.

[42] Deo, H. V., and Suh, N. P., “Variable Stiffness and Variable Ride-Height Suspension System and Application to Improve Vehicle Dynamics,” SAE Technical Paper, no. 2005-01-1924, 2005.

[43] Louca, L. S., Rideout, D. G., Stein, J. L., and Hulbert, G. M., "Generating Proper Dynamic Models for Truck Mobility and Handling," International Journal of Heavy Vehicle Systems 11, no. 3-4, pp. 209-236, 2004.

[44] Chang, F., Lu, Z. H., "Dynamic Model of an Air Spring and Integration into a Vehicle Dynamics Model," Proceedings of the Institution of Mechanical Engineers, Part D: Journal of Automobile Engineering, vol. 222, no. 10, pp. 1813-1825, 2008.

[45] Xu, X., Chen, Z.Z., Huang, J.J., Li, Z. X., "Dynamic Modeling and Characteristic Simulation of Charging-discharging System for Electronically Controlled Air Suspension," Journal of System Simulation, vol. 23, no. 6, June, 2011, pp.1225-1228.

[46] Nakajima, T., Shimokawa, Y., Mizuno, M., Sugiyama, H., "Air Suspension System Model Coupled with Leveling and Differential Pressure Valves for Railroad Vehicle Dynamics Simulation," Journal of Computational and Nonlinear Dynamics, vol.9, Jul. 2014, pp. 031006 1-9, doi: 10.1115/1.4026175.

[47] Qi, Z., Li, F., Huang, Y., Yu, D., "Study on the Pneumatic Simulation Model of Railway Vehicle Air Spring System Based on AMEsim," China Railway Science, vol. 34, no. 3, 2013.

[48] Moshchuk, N., Li, Y.J., Opiteck, S., "Air Suspension System Model and Optimization," SAE International, 2011, doi: 10.4271/2011-01-0067.

[49] Chen, Y., He, J., King, M. J., Chen, W., Wang, C., and Zhang, W., "Model Development and Dynamic Load-Sharing Analysis of Longitudinal-Connected Air Suspensions," Strojniški vestnik–Journal of Mechanical Engineering 59, no. 1, pp. 14-24, 2013.

[50] White, D. L., "Parametric Study of Leveling System Characteristics on Roll Stability of Trailing Arm Air Suspension for Heavy Trucks," SAE Technical Paper, no. 2000-01-3480, 2000.

[51] Docquier, N., Fisette, P., and Jeanmart, H., "Multidisciplinary Approach to Railway Pneumatic Suspensions: Pneumatic Pipe Modelling," Multi-body Dynamics 2007-ECCOMAS Thematic Conference, 2007.

[52] Kim, H., Lee, H., "Height and Leveling Control of Automotive Air Suspension System Using Sliding Mode Approach," Vehicular Technology, IEEE Transactions, vol. 60, no. 5, pp. 2027-2041, 2011.

[53] Chen, Y., "Modeling and Simulation Analysis of Hydro-pneumatic Coupled Suspension System," Master thesis, Jilin University, Changchun, China, 2009.

[54] Karnopp, D. C., Margolis, D. L., and Rosenberg, R. C., "System Dynamics: Modeling, Simulation, and Control of Mechatronic Systems," John Wiley & Sons, 2012.

[55] SMC company, "Modern Practical Pneumatic Technologies, Third Edition", ISBN: 978-7-111-23810-2, pp. 44-48.

[56] SA, LMS IMAGINE, "AMESim Library Manual," (2008).

[57] White, M. F., "Fluid Mechanics, WCB," McGraw-Hill, Boston (1999).

[58] Zhu, Z., "Flow Characterization and Redesign of Load-leveling Valves for Improving Transient Dynamics of Heavy Truck Air Suspension." Master thesis, Virginia Tech, 2016.

[59] Teng, S., and Shin-Yann H., "Failure Mode and Effects Analysis: an Integrated Approach for Product Design and Process Control," International Journal of Quality & Reliability Management 13, No. 5, pp. 8-26, 1996.

[60] Mohr, R. R., "Failure Modes and Effects Analysis," Panel Presentation at JE Jacobs Sverdrup, Feb, 2002.

[61] Dyadem, P., "Guidelines for Failure Mode and Effects Analysis for Automotive, Aerospace and General Manufacturing Industries," ISBN: 0-9731054-1-0.

[62] Lijesh, K.P., Muzakkir, S.M. and Hirani, H., "Failure Mode and Effect Analysis of Passive Magnetic Bearing," Engineering Failure Analysis, pp. 1-20, 2016.

[63] Guo, J., Jiao, N., Jiang, L., Han, X. and Zhang, X., "Hydro-pneumatic Suspension Gasbag Reliability Improvement Based on FMEA and FTA," In Reliability, Maintainability and Safety(ICRMS), International Conference, pp. 592-594, IEEE, 2014, doi: 10.1109/ICRMS.2014.710726459. SA, LMS IMAGINE, "AMESim Library Manual," (2008).

[64] Wang, J., Chen, X., Li, X. and Wu, Y., "Influence of Heavy Haul Railway Curve Parameters on Rail Wear," Engineering Failure Analysis, pp. 511-520, 2015.

[65] Woodrooffe, J., "Evaluation of Dangerous Goods Vehicle Safety Performance." Report TP, 13678-E, 2000.

[66] Cargo Tank Rollovers: Keep Load on the Road: https://www.fmcsa.dot.gov/sites/fmcsa.dot.gov/files/doc/HM_Cargo_Tank_Rollover-Safety_News_508CLN.pdf

[67] Ranganathan, R., Rakheja, S., and Sankar, S., "Influence of Liquid Load Shift on the Dynamic Response of Articulated Tank Vehicles," Vehicle System Dynamics, vol.19, no. 4 pp. 177-200, 1990.

[68] Saeedi, M. A., Kazemi, R., and Azadi, S., "Liquid Sloshing Effect Analysis on Lateral Dynamics of an Articulated Vehicle Carrying Liquid for Various Filled Volumes," International Journal of Engineering-Transactions B: Applications28, no. 11, pp. 1671, 2015.

[69] Ashtiani, I. Hazrati, A. Kolaei, M. Abedi, and S. Rakheja., "Application of Linear Slosh Theory on Stability of the B-train Combinations," In The Dynamics of Vehicles on Roads and Tracks: Proceedings of the 24th Symposium of the International Association for Vehicle System Dynamics (IAVSD 2015), Graz, Austria, , pp. 327, 2015.

[70] Shangguan, W., Chen, Y., Wang, X., and Rakheja, S., "Simulation of a Partly-filled Tank Vehicle Combination in TruckSim and Tank Design Optimisation," International Journal of Heavy Vehicle Systems, vol. 23, no. 3, pp. 264-282, 2016.

Appendix A Effective Area Change and Volume Variation for Airspring of 53-ft Trailer

The airspring used on the 53-ft trailer is manufactured by Goodyear, model number 1R12-095 (replaces: W01-358-8729). The design height typically ranges from 7 in to 10 in, set to be 8 in here for the simulation. Compared to the airspring mounted on the tractor, the trailer airspring has lower design height due to the limited mounting space (no training beam included). The variations of volumes and effective area with respect to heights needed by the airspring model are provided by the manufacturer, as shown in Figure A-1 and Figure A-2. They are fitted with the fourth- and second-order trend lines.

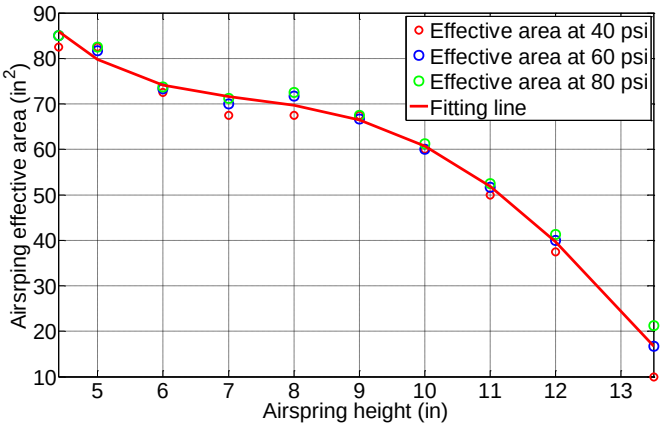

Figure A-1. Trailer's airspring effective area versus heights
(fitting function: $A=0.0253x^4-1.0713x^3+15.326x^2-93.6909x+283.1704$)

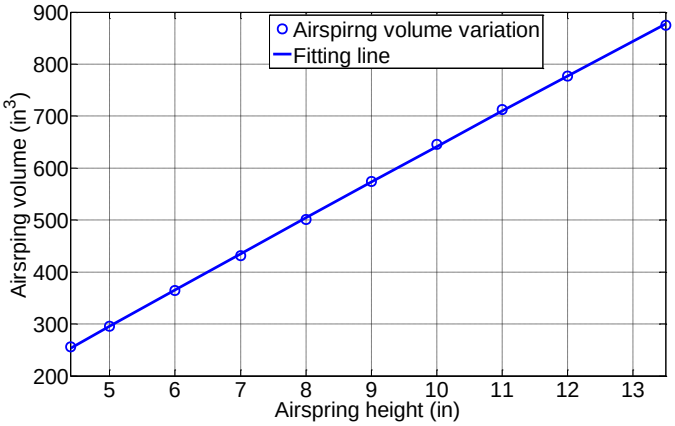

Figure A-2. Trailer's airspring volume versus heights
(fitting function: $V=-0.2159x^2+72.4868x-61.6213$)

Appendix B Schematics of 9-DOF Truck Dynamic Model and Parameters Used in Simulation

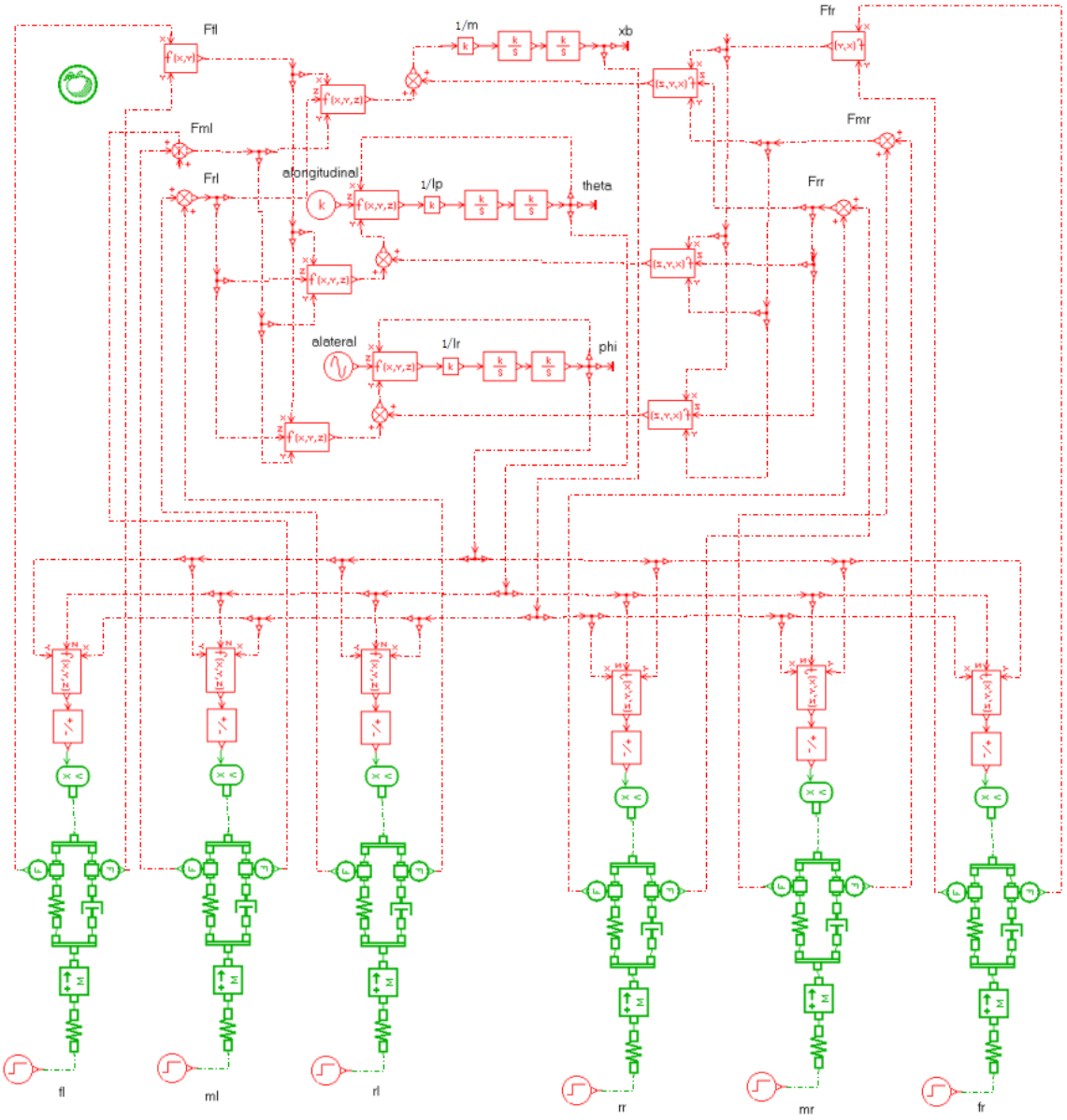

Figure B-1. 9-DOF truck model in AMEsim

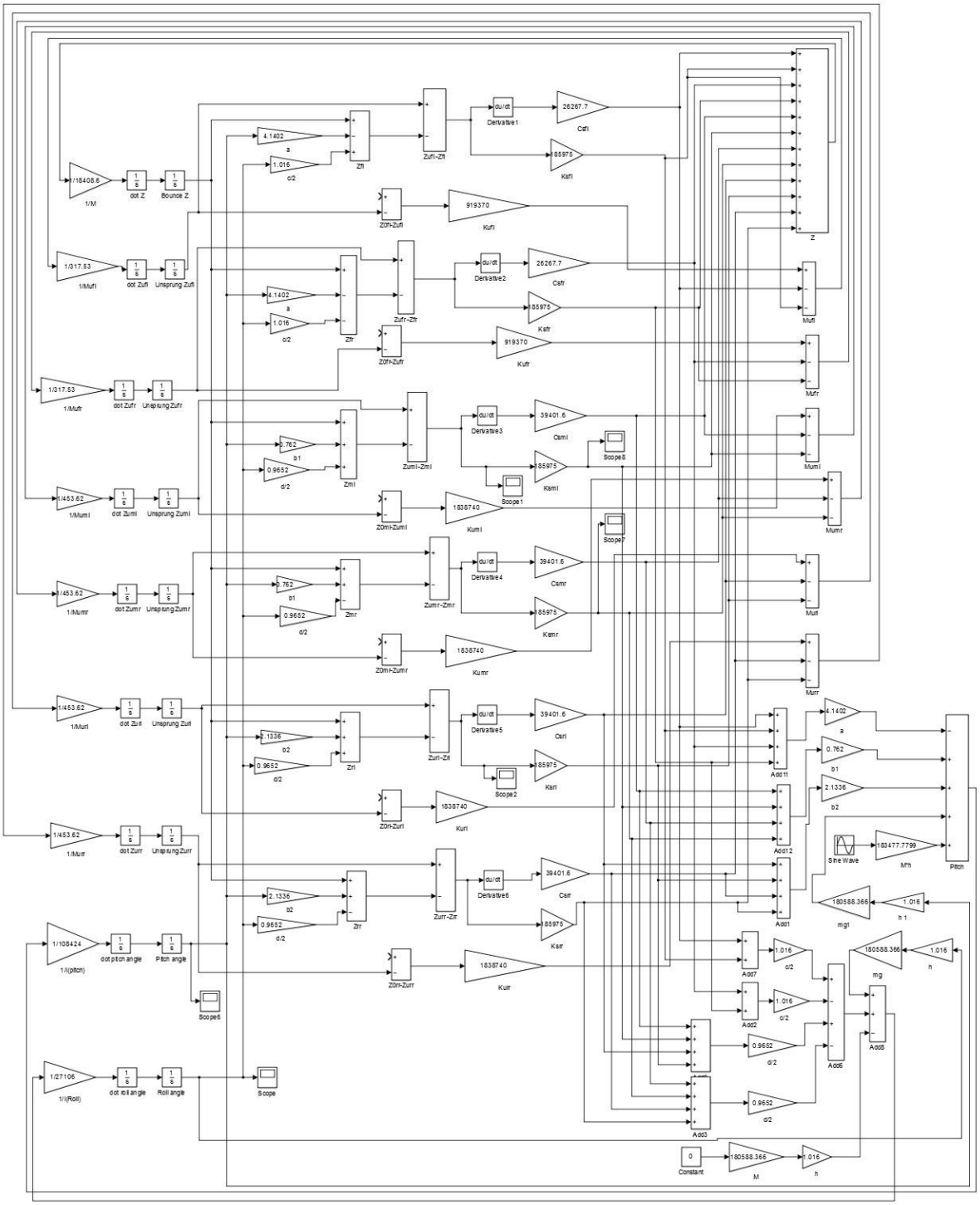

Figure B-2. 9-DOF truck dynamic model in Simulink

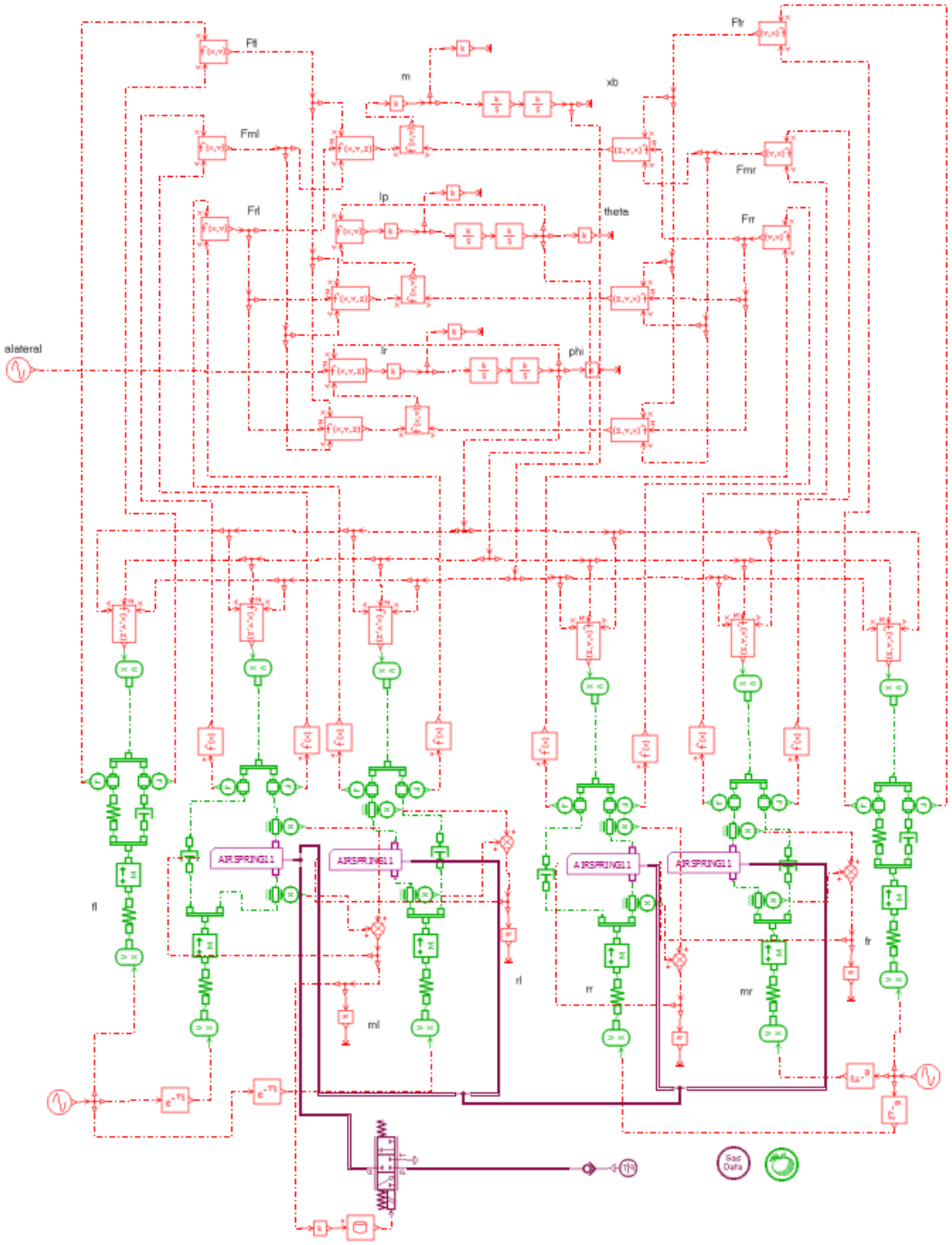

Figure B-3. Aligned truck dynamic model with OE suspensions in AMEsim

Table B-1. Main parameters selected for the 9-DOF truck dynamic simulation

Parameter	Value(English unit)	Value(SI unit)
Body (sprung) weight(loaded)	28357.824 lb.	126141.885 N
Roll moment of inertia, I_r	158044.1 $lbf \cdot in \cdot s^2$	17855.7 $kg \cdot m^2$
Pitch moment of inertia, I_p	632176.5 $lbf \cdot in \cdot s^2$	71422.8 $kg \cdot m^2$
Front leaf spring stiffness per suspension	692.71 lbf/in	121306 N/m
Front damping constant per suspension	97.36 $lbf \cdot s/in$	17049.3 $N \cdot s/m$
Rear damping constant per suspension	164.72 $lbf \cdot s/in$	28845.6 $N \cdot s/m$
Front unsprung weight per suspension	700 lbf	3114.97 N
Rear unsprung weight per suspension	1000 lbf	4450 N
Front unsprung stiffness per suspension	5250 lbf/in	919370 N/m
Rear unsprung stiffness per suspension	10500 lbf/in	1838740 N/m
Distance from the CG to the front axle, a	163 in	4.1402 m
Distance from the CG to the middle axle, b_1	30 in	0.762 m
Distance from the CG to the rear axle, b_2	84 in	2.1336 m
Front wheel track, c	80 in	2.032 m
Rear wheel track, d	76 in	1.9304 m

Table B-2. Main parameters selected for pneumatic suspension simulation

Parameter	Value(English unit)	Value(SI unit)
Airspring initial pressure, p_t	70 psi	482633 pa
Airspring initial height, h_0	11 in	0.254 m
Air tank pressure, p_{ta}	120 psi	827370.88 pa
Atmospheric pressure, p_a	14.7 psi	101300 pa
Initial temperature T_0	68 F^0	293.15 K
External temperature T_{ext}	68 FF^0	293.15 K
Pipe inner diameter(Balanced)	0.4 in	0.01016 m
Pipe inner diameter(OE)	0.236 in	0.006 m
Specific heat ratio γ	1.38	1.38
Gas constant R	287 J·K/kg	287 J·K/kg

Appendix C Schematics of Hybrid Models and Parameters Used in Co-Simulation

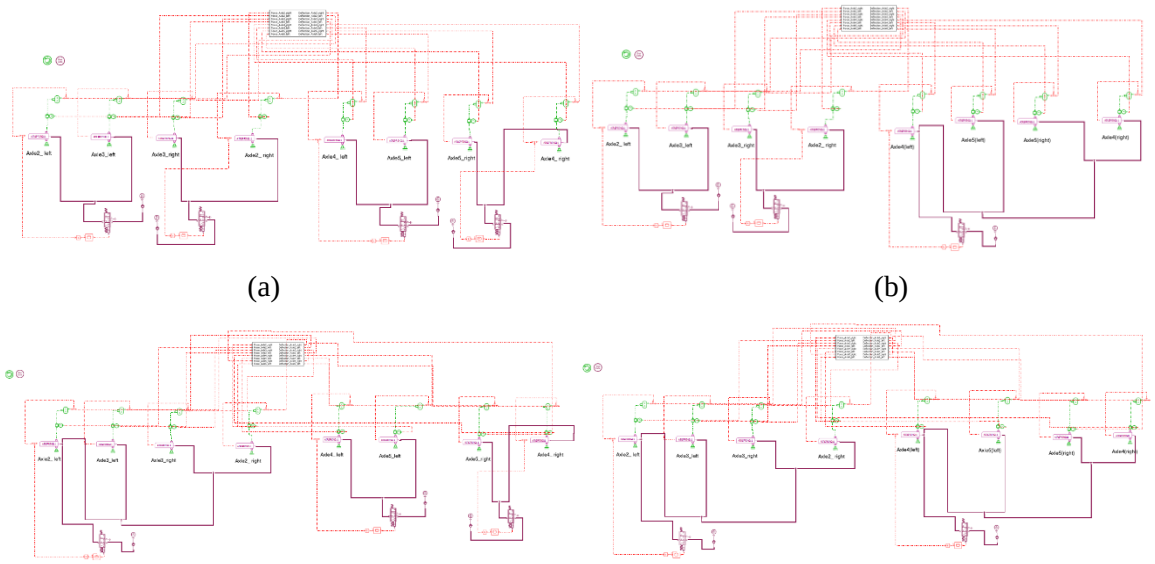

(a) (b)

(c) (d)

Figure C-1. Tractor and trailer suspension system model in AMEsim: a) OE/OE suspensions (b) Balanced/OE suspensions (c) OE/Balanced suspensions (d) Balanced/Balanced suspensions

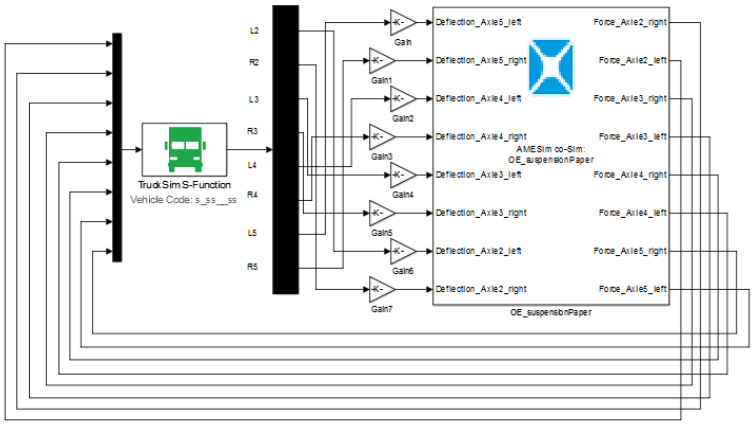

Figure C-2. Co-simulation model in Matlab/Simulink

Table C-1. Main parameters selected for truck dynamic simulation

Unit	Parameter	Value(English unit)	Value(SI unit)
Tractor	longitudinal distance from tractor CG to steering axle	75.67 in	1922.00 mm
	Vertical distance from tractor CG to ground	39.37 in	1000.00 mm
	Tractor body mass (Sprung mass)	14892.23 lb	6755.00 kg
	Roll inertia of tractor body mass	174714.78 lb-ft^2	7362.50 kg·m^2
	Pitch inertia of tractor body mass	551590.86 lb-ft^2	23244.10 kg·m^2
	Yaw inertia of tractor body mass	499365.08 lb-ft^2	21043.30 kg·m^2
	Longitudinal distance from fifth wheel to steering axle	198.93 in	5052.82 mm
	Vertical distance from fifth wheel to ground	43.31 in	1100.00 mm
	Fifth-wheel roll freedom	± 0.5 deg	±0.5 deg
	Fifth-wheel pitch freedom	-11 ~ 7 deg	-11 ~ 7 deg
	Fifth-wheel yaw freedom	±90 deg	±90 deg
	Distance from first drive axle to steering axle	185.98 in	4724.00 mm
	Distance from second drive axle to steering axle	237.75 in	6038.85 mm
	Track width of steering axle	83.62 in	2124.08 mm
	Leaf spring stiffness on steering axle	1427.54 lb/in	250.00 N/mm
	Damping coefficient on steering axle	1168.3 lb-s/ft	17.05 kN-s/m
	lateral spacing between leaf springs on steering axle	35.04 in	890.00 mm
	lateral spacing between dampers on steering axle	43.31 in	1100.00 mm
	Track width of front drive axle	72.62 in	1844.68 mm
	Damping coefficient on front drive axle	2124.18 lb-s/ft	31.00 kN-s/m
	Lateral spacing between airsprings on front drive axle	30 in	762.00 mm
	Lateral spacing between dampers on front drive axle	42 in	1066.80 mm
	Track width of rear drive axle	72.62 in	1844.68 mm
	Damping coefficient on rear drive axle	2124.18 lb-s/ft	31.00 kN-s/m
	Lateral spacing between airsprings on rear drive axle	30 in	762.00 mm
	Lateral spacing between dampers on rear drive axle	42 in	1066.80 mm
Trailer	Trailer tare mass (Sprung mass)	11358.22 lb	5152.00 kg
	Trailer unsprung mass	3042.38 lbf	1380.00 kg
	Vertical distance from kingpin to ground	43.31 in	1100.00 mm
	Distance from first trailer axle to kingpin	498.03 in	12650.00 mm
	Distance from second trailer axle to kingpin	546.02 in	13869.00 mm
	Track width of trailer axles	77.50 in	1968.5 mm
	Damping coefficient on trailer axles	2124.18 lb-s/ft	31.00 kN-s/m
	Lateral spacing between airsprings on trailer axles	39.37 in	1000.00 mm
	Lateral spacing between dampers on trailer axles	31.50 in	800.00 mm

Table C-2. Main parameters selected for pneumatic suspension simulation

Parameter	Value(English unit)	Value(SI unit)
Air tank pressure, P_{ta}	120 psi	827370.88 pa
Atmospheric pressure, Pa	14.7 psi	101300 pa
External temperature T_{ext}	68 F	293.15 K
Pipe inner diameter(Balanced)	0.4 in	0.01016 m
Pipe inner diameter(OE)	0.236 in	0.006 m
Pipe absolute roughness rr	3 e-6 in	0.00012 mm
Gas constant R	287 J·K/kg	8.314 m^2·Pa/(K·mol)
Specific heat ratio	1.38	1.38
Flow area of check valve S_c	0.155 in^2	100 mm^2
Tractor airspring initial height, $h_{tractor0}$	11 in	0.254 m
Trailer airspring initial height, $h_{trailer0}$	8 in	0.2032 m

Appendix D Schematics of the Liquid Cargo Tank Truck Model and Parameters Used in the Simulation

Matlab code used to calculate the initial CG height of liquid cargo load with given volume ratio.

```
% define interested volume ratio
vol_ratio = 0.9;
% define tank cross-sectional radius (ft)
R = 3.125; % ft

%%
h = FUNC_h(vol_ratio,R);

h = h*304.8;  % convert ft to mm
R = R*304.8;  % convert ft to mm

if h == 0
    M_ratio =0;
    Z0 = 0;

elseif 0<h && h<=R  % if the liquid is filled for no more than a half tank
    theta = acos((R-h)/R);
    S_bco = theta/2*R^2;
    S_abo = (R-h)*R*sin(theta)/2;
    S_abc = S_bco - S_abo;
    M_ratio = S_abc*2/(pi*R^2);
    OE = 4*R*sin(theta/2)/(3*theta);
    OF = OE*cos(theta/2);
    CF = R - OF;
    Z_abo = R - 2/3*(R-h);
    Z_abc = (S_bco*CF - S_abo*Z_abo)/(S_bco-S_abo);
    Z0 = Z_abc;

elseif R<h && h<2*R
    theta = acos((h-R)/R);
    AB = R*sin(theta);
    S_oab = (h-R)*R*sin(theta)/2;
    S_abc = theta/(2*pi)*pi*R^2 - S_oab;
    S_cbd = 2*S_abc;
    S_cob = theta/2*R^2;
    M_ratio = (pi*R^2-S_cbd)/(pi*R^2);
    OE = 4*R*sin(theta/2)/(3*theta);
    EF = OE*sin(pi/2-theta/2);
    OH = 2/3*(h-R);
    Z_abc = R + (S_cob*EF-S_oab*OH)/S_abc;
    Z_bdj = (pi*R^3-S_cbd*Z_abc)/(pi*R^2-2*S_abc);
    Z0 = Z_bdj;

elseif h == 2*R
    M_ratio = 1;
    Z0 = R;
```

```
end

fprintf('Z_0 is: %0.2f mm \n',Z0);
fprintf('Liquid level height is %0.2f mm \n',h);
fprintf('The mass ratio is %0.2f \n',M_ratio);
```

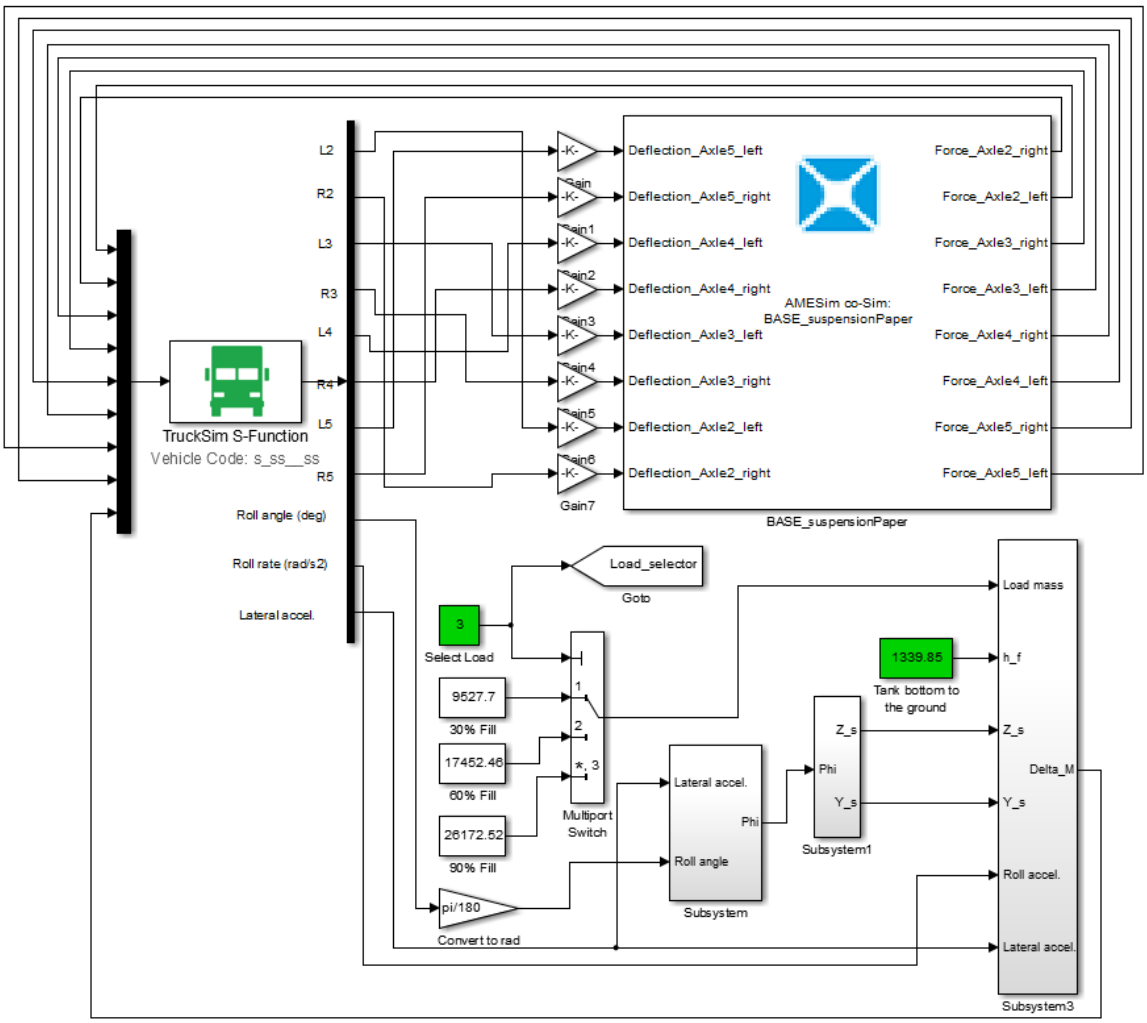

Figure D-1. Co-simulation model developed using AMEsim, Simulink, and TruckSim

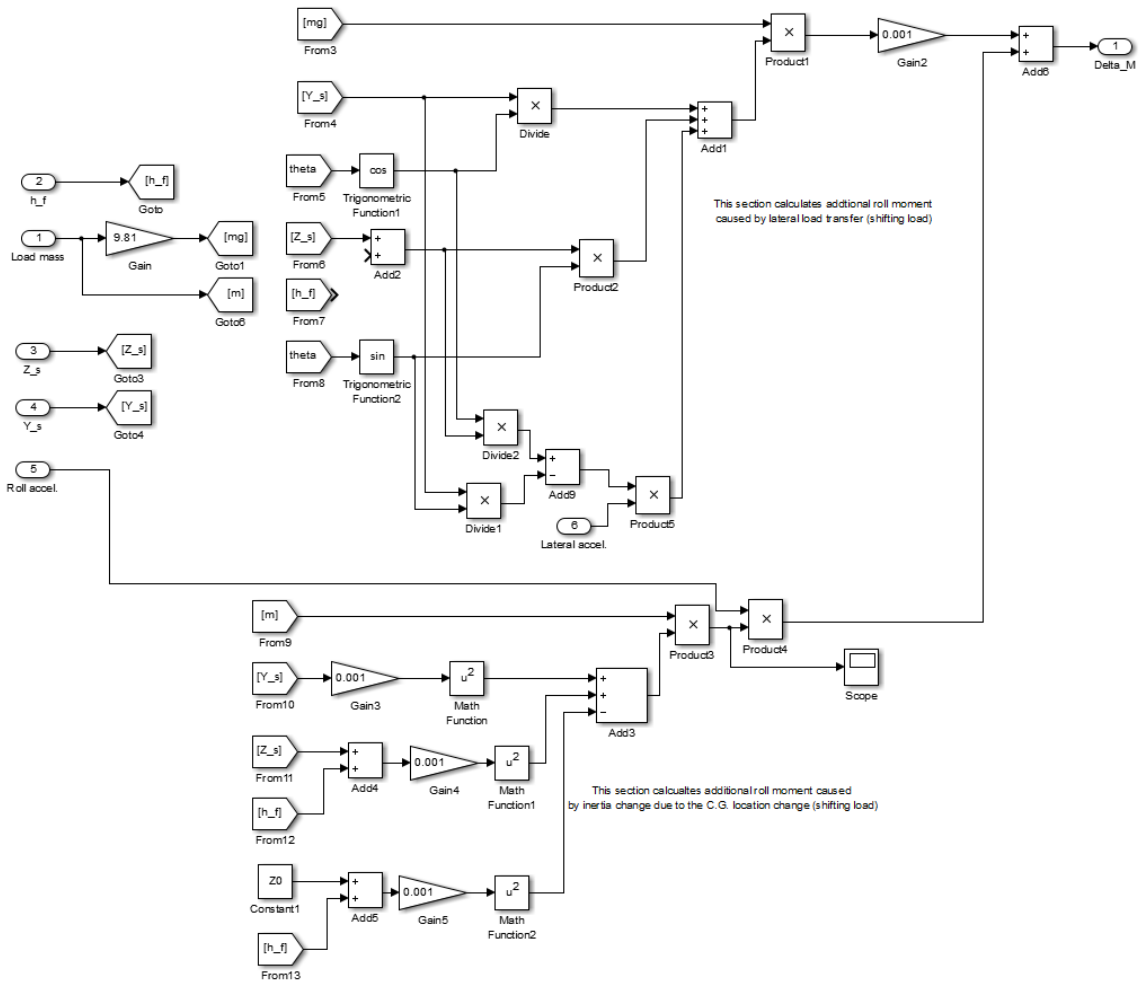

Figure D-2. Simulink diagram for calculation of the additional moment caused by the liquid load shift

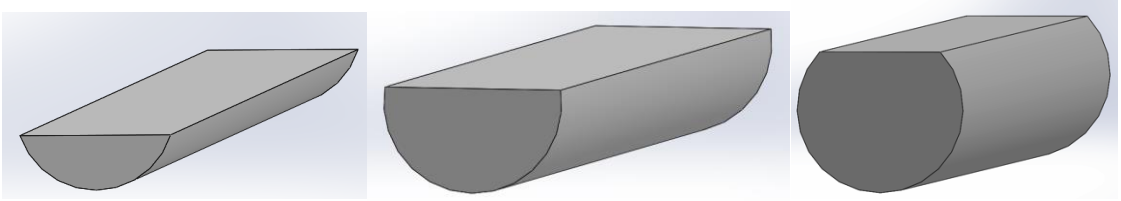

(a) (b) (c)

Figure D-3. Solidwork models of liquid cargo: (a) 30% fill volume, (b) 60% fill volume, and (c) 90% fill volume